Modeling and Control of an Unmanned Underwater Vehicle

J.H.A.M. Vervoort

DCT.2009.096

University of Canterbury
Department of Mechanical Engineering
Christchurch, New Zealand

University of Technology Eindhoven
Department of Mechanical Engineering
Eindhoven, The Netherlands

Master traineeship report

Title:	Modeling and Control of an Unmanned Underwater Vehicle			
Student:	J.H.A.M. Vervoort	ID number:	0577316	[TU/e]
			236146	[UC]
Supervisor:	Prof. Dr. H. Nijmeijer	[TU/e]		
Coach:	Dr. W. Wang	[UC]		
Host University:	University of Canterbury [UC] Department of Mechanical Engineering, Mechatronics			
Sending University:	University of technology Eindhoven [TU/e] Department of Mechanical Engineering, Dynamics and Control Group			

Christchurch, New Zealand, November 2008

Abstract

The Unmanned Underwater Vehicle (UUV) designed at the Mechanical Engineering Department of the University of Canterbury is in an early stage of development. With the design of the AUV completed, the primary focus now is to design control software. The control software has to be able to stabilize the vehicle at a desired position and let the vehicle follow a desired trajectory within a reasonable error.

The AUV is able to operate in six degrees of freedom and the dynamics of an AUV are nonlinear and subjected to a variety of disturbances. A kinematic and dynamic model of the AUV is derived for the six degrees of freedom operating range. The degrees of freedom are decoupled, where only the *surge*, *heave* and *yaw* degrees of freedom will be controlled. A system identification approach is proposed to estimate unknown mass/inertia and damping parameters, treating the *surge*, *heave* and *yaw* degrees of freedom separately. Unfortunately due to sensor malfunctioning the unknown mass/inertia and damping terms could not be estimated, a parameter selection method is used instead. The parameter selection is based on parameter estimation results of software programs and a parameter comparison with other similar shaped AUVs.

A feedback linearizing control technique is chosen to design control laws for control in the *surge*, *heave* and *yaw* degrees of freedom. The controller performed well under parameter perturbation and noise contamination on the feedback position and velocity signals. An under-actuated control problem arises in x-y plane, since one is only able to control two degrees of freedom while the AUV has three degrees of freedom. To steer the AUV smoothly, a path planning model is derived, which describes a path from A to B with the use of polar coordinates. It works as expected, except for planning a straight line trajectory due to singularity reasons.

The under-actuated control problem is again investigated, assuming sway motion of the AUV is not negligible, so Coriolis and centripetal forces need to be considered. A state feedback control method is explained, which is able to follow a reference trajectory in the *x-y* plane. The only disadvantage is that the yaw degree of freedom of the reference trajectory needs to be persistently exciting, which makes following a straight line impossible.

Contents

Chapter 1

Introduction

The first conceptual design of an underwater vehicle or submarine can be credited to the English mathematician William Bourne. He published his design in 1578; a wooden vehicle covered with waterproof leather could be submerged by decreasing the overall volume, an underwater rowing method could be used for steering and propulsion. The concept idea was finally realized by the Dutchman Cornelius Drebbel in 1620 [2]. Nevertheless, it was not until 1776 that a submarine was launched to take part in a naval operation. This submarine of David Bushnell was designed to participate in the American War of Independence. The little egg-shaped wooden submarine held together by iron straps could descend one person by operating a valve to admit water into the ballast tank and used pumps to eject the water [1]. Although the development of the submarine dates back to the 16th century, the first unmanned underwater vehicle or UUV was only to be designed in 1958 by the US Navy. The underwater recovery vehicle was controlled with a cable and used in 1963 to search for the USS Thresher and in 1966 to recover the US Navy hydrogen bomb lost at the coast of Spain [2]. The US Navy funded most of the early unmanned underwater vehicle technology in the 1960s. Building on this technology the first commercial use of the UUV started with the discovery of offshore oil and gas fields in the North Sea. These discoveries were done with a remotely operated vehicle or ROV. The ROV is still extensively used throughout the offshore industry but nowadays the autonomous type of UUV is becoming more popular.

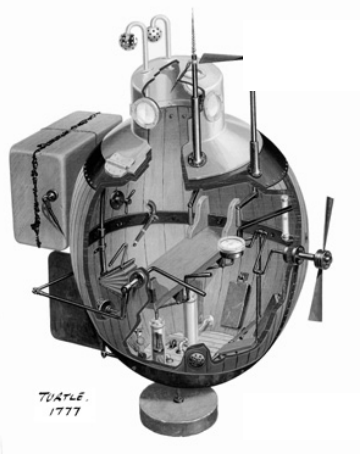

Figure 1.1: David Bushnell's Turtle Submarine *[U.S. Navy]*

The term UUV is a generic expression to describe both remotely operated and autonomous underwater vehicles. The difference between an autonomous underwater vehicle, or AUV, and a ROV is that the ROV is connected to a command platform (for instance a ship) with a tethered cable or an acoustic link [3]. The tethered cable ensures energy supply and information signals, in this way an operator is able to constantly monitor and control the vehicle. The AUV however, is equipped with a battery pack and sonar to fulfill its mission avoiding the use of an operator, which introduces conflicting control requirements. It has to be simple enough to ensure an online implementation of control techniques but at the same time has to cope with a time-varying vehicle/environment interaction [4].

Nowadays the AUV is becoming more and more popular since it can operate and explore in extreme depths (which is useful for the offshore industry) while at the same time it is a low-cost alternative capable of undertaking surveillance missions or mine laying and disposal operations for the navy [2].

The term AUV covers two different groups of vehicles, namely flight vehicles and hovering vehicles. Flight vehicles are often used for surveys, searches, object delivery and object location, while hovering vehicles are used for detailed inspection and physical work around fixed objects [6][7].

The AUV designed at the Mechanical Engineering Department of the University of Canterbury is a hovering AUV, see Figure 1.1. The basic design consists of a cylindrical PVC hull with aluminum end caps, a buoyancy system based on a dynamic diving method, four vertical and two horizon thrusters, a pressure sensor, an inertia measurement unit (IMU), motor controllers, batteries and a motherboard. More information about the design of the AUV can be found in Appendix B. The AUV has to be capable of self navigation, object detection, object avoidance and artificial intelligence to carry out simple tasks [5]. The final goal is to use the AUV for ship hull inspection in harbors. However the development of the AUV is in an early stage. With the design of the AUV completed, the primary focus now is to design control software. The control software has to be able to stabilize the vehicle at a desired position and let the vehicle follow a desired trajectory within a reasonable error. The AUV is able to operate in six degrees of freedom and the dynamics of an AUV are nonlinear and subjected to a variety of disturbances. The development of suitable algorithms for motion and position control of an AUV is a challenging task. When in operation the characteristics of the AUV will

change over time. The control system designed needs good robustness so that it can cope with plant uncertainties while it is suppressing noise and disturbances [2].

Before the development of control laws the design of the AUV is changed by implementing a special inner-sliding-mechanism, which is designed by the author and made by the author and R.C.Engelaar. The inner-sliding-mechanism, described in Appendix B.8, facilitates the exchange of the AUV electronics saving valuable experimental time. A vector representation and, the kinematic and dynamic model are drawn up in Chapter 2. The identification of the AUV, assumptions made to the dynamic model and parameter selection are explained in Chapter 3. In Chapter 4 a feedback linearization approach to control decoupled degrees of freedom is discussed and is extended to track a certain reference trajectory, afterwards a path planning method is explained which uses polar coordinates. Chapter 5 discusses an under-actuated tracking problem that occurs in the x-y plane and explains a control technique to tackle the problem. Finally the conclusion and recommendations are made in Chapters 6.

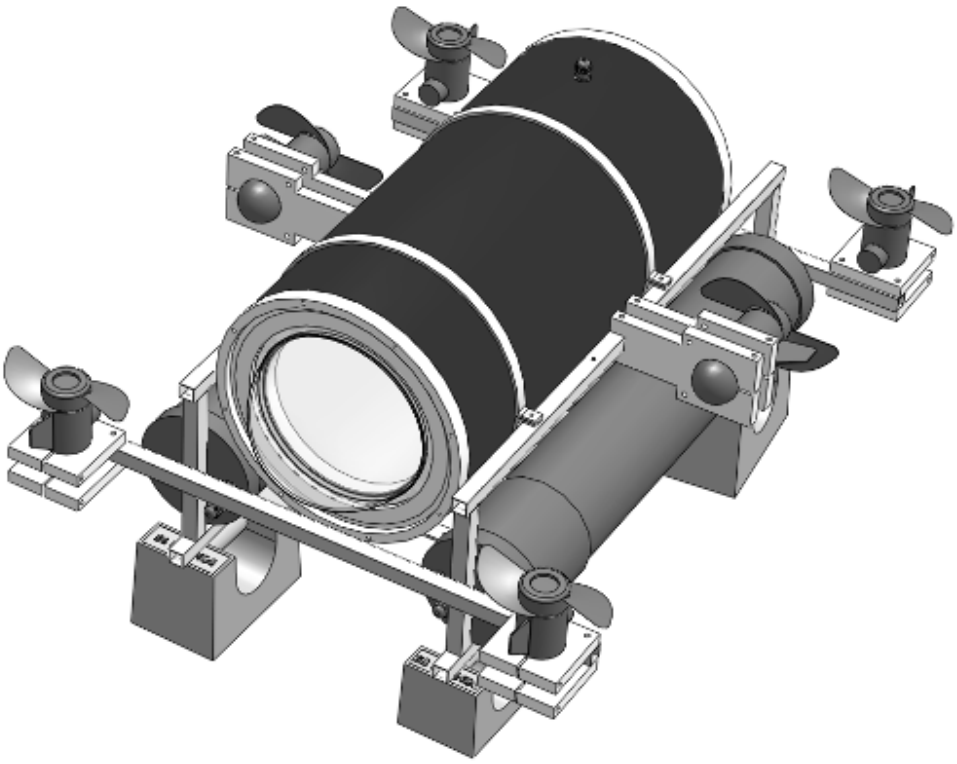

Figure 1.1: 3D CAD image of the AUV.

Chapter 2

Kinematic and Dynamic Model of the AUV

The existence of several complex and nonlinear forces acting upon an underwater vehicle, especially with open frame AUVs, makes the control of AUVs trickier. Several complex and nonlinear forces are, for example, hydrodynamic drag, damping, lift forces, Coriolis and centripetal forces, gravity and buoyancy forces, thruster forces, and environmental disturbances [17]. The kinematics and dynamics which are involved in controlling and modeling an AUV are explored in this chapter. The first section about the kinematics of the AUV will explain the reference frames, Euler angles and the state space representation. The second section about the dynamics will explain the dynamic model of the AUV, with a description of the mass and inertia, Coriolis and centripetal, hydrodynamic damping, and, gravitation and buoyancy forces.

2.1 AUV Kinematics

The reference frames, the use of Euler angles and the state space representation of the AUV will be explained in the following subsections.

2.1.1 Reference Frames

Two reference frames are introduced to model the AUV, a world-fixed reference frame (W) and a body-fixed reference frame (B). The W-frame is coupled to the world, where the *x*-axis points to the north, the *y*-axis to the east and the *z*-axis to the center of the earth. The B-frame is coupled to the vehicle, where the *x*-axis points to the forward direction, the *y*-axis to the right of the vehicle and the *z*-axis vertically down. The W-

frame and the B-frame are depicted in Figure 2.1; note the direction of every axis. Where the degrees of freedom (DOF) of the B-frame, respectively x_B, y_B, z_B, φ_B, θ_B and ψ_B are named *Surge*, *Sway*, *Heave*, *Roll*, *Pitch* and *Yaw*. The origins of the W-frame and B-frame are defined as O_W and O_B, respectively. All the DOF for the B-frame and W-frame which are used in this report are listed in a vector form in

$$\begin{aligned}\chi &= \begin{bmatrix} surge & sway & heave & roll & pitch & yaw \end{bmatrix}^T \\ &= \begin{bmatrix} x_B & y_B & z_B & \phi_B & \theta_B & \psi_B \end{bmatrix}^T \end{aligned} \tag{2.1}$$

and

$$\eta = \begin{bmatrix} x & y & z & \varphi & \theta & \psi \end{bmatrix}^T \tag{2.2}.$$

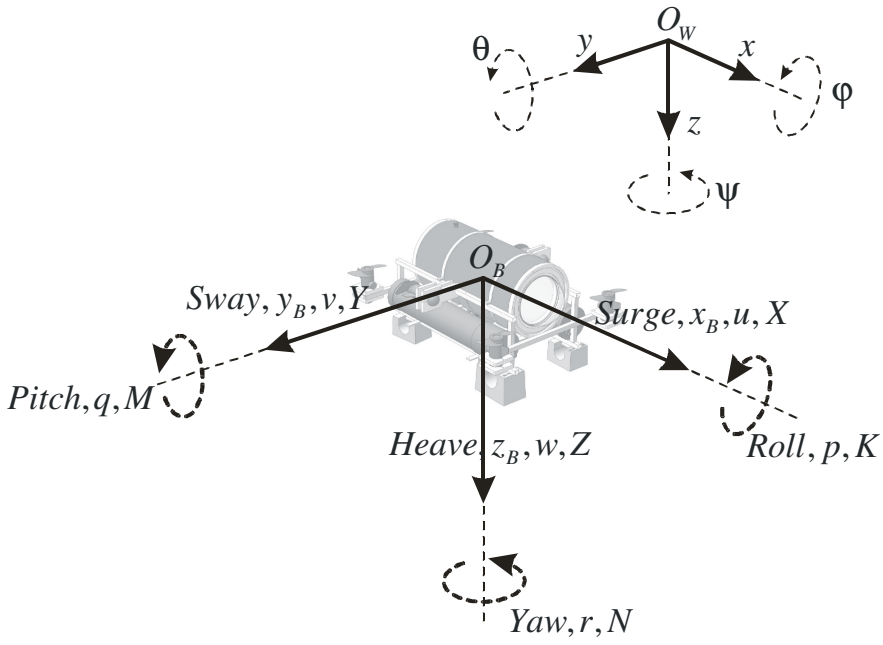

Figure 2.1: Definition of the reference frames, with the naming of all DOFs.

With these two reference frames one is able to determine the orientation of the vehicle with respect to the world and to determine the velocity and acceleration with respect to the world and vehicle coordinates, which is useful for the navigation of the AUV.

2.1.2 Euler Angles

Euler angles relate two coordinate systems in terms of orientation, i.e. the orientation of the B-frame with respect to the W-frame. To orientate one coordinate system with respect to another it may be subjected to a sequence of three rotations, the Euler convention used to describe the orientation from body to world is the *z*-*y*-*x* convention. The B-frame is first rotated around the *z*-axis, then around the *y*-axis and then around the *x*-axis, this corresponds to the rotation angles of *yaw* (ψ), *pitch* (θ), and *roll* (ϕ), respectively. The rotation matrix used to describe the orientation of the B-frame with respect to the W-frame is given by

$$\underline{R}^{BW}(\varphi,\theta,\psi) = \underline{R}_z(\psi)\underline{R}_y(\theta)\underline{R}_x(\varphi) \quad \text{or} \quad \underline{R}^{30}(\varphi,\theta,\psi) = \underline{R}^{32}(\psi)\underline{R}^{21}(\theta)\underline{R}^{10}(\varphi) \tag{3.3}.$$

The complete derivation of the rotation matrix can be found in Appendix A.1.

2.1.3 State Space Representation of the AUV

A state space representation is defined to provide a compact way to model and analyze the AUV. The vector notation includes the position vectors χ (2.1) and η (2.2) for the B and W-frame; the velocity vectors ν and $\dot{\eta}$ for the B and W-frame, respectively

$$\nu = \begin{bmatrix} \dot{x}_B & \dot{y}_B & \dot{z}_B & \dot{\phi}_B & \dot{\theta}_B & \dot{\psi}_B \end{bmatrix}^T = \begin{bmatrix} u & v & w & p & q & r \end{bmatrix}^T \tag{2.4.a}$$

and

$$\dot{\eta} = \begin{bmatrix} \dot{x} & \dot{y} & \dot{z} & \dot{\phi} & \dot{\theta} & \dot{\psi} \end{bmatrix}^T \tag{2.4.b};$$

and the force/torque vector τ of the thruster input,

$$\tau = \begin{bmatrix} \tau_u & \tau_v & \tau_w & \tau_\varphi & \tau_\theta & \tau_\psi \end{bmatrix}^T \tag{2.4.c}.$$

2.1.4 State Vector Transformation

The transformation of the position, velocity and acceleration vector from the B-frame to the W-frame is presented in the following subsections.

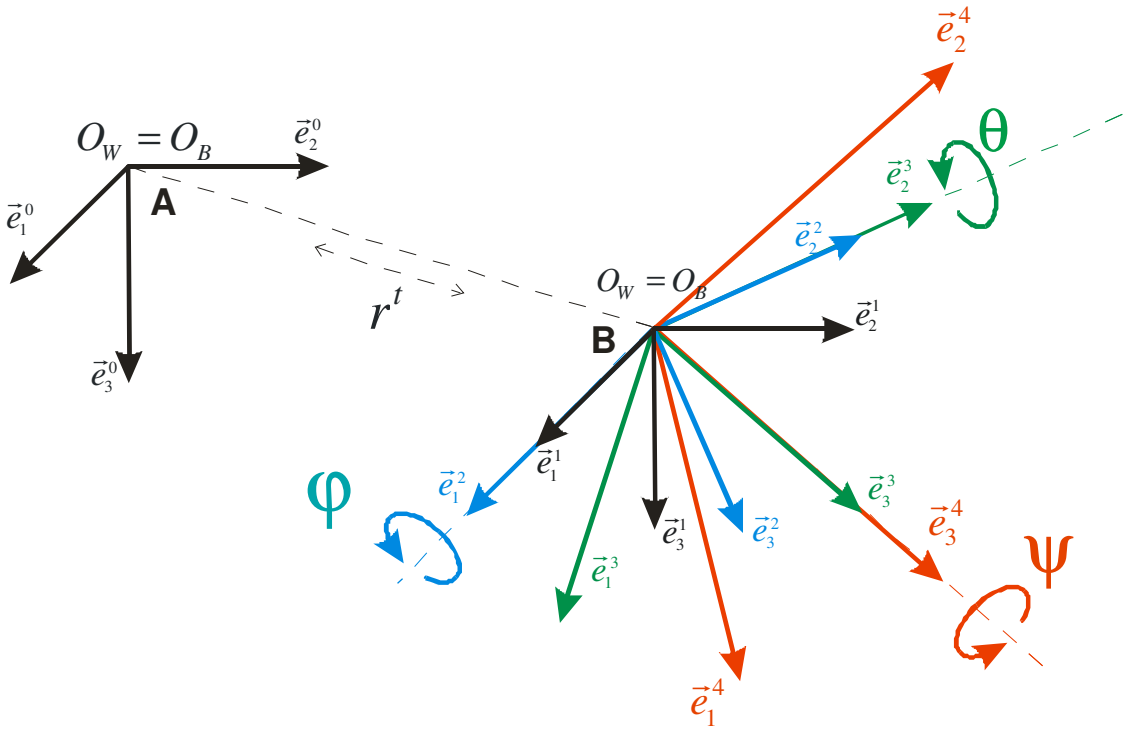

Figure 2.2: Visual explanation of the movement of the W-frame with the B-frame, where $\vec{e}^{\,0}$ and $\vec{e}^{\,1}$ correspond with the W-frame and $\vec{e}^{\,4}$ corresponds with the final position of the B-frame.

2.1.4.1 Position Vector Transformation

The position of the AUV can be described with the same position vector in the B and W-frame and a transformation of the position vector is not needed. The origin of the B and W-frame has the same position in the *surge*, *sway* and *heave* DOF and the position is always described relative to an initial position. Although the position of the B and W-frame in the *roll*, *pitch* and *yaw* DOF can be different. The W-frame has the orientation of the earth's magnetic field while the B-frame has the orientation of the vehicle. A visual explanation is provided in Figure 2.2. At point **A** the B and W-frame have the same orientation, named $\vec{e}^{\,0}$, when the position of the AUV is changed to point **B** with vector $\vec{r}^{\,t}$, the orientation of the B-frame is changed into $\vec{e}^{\,3}$ while the W-frame is changed into $\vec{e}^{\,1}$, which has the same orientation as $\vec{e}^{\,0}$, namely the orientation of the magnetic field of the earth.

2.1.4.1 Velocity Vector Transformation

The velocity vector consists of linear and angular velocities, the velocity vector can be transformed from the B-frame into the W-frame with the use of

$$\dot{\eta} = \underline{J}(\eta)\nu \qquad \text{with} \quad \dot{\eta} = \begin{bmatrix} \upsilon_W & \omega_W \end{bmatrix}^T, \qquad (2.5)$$

$$\nu = \begin{bmatrix} \upsilon_B & \omega_B \end{bmatrix}^T,$$

$$\underline{J}(\eta) = \begin{bmatrix} \underline{J}_1(\upsilon_W) & 0 \\ 0 & \underline{J}_2(\omega_W) \end{bmatrix}.$$

where, ν is the velocity vector of the B-frame, $\dot{\eta}$ is the velocity vector of the W-frame, υ_B is the linear velocity of the B-frame, ω_B is the angular velocity vector of the B-frame, υ_W is the linear velocity of the W-frame, ω_W is the angular velocity of the W-frame, $\underline{J}(\eta)$ is the coordinate transform matrix, which brings the W-frame into alignment with the B-frame.

The world linear velocities or accelerations can be calculated from the body linear velocities with the use of

$$\nu_W = \underline{J}_1(\nu_W)\ \nu_B \qquad \text{with} \qquad \underline{J}_1(\nu_W) = \underline{R}^{BW}(\nu_W) \qquad (2.6)$$

where

$$\underline{J}_1(\nu_W) = \begin{bmatrix} C(\theta)C(\psi) & -C(\varphi)S(\psi) + S(\varphi)S(\theta)C(\psi) & S(\varphi)S(\psi) + C(\varphi)S(\theta)C(\psi) \\ C(\theta)S(\psi) & C(\varphi)C(\psi) + S(\varphi)S(\theta)S(\psi) & -S(\varphi)C(\psi) + C(\varphi)S(\theta)S(\psi) \\ -S(\theta) & S(\varphi)C(\theta) & C(\varphi)C(\theta) \end{bmatrix}$$

note that the rotation matrix (2.3) is being used.

The world angular velocities or accelerations can be calculated from the body angular velocities with the use of

$$\vec{\omega}_W = \underline{J}_2(\omega_W)\vec{\omega}_B \qquad \text{with} \quad \underline{J}_2(\omega_W) = \begin{bmatrix} 1 & S(\varphi)T(\theta) & C(\varphi)T(\theta) \\ 0 & C(\varphi) & -S(\varphi) \\ 0 & S(\varphi)/C(\theta) & C(\varphi)/C(\theta) \end{bmatrix} \qquad (2.7)$$

where *S* denotes sine, *C* denotes cosine and *T* denotes tangent. The full derivation of J_2 can be found in Appendix A.2. Note that $\underline{J}_2$ is undefined if $\theta = \pm\frac{\pi}{2}$, which results in a singularity of the system kinematic equation and that $\underline{J}_2^{-1} \neq \underline{J}_2^T$. The coordinate transformation matrix $\underline{J}$ is still defined in Euler angles, since the AUV is unlikely to ever *pitch* anywhere near $\pm\frac{\pi}{2}$ ($\pm 90^\circ$). If in future applications the AUV needs to operate near to this singularity two Euler angle representations with different singularities can be used to avoid the singular point by simply switching between these. Another possibility is to use a quaternion representation [37, 38].

2.2 Dynamic Model of the AUV

The dynamic model for the AUV is defined to be able to formulate control algorithms and to perform simulations. The dynamic model

$$\underline{M}\dot{\nu} + \underline{C}(\nu)\nu + \underline{D}(\nu)\nu + \underline{g}(\eta) = \tau \tag{2.8}$$

is derived from the Newton-Euler equation of a rigid body in fluid [8, 9]. Where $\underline{M} = \underline{M}_{RB} + \underline{M}_A$ is the inertia matrix for the rigid body and added mass, respectively; $\underline{C}(\nu) = \underline{C}_{RB}(\nu) + \underline{C}_A(\nu)$ is the Coriolis and centripetal matrix for the rigid body and added mass, respectively; $\underline{D}(\nu) = \underline{D}_q(\nu) + \underline{D}_l(\nu)$ is the quadratic and linear drag matrix, respectively; $\underline{g}(\eta)$ is the gravitational and buoyancy matrix; τ is the force/torque vector of the thruster input. Note that (2.8) does not take into account environmental disturbances, such as underwater currents. The dynamic model which includes the environmental disturbances is given in Appendix C.

The hydrodynamic forces and moments where an AUV is dealing with can be separated into added mass and hydrodynamic damping. Added mass is a pressure-induced force and/or moment, which is generated by the forced motion of the vehicle body. Added mass can also be understood as a finite amount of water connected to the vehicle such that the mass of the AUV appears larger [16]. The forces generated by hydrodynamic damping, mass and inertia, Coriolis and centripetal, and, gravitation and buoyancy are explained in the following subsections.

2.2.1 Mass and Inertia Matrix

The mass and inertia matrix consists of a rigid body mass and an added mass, respectively $\underline{M}_{RB}$ and $\underline{M}_{A}$, where

$$\underline{M} = \underline{M}_{RB} + \underline{M}_{A} \tag{2.9}.$$

The rigid body mass term, $\underline{M}_{RB}\dot{\nu}$, from (2.8) can be written as

$$\underline{M}_{RB}\dot{\nu} = \begin{bmatrix} m\dot{\upsilon}_B + m\dot{\omega}_B \times r_G \\ I_B\dot{\omega}_B + mr_G \times \dot{\upsilon}_B \end{bmatrix} \tag{2.10},$$

where m is the mass of the AUV, I_B is the inertia tensor of the AUV with respect to the B-frame, given by

$$\underline{I}_B = \begin{bmatrix} I_{xx} & -I_{xy} & -I_{xz} \\ -I_{yx} & I_{yy} & -I_{yz} \\ -I_{zx} & -I_{zg} & I_{zz} \end{bmatrix} \tag{2.11},$$

and $r_G = \begin{bmatrix} x_G & y_G & z_G \end{bmatrix}^T$ is the definition of the center of gravity of the AUV with respect to the B-frame. The complete derivation of (2.10) can be found in [8]. The rigid body mass, $\underline{M}_{RB}$, used in (2.10) is defined by

$$\underline{M}_{RB} = \begin{bmatrix} m & 0 & 0 & 0 & mz_G & -my_G \\ 0 & m & 0 & -mz_G & 0 & mx_G \\ 0 & 0 & m & my_G & -mx_G & 0 \\ 0 & -mz_G & my_G & I_{xx} & -I_{xy} & -I_{xz} \\ mz_G & 0 & -mx_G & -I_{yx} & I_{yy} & -I_{yz} \\ -my_G & mx_G & 0 & -I_{zx} & -I_{zy} & I_{zz} \end{bmatrix} \tag{2.12}.$$

The AUV is symmetric in the *x*-*z* plane and almost symmetric about the *y*-*z* plane. Although the AUV is not symmetric about the *x*-*y* plane it can be assumed to be symmetric because the vehicle operates at relative low speeds [9]. When the AUV is symmetric in all planes and the origin of the B-frame is positioned at the center of gravity of the AUV, i.e. $r_G = \begin{bmatrix} 0 & 0 & 0 \end{bmatrix}^T$, then the rigid body mass, $\underline{M}_{RB}$, can be simplified into

$$\underline{M}_{RB} = \begin{bmatrix} m & 0 & 0 & 0 & 0 & 0 \\ 0 & m & 0 & 0 & 0 & 0 \\ 0 & 0 & m & 0 & 0 & 0 \\ 0 & 0 & 0 & I_{xx} & 0 & 0 \\ 0 & 0 & 0 & 0 & I_{yy} & 0 \\ 0 & 0 & 0 & 0 & 0 & I_{zz} \end{bmatrix} \tag{2.13}.$$

The effect of the hydrodynamic added mass is modeled with the use of

$$\underline{M}_{A} = \begin{bmatrix} X_{\dot{u}} & X_{\dot{v}} & X_{\dot{w}} & X_{\dot{p}} & X_{\dot{q}} & X_{\dot{r}} \\ Y_{\dot{u}} & Y_{\dot{v}} & Y_{\dot{w}} & Y_{\dot{p}} & Y_{\dot{q}} & Y_{\dot{r}} \\ Z_{\dot{u}} & Z_{\dot{v}} & Z_{\dot{w}} & Z_{\dot{p}} & Z_{\dot{q}} & Z_{\dot{r}} \\ K_{\dot{u}} & K_{\dot{v}} & K_{\dot{w}} & K_{\dot{p}} & K_{\dot{q}} & K_{\dot{r}} \\ M_{\dot{u}} & M_{\dot{v}} & M_{\dot{w}} & M_{\dot{p}} & M_{\dot{q}} & M_{\dot{r}} \\ N_{\dot{u}} & N_{\dot{v}} & N_{\dot{w}} & N_{\dot{p}} & N_{\dot{q}} & N_{\dot{r}} \end{bmatrix} \tag{2.14},$$

where the convention of SNAME (Society of Naval Architects and Marine Engineers, 1950) is used, where $X_{\dot{u}} = \frac{\partial X}{\partial \dot{u}}$, etc. The terms of the added mass matrix are dependent on the shape of the AUV. Since the AUV is assumed to be symmetric in all planes and the origin of the B-frame is positioned at the center of gravity the hydrodynamic added mass, $\underline{M}_A$, given in (2.14) can be simplified into

$$\underline{M}_{A} = \begin{bmatrix} X_{\dot{u}} & 0 & 0 & 0 & 0 & 0 \\ 0 & Y_{\dot{v}} & 0 & 0 & 0 & 0 \\ 0 & 0 & Z_{\dot{w}} & 0 & 0 & 0 \\ 0 & 0 & 0 & K_{\dot{p}} & 0 & 0 \\ 0 & 0 & 0 & 0 & M_{\dot{q}} & 0 \\ 0 & 0 & 0 & 0 & 0 & N_{\dot{r}} \end{bmatrix} \tag{2.15},$$

where only the diagonal terms are used. Note that, $\underline{M}_A > 0$ and $\dot{\underline{M}}_A = 0$, the parameters of the added mass matrix are constant when the vehicle is fully submerged. The parameters are usually in the vicinity of 10% to 100% of the corresponding parameters in the rigid body mass matrix [8, 9].

2.2.2 Coriolis and Centripetal Matrix

The Coriolis and Centripetal Matrix consists of a rigid body and an added mass term, respectively $\underline{C}_{RB}(\nu)$ and $\underline{C}_{A}(\nu)$,

$$\underline{C}(\nu) = \underline{C}_{RB}(\nu) + \underline{C}_{A}(\nu) \tag{2.16}.$$

The rigid body term in the form of $\underline{C}_{RB}\nu$ (2.8), can be written as

$$\underline{C}_{RB}(\nu)\nu = \begin{bmatrix} m\omega_B \times \upsilon_B + m\omega_B \times (\omega_B \times r_G) \\ \omega_B \times (I_B \omega_B) + mr_G \times (\omega_B \times \upsilon_B) \end{bmatrix} \tag{2.17},$$

where m is the mass of the AUV, I_B is the inertia tensor of the AUV with respect to the B-frame (2.11), $r_G = \begin{bmatrix} x_G & y_G & z_G \end{bmatrix}^T$ is the definition of the center of gravity of the AUV with respect to the B-frame. The complete derivation of (2.17) can be found in [8].

The rigid body term is given by

$$\underline{C}_{RB}(\nu) = \begin{bmatrix} 0 & 0 & 0 & 0 & mw & -mv \\ 0 & 0 & 0 & -mw & 0 & mu \\ 0 & 0 & 0 & mv & -mu & 0 \\ 0 & mw & -mv & 0 & I_{zz}r & -I_{yy}q \\ -mw & 0 & mu & -I_{zz}r & 0 & I_{xx}p \\ mv & -mu & 0 & I_{yy}q & -I_{xx}p & 0 \end{bmatrix} \tag{2.18},$$

note that it is assumed that the B-frame is positioned at the centre of gravity. The hydrodynamic added mass Coriolis-like matrix is given by

$$\underline{C}_{A}(\nu) = \begin{bmatrix} 0 & 0 & 0 & 0 & -\alpha_3(\nu) & \alpha_2(\nu) \\ 0 & 0 & 0 & \alpha_3(\nu) & 0 & -\alpha_1(\nu) \\ 0 & 0 & 0 & -\alpha_2(\nu) & \alpha_1(\nu) & 0 \\ 0 & -\alpha_3(\nu) & \alpha_2(\nu) & 0 & -\beta_3(\nu) & \beta_2(\nu) \\ \alpha_3(\nu) & 0 & -\alpha_1(\nu) & \beta_3(\nu) & 0 & -\beta_1(\nu) \\ -\alpha_2(\nu) & \alpha_1(\nu) & 0 & -\beta_2(\nu) & \beta_1(\nu) & 0 \end{bmatrix}$$

(2.19)

Where $\alpha_1(\nu) = X_{\dot{u}}u + Y_{\dot{v}}v + X_{\dot{w}}w + X_{\dot{p}}p + X_{\dot{q}}q + X_{\dot{r}}r,$

$\alpha_2(\nu) = X_{\dot{v}}u + Y_{\dot{v}}v + Y_{\dot{w}}w + Y_{\dot{p}}p + Y_{\dot{q}}q + Y_{\dot{r}}r,\ \alpha_3(\nu) = X_{\dot{w}}u + Y_{\dot{w}}v + Z_{\dot{w}}w + Z_{\dot{p}}p + Z_{\dot{q}}q + Z_{\dot{r}}r,$

$\beta_1(\nu) = X_{\dot{p}}u + Y_{\dot{p}}v + Z_{\dot{p}}w + K_{\dot{p}}p + K_{\dot{q}}q + K_{\dot{r}}r$, $\beta_2(\nu) = X_{\dot{q}}u + Y_{\dot{q}}v + Z_{\dot{q}}w + K_{\dot{q}}p + M_{\dot{q}}q + M_{\dot{r}}r$ and $\beta_3(\nu) = X_{\dot{r}}u + Y_{\dot{r}}v + Z_{\dot{r}}w + K_{\dot{r}}p + M_{\dot{r}}q + N_{\dot{r}}r$, also here the SNAME notation is used.

2.2.3 Hydrodynamic Damping Matrix

The hydrodynamic damping of underwater vehicles normally contains the drag and lift forces. However, the AUV only operates at a low speed which makes the lift forces negligible compared to the drag forces. The drag forces can be separated into a linear and a quadratic term, $\underline{D}(\nu) = \underline{D}_q(\nu) + \underline{D}_l(\nu)$, where $\underline{D}_q(\nu)$ and $\underline{D}_l(\nu)$ are the quadratic and the linear drag term, respectively. If the assumption of the vehicle symmetry about all planes holds then

$$D_l(\nu) = \begin{bmatrix} X_u & 0 & 0 & 0 & 0 & 0 \\ 0 & Y_v & 0 & 0 & 0 & 0 \\ 0 & 0 & Z_w & 0 & 0 & 0 \\ 0 & 0 & 0 & K_p & 0 & 0 \\ 0 & 0 & 0 & 0 & K_q & 0 \\ 0 & 0 & 0 & 0 & 0 & N_r \end{bmatrix} \tag{2.20}$$

describes the linear drag of the AUV [9].

The axial quadratic drag force of the AUV can be modeled with

$$X = -\left(\frac{1}{2}\rho C_d A_f\right)u|u| = X_{u|u|}u|u| \tag{2.21},$$

where $X_{u|u|} = \dfrac{\partial X}{\partial\left(u|u|\right)} = -\dfrac{1}{2}\rho C_d A_f$. The matrix notation of (2.21) which gives the quadratic drag matrix, is given by

$$D_q(\nu) = \begin{bmatrix} X_{u|u|}|u| & 0 & 0 & 0 & 0 & 0 \\ 0 & Y_{v|v|}|v| & 0 & 0 & 0 & 0 \\ 0 & 0 & Z_{w|w|}|w| & 0 & 0 & 0 \\ 0 & 0 & 0 & K_{p|p|}|p| & 0 & 0 \\ 0 & 0 & 0 & 0 & K_{q|q|}|q| & 0 \\ 0 & 0 & 0 & 0 & 0 & N_{r|r|}|r| \end{bmatrix} \tag{2.22}.$$

2.2.4 Gravitational and Buoyancy Matrix

The gravitational and buoyancy vector, $\underline{g}(\eta)$, can be denoted in matrix form by

$$\underline{g}(\eta) = \begin{bmatrix} f_B + f_G \\ r_B \times f_B + r_G \times f_G \end{bmatrix} \quad (2.23),$$

Where the gravitational force vector, f_G, is caused by the weight of the AUV,

$$f_G = \underline{R}^{BW^{-1}}(\upsilon_w)\begin{bmatrix} 0 & 0 & W \end{bmatrix}^T, \text{ with } \quad W = mg \quad (2.24)$$

and the buoyancy force vector, f_B, caused by the buoyancy,

$$f_B = \underline{R}^{BW^{-1}}(\upsilon_w)\begin{bmatrix} 0 & 0 & -B \end{bmatrix}^T, \text{ with } \quad B = \rho g \nabla \quad (2.25),$$

where g is the gravity constant $9.81\, m/s^2$, ρ is the fluid density, ∇ is the volume of fluid displaced by the AUV [m^3], $r_G = \begin{bmatrix} x_B & y_B & z_B \end{bmatrix}^T$ the center of gravity of the AUV, $r_B = \begin{bmatrix} x_B & y_B & z_B \end{bmatrix}^T$ the center of buoyancy of the AUV. Substitution of (2.24) and (2.25) into (2.23) gives

$$\underline{g}(\eta) = \begin{bmatrix} (W-B)\sin(\theta) \\ -(W-B)\cos(\theta)\sin(\phi) \\ -(W-B)\cos(\theta)\cos(\phi) \\ -(y_g W - y_b B)\cos(\theta)\cos(\phi) + (z_g W - z_b B)\cos(\theta)\sin(\phi) \\ (z_g W - z_b B)\sin(\theta) + (x_g W - x_b B)\cos(\theta)\cos(\phi) \\ -(x_g W - x_b B)\cos(\theta)\sin(\phi) - (y_g W - y_b B)\sin(\theta) \end{bmatrix} \quad (2.26).$$

2.2.5 Force and Torque Vector

The thrust force and torque of the AUV are provided by six trolling motors. The trolling motors can deliver a force or torque in the *surge*, *heave*, *roll*, *pitch* and *yaw* directions. The force and torque vector is defined by

$$\tau = LU \quad (2.27),$$

where L is the mapping matrix

$$L = \begin{bmatrix} 1 & 1 & 0 & 0 & 0 & 0 \\ 0 & 0 & 0 & 0 & 0 & 0 \\ 0 & 0 & 1 & 1 & 1 & 1 \\ 0 & 0 & -l_1 & l_2 & -l_1 & l_2 \\ l_3 & l_3 & -l_6 & -l_6 & l_5 & l_5 \\ -l_1 & l_2 & 0 & 0 & 0 & 0 \end{bmatrix} \tag{2.28}$$

and U the thrust vector

$$U = \begin{bmatrix} T_1 & T_2 & T_3 & T_4 & T_5 & T_6 \end{bmatrix}^T \tag{2.29}.$$

The mapping matrix indicates the direction of the force in the *surge* and *heave* degrees of freedom and the direction and arm of the torque for the *roll*, *pitch* and *yaw* degrees of freedom. The thrust vector indicates the thrust that every trolling motor delivers, where T_1 to T_6 represent trolling motor 1 to 6, indicated in Figure 2.3. The figure also shows the trolling motor numbering of the AUV and distances l_i which the trolling motors are separated from the center of gravity. Here the distances l_i are $l_1 = l_2 = 400mm$, $l_3 = 50mm$, $l_5 = 400mm$ and $l_6 = 600mm$.

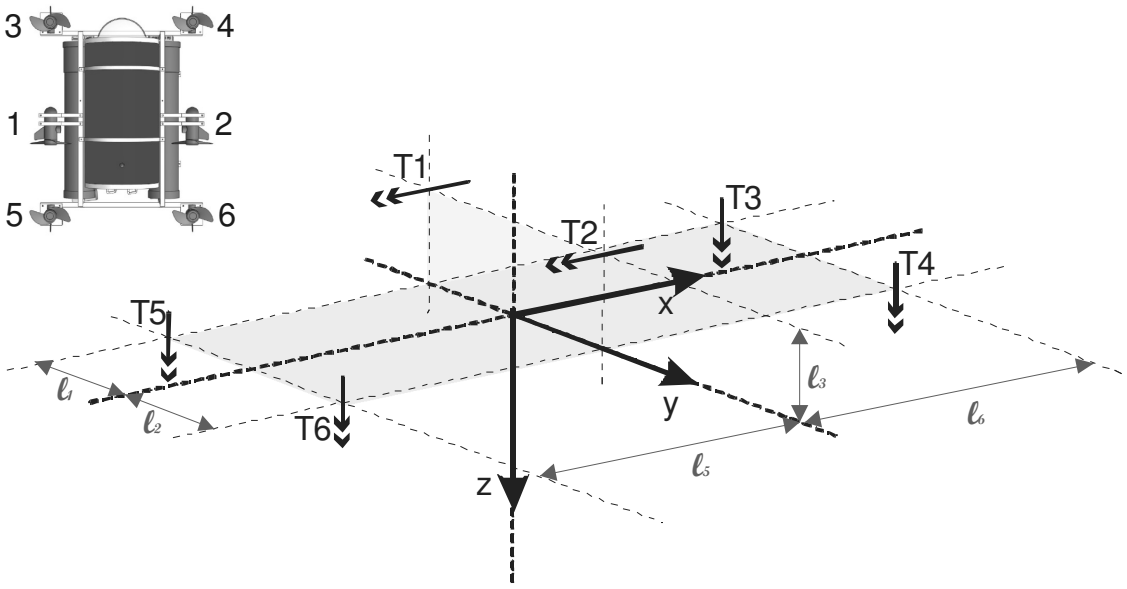

Figure 2.3: Numbering of the trolling motors on the AUV, the definition of the distances of the trolling motor from the center of gravity and direction of positive thrust.

Chapter 3

System Identification of the AUV

The dynamic model of the AUV introduced in Chapter 2 is a complex model, which is simplified with a number of assumptions. This chapter will first sum the assumptions made for the dynamic model and explain why these assumptions can be made. Afterwards the chapter explains the parameter estimation, where the main problem is overparametrisation. An approach to decouple the degrees of freedom of the AUV to identify the model parameters is discussed. The dynamic model can later on be used in numerical simulations; therefore reasonably accurate model parameters should be obtained.

3.1 Assumptions on the AUV Dynamics

Obtaining the parameters of the dynamic model is a difficult time consuming process. Therefore assumptions on the dynamics of the AUV are made to simplify the dynamic model and to facilitate modeling. The following assumptions are made:

1. *Relative low speed, so lift forces can be neglected.*
   The AUV operates at relative low speed, i.e. max. 1 m/s, which means that lift forces can be neglected. The low speed was verified during underwater experiments (wet tests).

2. *AUV symmetry about the three planes.*
   The AUV is symmetric about the *x-z* plane and close to symmetric about the *y-z* plane. Although the AUV is not symmetric about the *x-y* plane it is assumed that the vehicle is symmetric about this plane, so one able to decouple the degrees of freedom. The AUV can be assumed to be symmetric about three planes since the vehicle operates at relative low speed.

3. *The aligning moment ensures horizontal stability.*
   The AUV remains close to horizontal in all maneuvers and stabilizes itself, since the center of gravitation and center of buoyancy are correctly in right order aligned (i.e. aligning moment). This could be concluded from underwater videos made during underwater experiments.

4. *Roll and pitch movement are neglected.*
   The *roll* and *pitch* movement of the AUV are passively controlled and can therefore be neglected, since the AUV stabilizes itself due to the aligning moment. Therefore, the corresponding parameters do not have to be identified.

5. *The B-frame is positioned at the center of gravity,* $r_G = [0 \quad 0 \quad 0]^T$.

6. *The mapping matrix* L *is ignored*
   The trolling motor mapping matrix L is ignored; one just assumes that a certain amount of thrust is delivered in a certain degree of freedom.

7. *Model with and without environmental disturbances.*
   Underwater currents are the only environmental disturbances acting on a deeply submerged AUV. Underwater currents are slowly varying [6] and can result in a movement of the AUV in *sway* direction, see Appendix C for more information.. A dynamic model is made with and without underwater currents. The s*way* movement is hard to control, since no trolling motors are aligned in the *sway* direction and an action in *yaw* and *surge* is needed to correct an error in the *sway* degree of freedom. The movement of the AUV in the *sway* direction is neglected in the model that does *not include* the ocean currents.

8. *The degrees of freedom of the AUV can be decoupled.*

   Decoupling assumes that a motion along one degree of freedom does not affect another degree of freedom. Decoupling is valid for the model that does not include ocean currents since the AUV is symmetric about its three planes, the off-

diagonal elements in the dynamic model are much smaller than their counterparts and the hydrodynamic damping coupling is negligible at low speeds. When the degrees of freedom are decoupled the Coriolis and centripetal matrix becomes negligible, since only diagonal terms matter for the decoupled model. The resulting dynamic model is

$$\underline{M}\dot{\nu} + \underline{D}(\nu)\nu + \underline{g}(\eta) = \tau \tag{3.1}.$$

3.2 Parameter Estimation, a System Identification Approach

To validate the dynamic model of the AUV, the mass and damping parameters used in the dynamic model need to be estimated. There are different methods available to estimate these parameters, for instance system identification or nonlinear optimization methods. The main problem with these methods is overparametrisation [6]. A system identification approach explained in [17], [45] and [66] can be used to identify the parameters of the dynamic model. Decoupling between the degrees of freedom is used to treat every degree of freedom separately. As already explained in Section 3.1, only the parameters for the *surge, heave* and *yaw* degrees of freedom need to be estimated, since the other degrees of freedom are neglected.

The dynamic model defined in (2.8) is, with respect of the assumptions made in section 3.1, rewritten into

$$m_{\dot{x}}\ddot{x} + d_{\dot{x}}\dot{x} + d_{\dot{x}|\dot{x}|}\dot{x}|\dot{x}| + g_{\dot{x}} = \tau_{\dot{x}} \tag{3.2}.$$

Note that the dynamic model without ocean currents is used to describe the equation of motion for only one degree of freedom, where $m_{\dot{x}}$ represents the mass and inertia relative to the considered degree of freedom, $d_{\dot{x}}$ and $d_{\dot{x}|\dot{x}|}$ the linear and quadratic damping respectively, $g_{\dot{x}}$ the gravitation and buoyancy, $\tau_{\dot{x}}$ the input force/torque and $\dot{x}$ the velocity component, mind that only one specific degree of freedom is represented by (3.2) and its parameters. Note that $g_{\dot{x}}$ the gravitation and buoyancy parameter is zero for the *surge* and *yaw* degrees of freedom.

To determine the behavior of the AUV with the use of (3.2) all parameters in the equation need to be known. The input force/torque $\tau_{\dot{x}}$ is assumed to be known and can be calculated directly from duty cycle/voltage measurements, which is further explained in Appendix D.1. *A priori* information is used to calculate the gravitation and buoyancy

parameter $g_{\dot{x}}$, which consist of the parameters: m the total 'dry' mass of the AUV; ρ the fluid density; ∇ the volume of fluid displaced by the AUV; l_1 the distance between the center of gravitation and the horizontal trolling motor; x_b, y_b and z_b the location of the center of buoyancy; x_g, y_g and z_g the location of the center of gravity. All these parameters can easily be measured or determined by a CAD program and are given in Table 3.1. The remaining parameters of (3.2), i.e. the inertia and drag parameters $m_{\dot{x}}$, $d_{\dot{x}}$ and $d_{\dot{x}|\dot{x}|}$, are unknown parameters, which can be obtained from a static and dynamic experiment. A static experiment to determine the damping terms, where the acceleration is zero, and, a dynamic experiment to determine the mass terms, with the use of constant acceleration. A least squares technique is used to estimate the unknown parameters from the experimental data which is retrained from the static and dynamic experiment. The static and dynamic experiment are discussed in Appendix D.2 and D.3, respectively, and the least squares technique is explained in Appendix E. During the experiments the AUV will be remotely controlled with specially made software, which is explained in Appendix F.

Parameter	Value
m	161 kg
ρ	998 kg/m3
∇	151 L
l_1	400 mm
x_b	0 mm
y_b	0 mm
z_b	100 mm
x_g	0 mm
y_g	0 mm
z_g	0 mm

Table 3.1: *a priori* information needed to calculate the gravitation and buoyancy term.

Three different wet tests were performed in order to obtain the unknown parameters; none of the tests were successful due to failure of the Inertial Measurement Unit (IMU). Information about the IMU can be found in Appendix B.2. After the wet tests the following could be concluded about the IMU sensor:

1. The magnetometer of the IMU is disrupted by the magnetic field created by the other electronic components. Instead of measuring the earths magnetic field as reference frame the IMU started measuring the magnetic field of the electronic equipment as reference frame, which led to an inaccurate orientation matrix. Relocating the IMU within the hull of the AUV did not solve this problem.
2. The accelerometers within the IMU are not accurate enough to determine the velocity of the AUV. The noise level is too high and the bias stability is to low for measuring the velocity and position of the AUV correctly. Note that the errors in the acceleration measurement are integrated into progressively larger errors in velocity.

Due to the IMU failure the system identification approach with the use of a static and dynamic experiment can not be completed successfully, since the velocity of the AUV is unknown.

3.3 Parameter Selection

The unknown parameters, i.e. the mass and damping parameters, could not be estimated because of the IMU failure; therefore software programs are used instead. The program "ANSYS" is used to determine the drag coefficients and the program "Solid Works" is used to determine the mass and inertia parameters. The data from the program is obtained by the team of bachelor students of the University of Canterbury. The team determined the drag force of the AUV in both directions for the *surge* and *heave* degrees of freedom for a water velocity of 0, 0.2, 0.4 and 0.6 [m/s], the results are given in Table 3.2 [94].

Velocity $[m/s]$	**Drag Force** $[N]$			
	Positive Surge Forward	*Negative Surge* Backward	*Positive Heave* Down	*Negative Heave* Up
0.00	0.00	0.00	0.00	0.00
0.20	3.30	3.80	11.5	7.60
0.40	13.1	14.7	45.2	30.4
0.60	29.3	33.0	96.2	67.7

Table 3.2: Drag force results from ANSYS for the *surge* and *heave* degrees of freedom at different velocities.

The drag force results obtained by the team of bachelor students are analyzed by the author. First a quadratic fit of the data is made with the program Matlab, which estimates the unknown terms of the drag force equation

$$F_d = p_1 v^2 + p_2 v + p_3 \qquad (3.3),$$

where F_d denotes the drag force, v the velocity, p_1 the quadratic drag term, p_2 the linear drag term and p_3 the equation offset for basic fitting. The parameters are found by the basic fitting option of Matlab and are given in Table 3.3. The data points obtained and the quadratic fitting are shown in Figure 3.4. Note that the quadratic fitting goes through all data points because the data points were calculated with a quadratic solver in ANSYS. Later on the obtained drag terms will be compared with other AUV's to see if the analysis with ANSYS made sense.

Quadratic Fit Parameter	*Positive Surge* Forward	*Negative Surge* Backward	*Positive Heave* Down	*Negative Heave* Up
p_1	80.625	90.625	246.88	185.63
p_2	0.475	0.575	13.025	1.575
p_3	-0.005	0.015	-0.245	-0.035

Table 3.3: Quadratic fitting parameters, for drag force data fitting in *surge* and *heave* degrees of freedom.

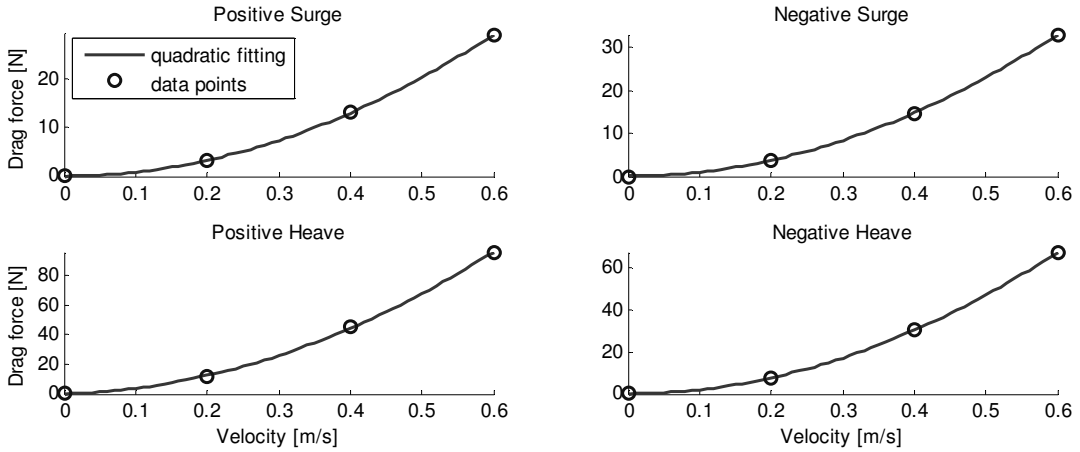

Figure 3.4: Quadratic fitting of the obtained drag force data, velocity versus drag force, for both directions of the *surge* and *heave* degrees of freedom.

The mass and inertia parameters are obtained with the program Solid Works. The complete AUV is built in Solid Works by the team of bachelor students and they were

able to obtain the mass and inertia parameters of the vehicle, which are shown in Table 3.4.

Parameters	$m\ [kg]$	$I_{xx}\ [kgm^2]$	$I_{yy}\ [kgm^2]$	$I_{zz}\ [kgm^2]$
Value	160	13.4	15.7	8.8

Table 3.4: The mass and inertia parameter obtained with the program Solid Works.

The obtained mass/inertia and drag parameters given in Table 3.3 and Table 3.4, respectively, are compared with the parameters of two other similar shaped/looking UUV's in Table 3.5. The UUV's compared with, are the "Kambara" of the University of Australia [16] and the "Romeo" ROV of CNR-IAN [17], which are both hovering underwater vehicles.

Parameters	**AUV**	**Kambara**	**Romeo**
$m\ [kg]$	160	175	675
$I_{xx}\ [kgm^2]$	13.4	14	N.A.
$I_{yy}\ [kgm^2]$	15.7	13	N.A.
$I_{zz}\ [kgm^2]$	8.98	16	88
$X_u\ [Ns/m]$	0.525 ± 0.5	120	50 ± 8
$Y_v\ [Ns/m]$	N.A.	90	150 ± 20
$Z_w\ [Ns/m]$	7.25 ± 5.5	150	25 ± 14
$N_r\ [Ns/m]$	N.A.	18	34 ± 2
$X_{u\|u\|}\ [Ns^2/m^2]$	85.625 ± 5	90	322 ± 26
$Y_{v\|v\|}\ [Ns^2/m^2]$	N.A.	90	363 ± 101
$Z_{w\|w\|}\ [Ns^2/m^2]$	215 ± 30	120	411 ± 24
$N_{r\|r\|}\ [Ns^2/m^2]$	N.A.	15	0

Table 3.5: Comparison between the mass/inertia and damping parameter with Kambara and Romeo.

Comparing the results one sees that the mass/inertia and quadratic drag parameters are obtained in a right order, however a large difference exists between the linear drag parameters. Due to the difference in the linear drag parameters and the non-available drag parameters for the *sway* and *yaw* degrees of freedom one will select

mass/inertia and drag parameters which are in the right order and similar to the parameters of other underwater vehicles. However, this will lead to estimated parameters which are not close to the exact parameters of the AUV, the parameters will still be suitable to run the simulations made in Chapters 6 and 7. Note that these parameters can not be used to run wet tests, therefore parameters should be estimated according to Section 3.2. The selected parameters can be found in Table 3.6 and are based on the results of the software programs and on the parameters of the Kambara UUV, since this underwater vehicle has most similarities in the mass/inertia parameters and shape.

Parameters	**AUV**
$m \ [kg]$	160
$I_{xx} \ [kgm^2]$	15
$I_{yy} \ [kgm^2]$	15
$I_{zz} \ [kgm^2]$	15
$X_u \ [Ns/m]$	60
$Y_v \ [Ns/m]$	60
$Z_w \ [Ns/m]$	100
$N_r \ [Ns/m]$	20
$X_{u\|u\|} \ [Ns^2/m^2]$	90
$Y_{v\|v\|} \ [Ns^2/m^2]$	90
$Z_{w\|w\|} \ [Ns^2/m^2]$	150
$N_{r\|r\|} \ [Ns^2/m^2]$	15

Table 3.6: Selected mass/inertia and damping parameter which will be used to run simulations for the AUV.

Chapter 4

Control of AUVs

The control of AUVs presents several difficulties caused by the nonlinear dynamics of the vehicle and model uncertainties. It is important to explore different controllers that have been implemented on AUVs. Therefore, problems of controlling AUVs and control techniques are discussed in Section 4.1. A feedback linearizing control technique is chosen to design control laws for control in the *surge*, *heave* and *yaw* degrees of freedom. The feedback linearizing control technique is derived and discussed in Section 4.2. In the *x-y* plane the AUV is only actuated in the *surge* and *yaw* degrees of freedom caused by the trolling motor configuration. An under-actuated control problem arises since the AUV, in the *x-y* plane, is able to move in three directions (x, y, ψ). To steer the AUV with a smooth motion from an initial position *A* to a different position *B*, in the *x-y* plane, a path planning model is derived in Section 4.3.

4.1 Control Problems

Complex nonlinear forces acting upon an underwater vehicle, especially with open frame AUVs, make the control more tricky, which has been explained in Chapters 2 and 3. Several complex nonlinear forces are, for example, hydrodynamic drag, lift forces, Coriolis and centripetal forces, gravity and buoyancy forces, thruster forces, and environmental disturbances [17]. These forces are not added to the equation of motion in the complex form: some are simplified and others are left out. Assumptions and simplifications made to the dynamics have been explained in Chapter 3. Control gets

even more complicated due to the difficulties in observing and measuring the AUV's response in the water [18].

Many universities and companies have interest in developing control techniques for underwater vehicles with the aim to improve the dynamic response of underwater vehicles. A great amount of research work on the design and implementation of different controllers is already available. A few control techniques used for underwater vehicles control are explained in Appendix H, the explanation includes PID Control, Linear Quadratic Gaussian Control, Fuzzy Logic Control, Adaptive Control and Sliding Mode Control.

4.2 Feedback Linearization

A common approach used in controlling nonlinear systems is feedback linearization. The basic idea of the approach is to transform, if possible, the nonlinear system into a linear system via a change of variables and/or a suitable control input and then use a linear control technique to stabilize the linear system. The feedback linearization approach requires full state measurement and according to J.E.Slotine and W.Li [73] is used to solve a number of practical nonlinear control problems. However, it should be noted that in combination with parameter uncertainty and/or disturbances does not always guarantee a robust system.

Control of the one degree of freedom dynamical model via feedback linearization is derived in subsection 4.2.1. The nonlinear model is transformed into a linear model which is stabilized with a PD controller. Afterwards in subsection 4.2.2 the control law is extended to a tracking controller and the PD controller is changed into a PID controller for better robustness to account for parameter perturbations. The tracking controller is implemented in Matlab Simulink and simulations are run in section 4.2.3.

4.2.1 Derivation of the Feedback Linearization

The one degree of freedom dynamical model

$$m_{\dot{x}}\ddot{x} = \tau_{\dot{x}} - d_{\dot{x}}\dot{x} - d_{\dot{x}|\dot{x}|}\dot{x}|\dot{x}| - g_{\dot{x}} \tag{4.1}$$

derived in Chapter 3 can be rewritten as

$$\ddot{x} = -a\dot{x} - b\dot{x}|\dot{x}| - c + d\tau_{\dot{x}} \tag{4.2},$$

where $a = \frac{d_{\dot{x}}}{m_{\dot{x}}}$, $b = \frac{d_{\dot{x}|\dot{x}|}}{m_{\dot{x}}}$, $c = \frac{g_{\dot{x}}}{m_{\dot{x}}}$, $d = \frac{1}{m_{\dot{x}}}$, x is the position and $\tau_{\dot{x}}$ is the force/torque or control input. Under steady state condition where $\ddot{x} = 0$ and $\dot{x} = 0$ the dynamic model (4.2) changes into

$$0 = -c + d\tau_{\dot{x},ss} \tag{4.3},$$

where the force/torque has a steady state component, $\tau_{\dot{x},ss}$, which satisfies

$$\tau_{\dot{x},ss} = \frac{c}{d} = g_{\dot{x}} \tag{4.4}.$$

To control the AUV the position output of the AUV is measured, turning the system into a single input single output (SISO) system, given in state space form by

$$\dot{x} = f(x) + g(x)u \tag{4.5.a},$$

$$y = h(x) \tag{4.5.b},$$

where u is the control variable denoted by $u = \tau_{\dot{x}} - \tau_{\dot{x},ss}$. The state variables are now defined as $x_1 = x$ and $x_2 = \dot{x}$. The one degree of freedom dynamic model (4.2) is now rewritten into the state equation

$$\dot{x}_1 = x_2 \tag{4.6.a},$$

$$\dot{x}_2 = -ax_2 - bx_2|x_2| + du \tag{4.6.b},$$

$$y = x_1 \tag{4.6.c}.$$

Inspection of the state equation shows that if the state feedback control law u is defined as

$$u = \frac{1}{d}\left(ax_2 + bx_2|x_2| + v\right) \tag{4.7}$$

the nonlinearity of the system will be canceled (note that exact knowledge of the parameters a and b is required) and after substitution will form the system given by

$$\dot{x}_1 = x_2 \tag{4.8.a},$$

$$\dot{x}_2 = v \tag{4.8.b}.$$

Note that exact knowledge of the parameter a and b is required to cancel the nonlinearity of the system.

This choice of *u* can be confirmed by the input-output linearization of the state equation (4.6), which is given in Appendix G.1. After the implementation of the state feedback control law the state equation is linearized to

$$\dot{x} = Ax + Bv \tag{4.9},$$

where $A = \begin{bmatrix} 0 & 1 \\ 0 & 0 \end{bmatrix}$ and $B = \begin{bmatrix} 0 \\ 1 \end{bmatrix}$. Now the linear state feedback control $v = -Kx$ is introduced to the nonlinear system, where $K = \begin{bmatrix} k_1 & k_2 \end{bmatrix}$, which changes the linear state equation into

$$\dot{x} = (A - BK)x \tag{4.10}.$$

The linear state feedback control $v = -Kx$ has now to be designed such that $(A - BK)$ is Hurwitz in order to have an asymptotically stable system, which means that all the eigenvalues have to satisfy $\mathrm{Re}(\lambda_i) < 0$. $(A - BK)$ is Hurwitz for $k_1 > 0$ and $k_2 > 0$, which is verified in Appendix G.4.

The overall feedback control law $\tau_{\dot{x}}$, can now be derived with the use of the linear state feedback control *v*, the state feedback control law *u* and the steady state component $\tau_{\dot{x},ss}$, which results in

$$\tau_{\dot{x}} = u + \tau_{\dot{x},ss} = \frac{1}{d}\left(ax_2 + bx_2|x_2| + c - k_1x_1 - k_2x_2\right) \tag{4.11},$$

where $u = \frac{1}{d}\left(ax_2 + bx_2|x_2| + v\right)$, $v = -k_1x_1 - k_2x_2$ and $\tau_{\dot{x},ss} = \frac{c}{d}$. The overall state feedback control law $\tau_{\dot{x}}$, is written down in the original coordinates in

$$\tau_{\dot{x}} = d_{\dot{x}}\dot{x} + d_{\dot{x}|\dot{x}|}\dot{x}|\dot{x}| + g_{\dot{x}} - m_{\dot{x}}k_1x - m_{\dot{x}}k_2\dot{x} \tag{4.12}$$

and changes the systems dynamics into

$$\ddot{x} + k_2\dot{x} + k_1x = 0 \tag{4.13}.$$

The overall state feedback control law is also known as computed torque control law. A thumb rule in computed torque control is to choose k_1 as k^2 and k_2 as $2k$ [73]. The system dynamics (4.13) are hereby changed into

$$\ddot{x} + 2k\dot{x} + k^2x = 0 \tag{4.14}.$$

Mind that *k* has to be larger than zero for stable closed loop dynamics.

4.2.2 Tracking

If the AUV needs to follow a certain trajectory then the control law $\tau_{\dot{x}}$ needs to be extended, so that the output *y* tracks a reference signal *r(t)*. The error between the output and the reference signal is called the tracking error *e* and is defined together with its derivatives by

$$e = x - r \quad (4.15.a),$$
$$\dot{e} = \dot{x} - \dot{r} \quad (4.15.b),$$
$$\ddot{e} = \ddot{x} - \ddot{r} \quad (4.15.c).$$

The tracking control law can be derived by taking $e_1 = x_1 - r$ and $e_2 = x_2 - \dot{r}$, which gives the state equation

$$\dot{e}_1 = e_2 \quad (4.16.a),$$
$$\dot{e}_2 = -ax_2 - bx_2|x_2| + du - \ddot{r} \quad (4.16.b).$$

It is clear the state feedback control law *u* will now have to take the form

$$u = \frac{1}{d}\left(ax_2 + bx_2|x_2| + \ddot{r} - k_1 e_1 - k_2 e_2\right) \quad (4.17),$$

which results in the overall state feedback control law

$$\tau_{\dot{x}} = \frac{1}{d}\left(ax_2 + bx_2|x_2| + c + \ddot{r} - k_1 e_1 - k_2 e_2\right) \quad (4.18).$$

The tracking control law which is the overall state feedback control law in original coordinates is given by

$$\tau_{\dot{x}} = d_{\dot{x}}\dot{x} + d_{\dot{x}|\dot{x}|}\dot{x}|\dot{x}| + g_{\dot{x}} + m_{\dot{x}}\ddot{r} - m_{\dot{x}}k_1 e - m_{\dot{x}}k_2\dot{e} \quad (4.19),$$

with $k_1 = k^2$ and $k_2 = 2k$. Note that this tracking control law requires the reference signals $r, \dot{r}, \ddot{r}$ to be available on-line at any time. When this is not possible during experiments, due to a shortcoming of measurement equipment, the control law should be extended with an observer in order to estimate unmeasured states. The system dynamics are now reduces to the error dynamics (the tracking error of the closed loop system)

$$\ddot{e} + 2k\dot{e} + k^2 e = 0 \quad (4.20).$$

Note that the error dynamics are formed by the substitution of the error equation (4.15.c) and the tracking control law (4.19) into the system dynamics (4.1). If *k* is chosen positive

the error dynamics (4.20) will be stable and the error will go to zero, assuming that the dynamic model is accurate. However the model parameters of the AUV are not known exactly and the system dynamics are simplified, which means that the system can still behave unacceptable.

An integral term is added to the linear feedback controller *v* in order to cope with parameter perturbations. A parameter perturbation is caused, for example, by a reconfiguration on the AUV, for instance a change of mass. Integrating the error between the output and the reference signal will compensate the steady state error created by the perturbed parameters.

An integral gain k_i determines the magnitude of contribution of the integral term to the tracking controller $\tau_{\dot{x}}$. The integral term is described as $k_i \int e$ and is added to the linear feedback controller *v*, which can be seen in

$$v = -k_1 e - k_2 \dot{e} - k_i \int e \tag{4.21}$$

Note that this linear feedback controller is also known as a PID controller, where k_1 forms the proportional gain, k_i the integral gain and k_2 the derivative gain. More information about PID control can be found in Appendix H.1. The tracking control law in combination with the PID controller is now given in

$$\tau_{\dot{x}} = d_{\dot{x}} \dot{x} + d_{\dot{x}|\dot{x}|} \dot{x} |\dot{x}| + g_{\dot{x}} + m_{\dot{x}} \ddot{r} - m_{\dot{x}} k_1 e - m_{\dot{x}} k_2 \dot{e} - m_{\dot{x}} k_i \int e \tag{4.22}$$

and the error dynamics can now be described by

$$\ddot{e} + 2k\dot{e} + k^2 e + k_i \int e = 0 \tag{4.23}.$$

4.2.3 Simulation Results

Simulations will be run in Matlab Simulink to test the tracking control law defined in (4.22). To be able to run a simulation a reference and plant model are made. The reference model defines a reference trajectory for the AUV to follow. Note that the reference signals r, $\dot{r}$ and $\ddot{r}$ need to be available online. The plant model will replace the real AUV and represent the AUV dynamics. A more extensive explanation of the implementation of the tracking control laws into Matlab Simulink is given in Appendix K.

A cosine function will define the reference signal for acceleration, with a frequency of 0.3 Hz and a maximum amplitude of 0.1 m/s^2. The cosine function will be integrated twice to obtain the reference signals for velocity and position. Table 4.1 shows the maximum r, $\dot{r}$ and $\ddot{r}$ values reached; the AUV was able to reach these values during wet tests.

Max($\ddot{r}$)	0.10 m/s^2
Max($\dot{r}$)	0.33 m/s
Max(r)	2.22 m
Function	$\ddot{r} = 0.1\cos(0.6\pi t)$

Table 4.1: Reference model information.

In reality the current position and velocity of the AUV (or plant) will be measured with a certain level of noise, therefore white noise is added to the determined position and velocity of the plant. The noise amplitude of the position will be 0.01 m and 0.02 m/s for the velocity.

A rate limiter is added to the thrust output, since in reality the trolling motors are not able to immediately switch thrust, from for instance a maximum negative thrust to a maximum positive thrust, since the propellers have inertia. The rate limiter will limit the rate of change of thrust to maximum 100 N in one second per trolling motor, for the *surge* degree of freedom this will mean a maximum change of 200N since the AUV has two trolling motors operating in this degree of freedom.

Saturation is added to the thrust output, since in reality the trolling motors can only get a certain amount of power (i.e. thrust). One trolling motor is able to deliver a maximum thrust of 50 N, and the assumption is made that it will be able to provide this power in both directions. For the *surge* degree of freedom this means that the saturation is set to 100 N, since two trolling motors are operating in this degree of freedom. According to wet tests and simulation results the amount of thrust is sufficient to follow the reference trajectory in a swimming pool.

Simulations are only run for the controller in the *surge* degree of freedom, since for the controllers in the other degrees of freedom similar procedures hold. From different simulations could be concluded, that the tracking controller defined in (4.22) performs well under parameter perturbation and measurement noise. In the simulation results shown below two different control options are compared. For control option 1 a PD controller and for option 2 a PID controller is chosen for the linear controller within the tracking controller. The tracking controllers are tested under a perturbed parameter situation where the mass of the controller is half the mass of the plant, which can be seen

in Table 4.2. Further noise is added to the position and velocity measurement signals. The noise level can be seen in Table 4.3. The controller gains which are obtained by trial and error are given in Table 4.4. For both control options the AUV is able to track the reference signal. The trajectory is visualized in Figure 4.1.a and the position and velocity errors are shown in Figure 4.2. If one looks at the position error signal of the PD controller, option 1, see Figure 4.2.a, then a sinusoidal error can be seen, this indicates that control can be improved. After implementing an integral gain, which will give the PID controller of option 2, the position error is decreased to 0.01 *m*. Note that this position error has the same value as the implemented measurement noise on the position. Note that even this system can be improved by for instance adding a Kalman filter to filter the noise.

Parameters	**Controller**	**Plant**
$m_{\dot{x}}$	80	160
$d_{\dot{x}}$	60	60
$d_{\dot{x}\lvert\dot{x}\rvert}$	90	90
$g_{\dot{x}}$	0	0

Table 4.2: Controller and plant parameters.

	Option 1	**Option 2**
Parameters		
k_p	9	9
k_i	0	10
k_d	6	6
Noise		
Position [m]	0.0093	0.0093
Velocity [m/s]	0.0186	0.0186

Table 4.3: PID gain terms for options 1 and 2.

Maximum tracking error	**Option 1**	**Option 2**
Position	0.0185	0.0118
Velocity	0.0249	0.0276

Table 4.4: Maximum tracking error for options 1 and 2.

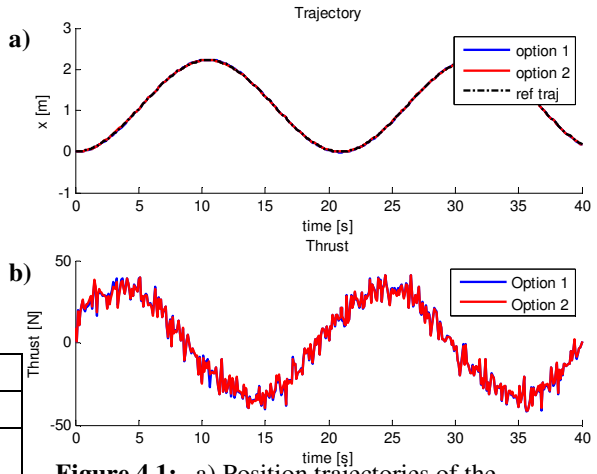

Figure 4.1: a) Position trajectories of the reference, option 1 and option 2.
b) Thrust input of options 1 and 2.

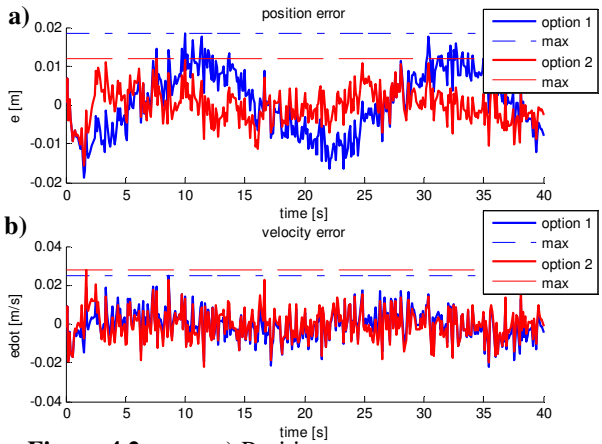

Figure 4.2: a) Position error.
b) Velocity error.

Next to the simulations described above other different simulations are run these are described in Appendix I. The subject of these simulations and there appendices are listed below:

- The effect of a high gain PD controller for the linear controller within the tracking controller without noise and perturbation is described in Appendix I.1.
- The effect of perturbed parameters on low gain P control and high gain PD control for the linear controller within the tracking controller is described in Appendix I.2.
- The effect of the implementation of noise on low gain P control and high gain PD control for the linear controller within the tracking controller is described in Appendix I.3.
- The effect of the thrust rate limiter on high gain PD control for the linear controller within the tracking controller is described in Appendix I.4.
- The effect of extreme parameter perturbation on the tracking controller which had a PID controller for the linear controller within the tracking controller is described in Appendix I.5.

The tracking controller defined in (4.22) with the PID gains given in Table 4.3 is able to control the AUV in one degree of freedom and will track a position reference trajectory with a maximum position error of 0.012 *m*. The tracking controller is optimized to perform in the *surge* degree of freedom but a similar method can be applied for the *heave* and *yaw* degrees of freedom. After doing so the AUV will be able to move controlled in these degrees of freedom, but the AUV is still not able to move from an initial position *A* to a different position *B*. Therefore path planning equations are needed, to define reference signals for the *surge*, *heave* and *yaw* degrees of freedom.

4.3 Path Planning

With the controllers for the *surge*, *heave* and *yaw* degrees of freedom working, it is time for the AUV to move from an initial position, named set-point *A*, to another position, named set-point *B*, which has a different *x*, *y*, *z* and/or *yaw* position in the earth fixed frame. The AUV is only able to move in the *surge*, *heave* and *yaw* degrees of freedom, since only these degrees of freedom are controlled. An under-actuated problem arises in the *x-y* plane because the AUV is unable to move in the *sway* direction. Take for instance the relative positions *A* and *B* given in Figure 4.16. Note that set-point *B* has a

different *x*, *y* and *yaw* position compared with set-point *A*. With only *surge* and *yaw* controlled, there are two options to go from *A* to *B*:

Option 1: to first change the *yaw* angle, so the AUV is pointing towards set-point *B*, then moving in *surge* until the *x* and *y* position of set-point *B* are reached and afterwards change the *yaw* angle again so the *yaw* position of set-point *B* is reached.

Option 2: a smooth curved motion, where *surge* and *yaw* are controlled at the same time. This smooth motion is visualized in Figure 4.16 by the dashed arrow.

One prefers the second option since this option will save time and has a more "delicate" way of moving. This section will first, in section 4.3.1, explain a path planning method which will define the desired reference trajectory for the *surge* and *yaw* degrees of freedom to accomplish a smooth motion. Finally in section 4.3.2 simulations are performed with the path planning equations, to see its performance.

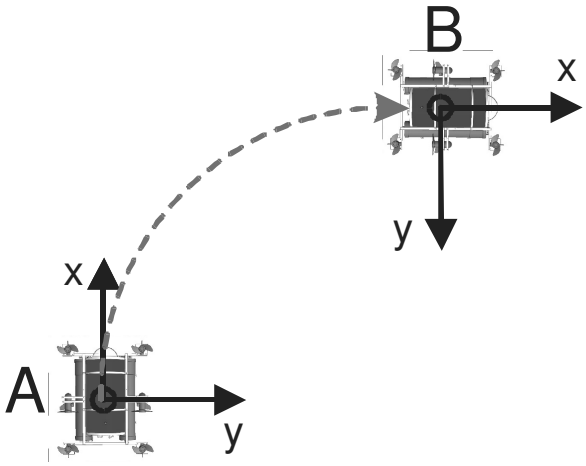

Figure 4.16: Visualization of the initial position, set-point A, and the desired position, set-point B.

4.3.1 A Path Planning Method

A reference model is needed to provide reference signals for the velocity in the *surge* and *yaw* degrees of freedom, as a function of time to go from set-point *A* to set-point *B* in a smooth curved motion. In the *x*-*y* plane and under the assumption that *sway* motion is neglected, the following kinematic equations hold:

$$\dot{x} = u\cos(\psi) \tag{4.24.a}$$

$$\dot{y} = u\sin(\psi) \tag{4.24.b}$$

$$\dot{\psi} = r \tag{4.24.c}$$

Inspired by M.Aicardi, G.Casalino, et.al. [78] the kinematic equations are rewritten into polar coordinates given by

$$\dot{e} = -u\cos(\alpha) \qquad (4.25.a),$$

$$\dot{\alpha} = -r + \frac{u}{e}\sin(\alpha) \qquad (4.25.b),$$

$$\dot{\beta} = \frac{u}{e}\sin(\alpha) \qquad (4.25.c),$$

where e describes the error distance between the centers of gravity of the AUV in set-point A and B, β describes the current orientation of the AUV with respect to the body fixed frame of a virtual AUV in set-point B and α describes the angle between the principal axis of the AUV and the distance error vector e. A visual representation for better understanding of these parameters is given in Figure 4.17 where e describes the error distance vector, and, α and β describe the alignment error vector. Note that the kinematic equations given by the polar coordinates are only valid for $e > 0$ and that the kinematic equations are only valid for non zero values since α and β are undefined when $e = 0$. The system and its kinematic equations given in (4.25) will, from now on, simply be named "the P-system".

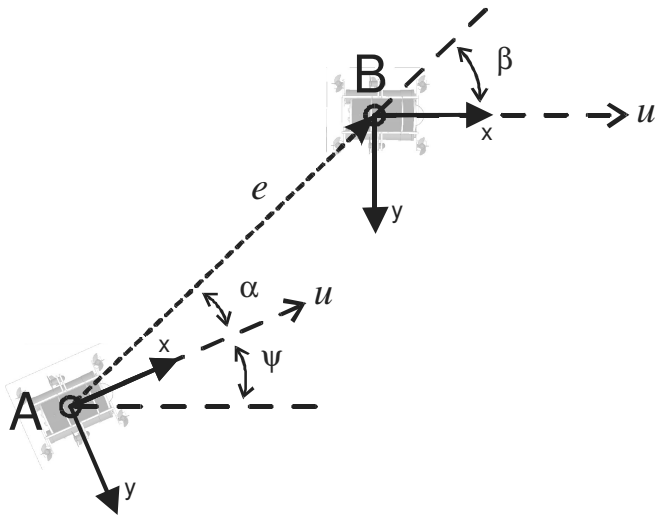

Figure 4.17: Visualization of the polar coordinate parameters e, α and β.

To fulfill option 2 defined above suitable chosen control laws for u and r need to guide the P-system asymptotically towards the limiting point $[e, \alpha, \beta] = [0, 0, 0]$, without

reaching the condition $e = 0$. Lyapunov's stability theorem is used to derive control laws for u and r which asymptotically stabilize the system.

Lyapunov theory suggests that when the energy of a system keeps decreasing it will finally arrive at a stable equilibrium point, or in other words, if the derivative of the energy function of a certain system remains smaller than zero at any time, the system will be asymptotically stable. Lyapunov found out that this also works for other functions rather than energy functions, which led to Lyapunov's stability theorem [74], see Appendix G.5.

A proper Lyapunov candidate function for the P-system is given by

$$V = 0.5\left(e^2 + \alpha^2 + \beta^2\right) \tag{4.26},$$

which is in positive definite quadratic form, lower bounded and satisfies $V(0) = 0$ and $V(x) > 0$ in $D - \{0\}$. Note that the Lyapunov candidate function can be separated into $V_1 = 0.5e^2$ and $V_2 = 0.5\left(\alpha^2 + \beta^2\right)$, which represent the Lyapunov candidate function for the error distance vector and the alignment vector, respectively.

The derivative of the Lyapunov candidate function is given by

$$\dot{V} = \dot{V}_1 + \dot{V}_2 = e\dot{e} + \alpha\dot{\alpha} + \beta\dot{\beta} \tag{4.28},$$

where the derivatives of its separates are

$$\dot{V}_1 = -eu\cos(\alpha) \tag{4.29},$$

$$\dot{V}_2 = \alpha\left(-r + \frac{u}{e}\sin(\alpha)\right) + \beta\frac{u}{e}\sin(\alpha) \tag{4.30}.$$

One needs to design a control law for u and r in such a way that the derivative of the Lyapunov's candidate function, $\dot{V}$, is always smaller than zero (see Appendix G.5). Note that in case of $e = 0$ the Lyapunov candidate function is not well defined. However, when one defines the control law u as

$$u = k_1 e\cos(\alpha) \tag{4.31},$$

with $k_1 > 0$ than $\dot{V}_1$ becomes negative semi definite. Since V is lower bounded by zero and is non increasing in time ($\dot{V}_1 \leq 0$) V_1 will asymptotically converge towards a non negative finite limit. After implementation of the control law u the derivative of the Lyapunov candidate functions $\dot{V}_1$ and $\dot{V}_2$ become

$$\dot{V}_1 = -eu\cos(\alpha) = -k_1 e^2 \cos^2(\alpha) \le 0, \qquad k_1 > 0 \tag{4.32},$$

and

$$\dot{V}_2 = \alpha\left(-r + k_1 \cos(\alpha)\sin(\alpha)\right) + \beta k_1 \cos(\alpha)\sin(\alpha) \tag{4.32},$$

respectively.

After the implementation of the control law r given by

$$r = k_1 \cos(\alpha)\sin(\alpha) + k_1 \frac{\beta}{\alpha}\cos(\alpha)\sin(\alpha) + k_2\alpha \tag{4.33},$$

with $k_2 > 0$, $\dot{V}_2$ becomes negative semi definite as can be seen in

$$\dot{V}_2 = -k_2\alpha^2 \le 0, \qquad k_2 > 0 \tag{4.34}$$

The summation of $\dot{V}_1$ and $\dot{V}_2$ gives the derivative of the Lyapunov's candidate function

$$\dot{V} = -k_1 e^2 \cos^2(\alpha) - k_2\alpha^2 \le 0, \qquad k_1 > 0, \quad k_2 > 0 \tag{4.35},$$

which is in a negative semi definite form. According to Barbalat's lemma $\dot{V}$ converges to zero for increasing time [73], since V is lower bounded and $\dot{V}$ is negative semi-definite and uniformly continuous in time. Barbalat's lemma is given in Appendix G.6 and for the application of Barbalat's lemma a "Lyapunov-Like" method is used, which is given in Appendix G.7. Since $\dot{V}$ converges to zero for increasing time and $\dot{V}$ can only become zero when e and α are zero the P-system will have to converge to the line $[e, \alpha, \beta] = [0, 0, \beta]$. The substitution of $(e, \alpha) = (0, 0)$ into the kinematic equations, with the implementation of the control laws for u and r, given by

$$\dot{e} = k_1 e \cos^2(\alpha) \tag{4.36.a}$$

$$\dot{\alpha} = -k_1 \frac{\beta}{\alpha}\cos(\alpha)\sin(\alpha) - k_2\alpha \tag{4.36.b}$$

$$\dot{\beta} = k_1 \cos(\alpha)\sin(\alpha) \tag{4.36.c},$$

indicates that $\dot{e}$ and $\dot{\beta}$ also converge to zero. The convergence of $\dot{\beta}$ to zero implies that β goes to a finite limit, named $\bar{\beta}$. Since β goes to a finite limit $\dot{\alpha}$ will converge to the finite limit $-k_1\bar{\beta}$, note that $\lim_{\alpha\to 0} \frac{\cos(\alpha)\sin(\alpha)}{\alpha} = 1$. According to Barbalat's lemma, see Appendix G.6, $\dot{\alpha}$ converges to zero for increasing time since $\dot{\alpha}$ is a uniformly continuous in time and α has a finite limit for increasing time. The convergence of $\dot{\alpha}$ to

zero implies that $\bar{\beta}$ will have to converge to zero, since $\dot{\alpha}$ can only be zero when all its parameters are zero. Since $\bar{\beta}$ will also converge to zero it is proven that the P-system will not only converge to the line $[e,\alpha,\beta]=[0,0,\beta]$ but towards the limiting point $[e,\alpha,\beta]=[0,0,0]$.

4.3.2 Simulation Results

The kinematic equation are written in polar coordinates, so only the relative distance between set-point *A* and set-point *B* will matter. Set-point *B* will always positioned at $[e,\alpha,\beta]=[0,0,0]$, which means that the polar coordinate system will always align with the body-fixed frame of the AUV in set-point *B*. Lets take, for example, the following earth fixed coordinates for set-point *A* $[x,y,\psi]=[0,0,0]$ and for set-point *B* $[x,y,\psi]=[1,0,0]$, in polar coordinates the same distance would denote $[e,\alpha,\beta]=[1,0,0]$ for set-point *A* and $[e,\alpha,\beta]=[0,0,0]$ for set-point *B*.

To simulate the path planning model defined in subsection 4.3.1 the AUV will start from fourteen different initial positions, which means fourteen different locations for *A*. All these locations are defined in earth fixed coordinates in Table 4.20. For easy set-point *B* will always have the earth fixed coordinates $[x,y,\psi]=[0,0,0]$.

Coordinates of set-point *A*														
x	-1	-1	-1	-1	-0.5	-0.5	0	0	0.5	0.5	1	1	1	1
y	-1	-0.5	0.5	-0.001	-1	1	1	-1	1	-1	-0.001	-0.5	0.5	1
ψ	0	0	0	0	0	0	0	0	0	0	0	0	0	0

Table 4.20: the coordinates of set-point *A* denoted in the earth fixed frame.

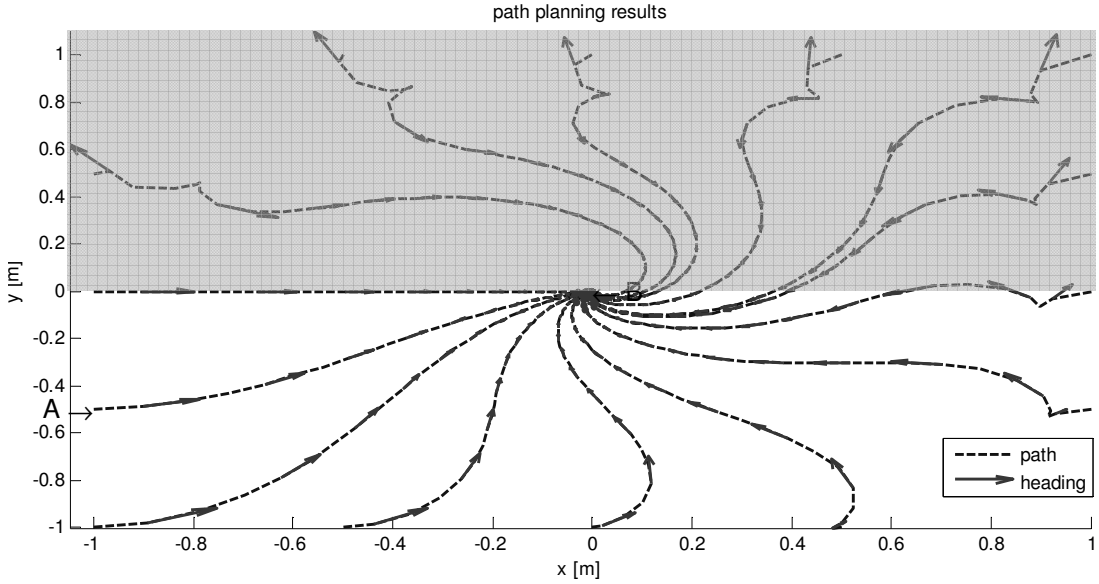

Figure 4.19: The path for the AUV defined from set-point A to set-point B at (x,y)=(0,0).

The simulation reveals fourteen different paths, which can be seen in Figure 4.19. Note that the AUV will move asymptotically towards set-point *B* and that all initial positions which are located in the earth-fixed frame (x, y, ψ) with $y < 0$ have a suitable path. However the paths with initial positions located at $y > 0$ are not suitable (depicted grey shaded in Figure 4.19). Note that a path similar shaped to a path starting from the initials position with $y < 0$ is also possible and more obvious for the other initial positions. The only difference will be the sign in the velocity in the *yaw* degree of freedom. To determine a correct path the positive sign of *y*, from initial conditions with $y > 0$, is transformed to a negative sign and the sign of the resulting velocity in the *yaw* degree of freedom is transformed into the opposite sign. The simulation now reveals fourteen smooth satisfying paths, which can be seen in Figure 4.20. Note that for paths with initial positions $(1, y, \psi)$ the velocity in the *surge* degree of freedom changes sign, which means that the AUV will first move backwards.

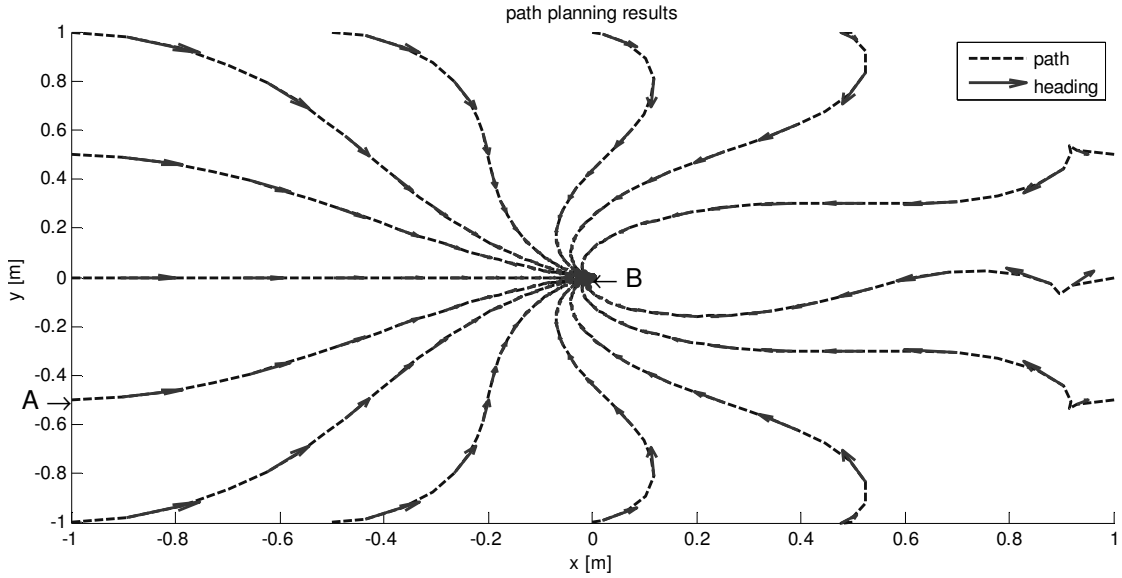

Figure 4.20: The path for the AUV defined from set-point A to set-point B at (x,y)=(0,0).

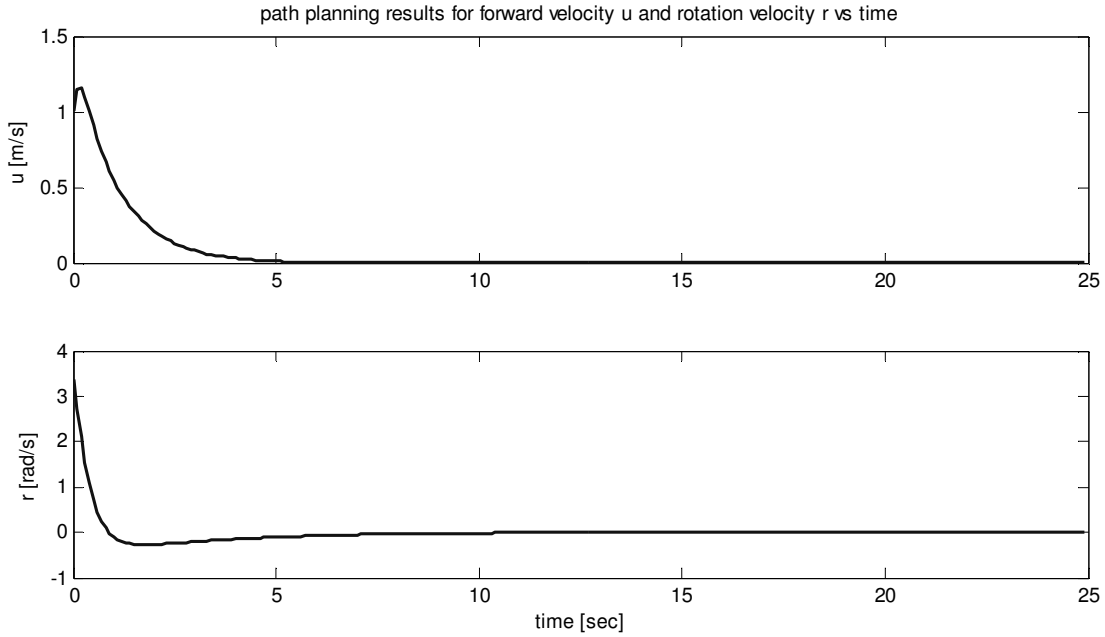

Figure 4.21: The forward velocity *u* and rotation velocity *r* of the AUV while following the path from point A at (x,y)=(-1,-1) to point B at (x,y)=(0,0).

The forward velocity *u* and rotation velocity *r* prescribed for the AUV to follow the path from set-point *A (x,y)=(-1,-1)* to set-point *B (x,y)=(0,0)* are visualized in Figure 4.21. Note that both velocity profiles approach zero in finite time and with a given accuracy one is able to conclude that the AUV will move to set-point B. However when

noise is implemented on the position measurement (i.e. the implementation of noise on the forward velocity *u*) and the AUV reaches the limiting point an overshoot will occur resulting in a $k\pi$ *[rad]* value shift of the angle α, which on its turn causes the AUV to behave "nervous" around the limiting point infinitely changing its rotation angle. This behavior can be seen in Figure 4.22 and Figure 4.23 which visualizes the predefined path of the AUV and in Figure 4.24 which shows the forward velocity *u* and rotation velocity *r* of the AUV. A solution to this problem could be to switch to a different control law in a predefined area around set-point *B*.

The paths provided by the path planning model can be executed by the control laws derived in Section 3.2.

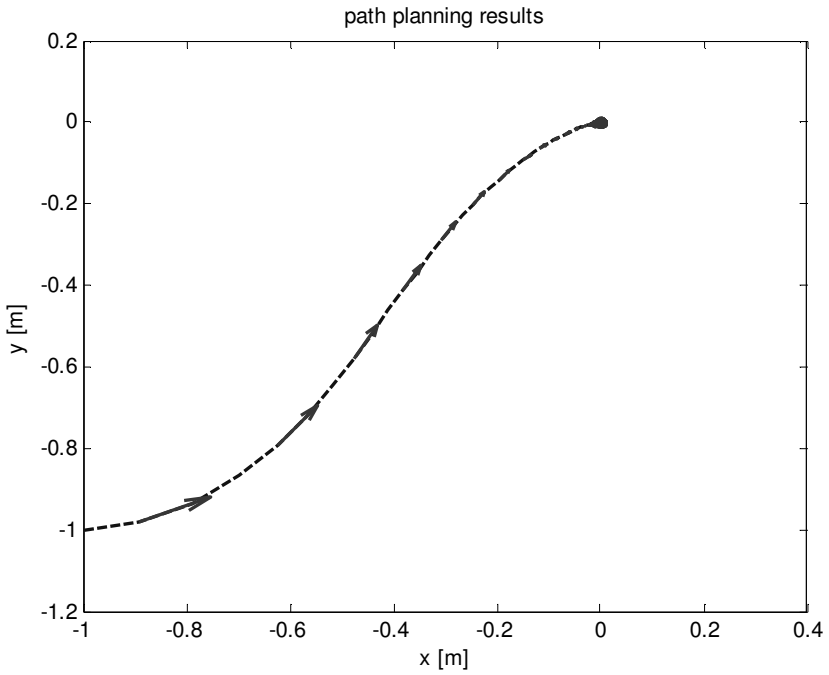

Figure 4.22: The path for the AUV defined from set-point A to set-point B in case of noise implementation.

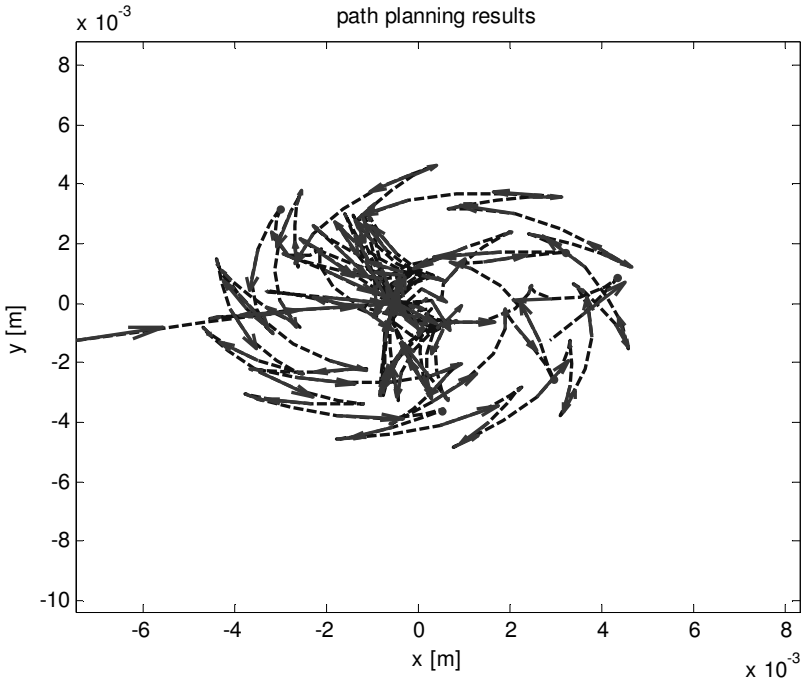

Figure 4.23: The path for the AUV defined from set-point A to set-point B in case of noise implementation.

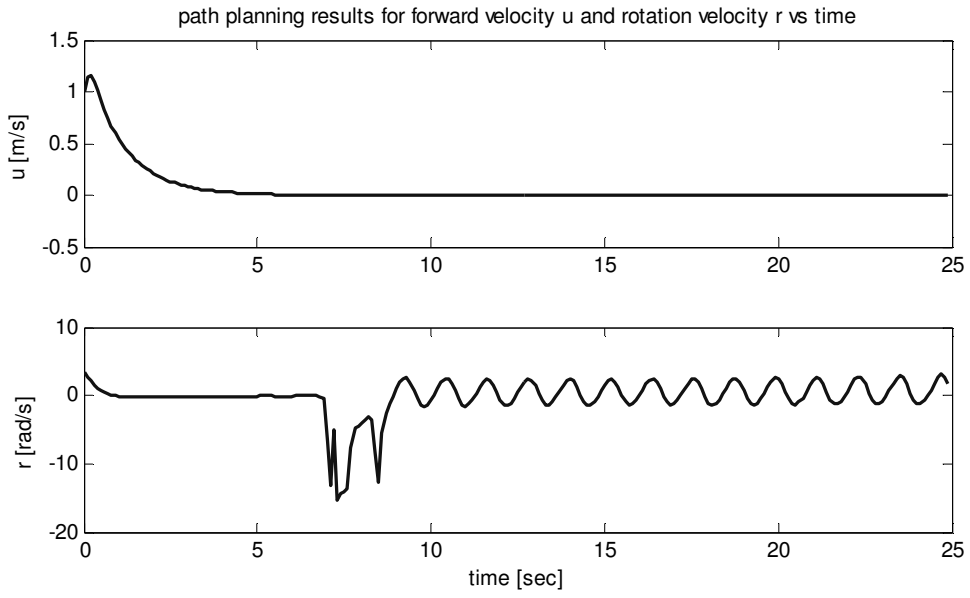

Figure 4.24: The forward velocity *u* and rotation velocity *r* of the AUV while following the path from point A at (x,y)=(-1,-1) to point B at (x,y)=(0,0) in case of noise implementation.

4.4 Summary

In the *x-y* plane the AUV is only able to move in the *surge* and *yaw* degrees of freedom due to the trolling motor configuration. An under-actuated control problem arises, since one is only able to control two degrees of freedom while the AUV is able to move in three degrees of freedom. To steer the AUV with a smooth motion from an initial position *A* to a different position *B*, in the *x-y* plane, a path planning model is derived. The path planning model describes a path from *A* to *B* with the use of polar coordinates which the AUV is able to follow controlling only the *surge* and *yaw* degrees of freedom. The assumption is made that *sway*-motion of the AUV can be neglected. Simulations with the model reveal that the path planning works correct, except for planning a straight line due to singularity reasons. This problem can be solved by introducing a switching controller which is able to switch between different path planning models.

A feedback linearizing controller extended to a tracking controller is designed in order to track a reference trajectory in one degree of freedom. The reference trajectory can be provided by the path planning model, however a separate feedback linearizing controller is needed for the *surge*, *heave* and *yaw* degrees of freedom. The feedback linearizing control technique changes the nonlinear dynamical system into a linear system through a suitable chosen control input. The linear system is stabilized with the use of PID control. In simulations the controller performed well under parameter perturbation and the implementation of noise on the feedback position and velocity signals of the plant. It should be noted that all states need to be available online to control the AUV. When during experiments full state measurement is not possible then the control law should be extended with an observer in order to estimate unmeasured states.

Chapter 5

Tracking control of an under-actuated AUV

In this chapter a state feedback control technique is proposed to control the AUV in an under-actuated situation, where motion in sway is no longer neglected. Section 5.1 will explain the control technique and section 5.2 will show simulation results.

5.1 An Under-Actuated AUV

The AUV is able to follow a predefined path in 3D space by enabling different trolling motors. The setup of the trolling motors makes it possible to control all degrees of freedom except for the *sway* direction. No trolling motors are aligned in the *sway* direction, so there is no *sway* control force. The *roll* and *pitch* degrees of freedom are stabilized by the aligning moment of buoyancy and gravity and are therefore not controlled. This means that one is able to control the *surge*, *heave* and *yaw* degrees of freedom, where an error in the *sway* direction can only be adjusted by *surge* and *yaw* control.

The control laws for the *surge* and *yaw* degrees of freedom need to control three degrees of freedom, which means that one is dealing with an under-actuated problem. Motion in *heave* is neglected in this situation, since the under-actuated problem only concerns the *surge*, *sway* and *yaw* degrees of freedom. In this section control laws for the *surge* and *yaw* degrees of freedom will be derived, these control laws are different from control laws derived in Chapter 4. The idea is to derive new control laws is such way that the controlled system is able to follow a path in the *x*-*y* plane and an error in *sway* is corrected by controlling the system in the *surge* and *yaw* direction. The assumptions made in Chapter 4 apply to this problem, only the motion in the *sway* direction and the

Coriolis and Centripetal Matrix are not neglected anymore. Note that when the AUV is making a curve and is able to move in *sway* the control laws will need to take in consideration the Coriolis and Centripetal forces will try to "push" the vehicle out of track.

The dynamics of the AUV in the *surge*, *sway* and *yaw* degrees of freedom are defined in matrix form by

$$\dot{\eta} = \underline{J}(\eta)\dot{\nu} \tag{5.1}$$

$$\underline{M}\dot{\nu} = -\underline{C}(\nu)\nu - \underline{D}(\nu)\nu + \tau \tag{5.2},$$

which follow directly from the dynamic model (2.8) for 6 degrees of freedom. Under the modeling assumptions made in Section 3.1 the matrix form of the AUV dynamics is rewritten into

$$\dot{x} = uC(\psi) - vS(\psi) \tag{5.3.a}$$

$$\dot{y} = uS(\psi) + vC(\psi) \tag{5.3.b}$$

$$\dot{\psi} = r \tag{5.3.c}$$

$$m_{11}\dot{u} = m_{22}vr - d_{11}u + \tau_u \tag{5.3.d}$$

$$m_{22}\dot{v} = -m_{11}ur - d_{22}v \tag{5.3.e}$$

$$m_{33}\dot{r} = (m_{11} - m_{22})uv - d_{33}r + \tau_r \tag{5.3.f}$$

Where $\nu = [u \quad v \quad r]^T$, $\eta = [x \quad y \quad \psi]^T$, $\underline{M} = diag(m_{11}, m_{22}, m_{33})$,

$\underline{D}(\nu) = diag(d_{11}, d_{22}, d_{33})$, $\tau = [\tau_u \quad 0 \quad \tau_r]^T$,

$$\underline{J}(\eta) = \begin{bmatrix} C(\psi) & -S(\psi) & 0 \\ S(\psi) & C(\psi) & 0 \\ 0 & 0 & 1 \end{bmatrix} \text{ and } \underline{C}(\nu) = \begin{bmatrix} 0 & 0 & -m_{22}v \\ 0 & 0 & m_{11}u \\ m_{22}v & -m_{11}u & 0 \end{bmatrix}.$$

Where *x*, *y* and ψ represent the position and orientation of the AUV in the earth-fixed frame and *u*, *v* and *r* are the velocities in *surge*, *sway* and *yaw* respectively. The parameters m_{11}, m_{22} and m_{33} represent the rigid body and added mass of the inertia and mass of the AUV and d_{11}, d_{22} and d_{33} represent the linear damping terms of the AUV.

According to [92, 93] no pure state feedback control law exists to asymptotically stabilize the system given in (5.3). This problem is solved by introducing time-variance in the feedback law, an approach which is used for mobile robots in [80, 81], and is

extended to the control of ships in [83, 88, 89], and used for AUV's with the use of backstepping techniques in [82, 84, 85, 86, 87, 90, 91].

The position error between the current position of the AUV and a reference position of a virtual AUV is given by

$$x - x_r \tag{5.4.a}$$

$$y - y_r \tag{5.4.b}$$

$$\psi - \psi_r \tag{5.4.c},$$

which represents the position errors in the earth fixed frame. Where x, y and ψ represent the current position of the AUV and x_r, y_r and ψ_r the reference position of a virtual AUV. The problem with the position error proposed in (5.4) is that the error depends on the initial position of the earth fixed frame. Lefeber [83] inspired by the work of Pettersen and Egeland [93] solved this problem by a change of coordinates, which led to the natural error coordinates given by

$$\begin{bmatrix} x_e \\ y_e \\ \psi_e \end{bmatrix} = \begin{bmatrix} C(\psi) & S(\psi) & 0 \\ -S(\psi) & C(\psi) & 0 \\ 0 & 0 & 1 \end{bmatrix} \begin{bmatrix} x - x_r \\ y - y_r \\ \psi - \psi_r \end{bmatrix} \tag{5.5}$$

The position errors (5.4) are now considered in the body fixed frame of the AUV, so the tracking errors of the AUV can now be defined by

$$x_e = C(\psi)\left(x - x_r\right) + S(\psi)\left(y - y_r\right) \tag{5.6.a},$$

$$y_e = -S(\psi)\left(x - x_r\right) + C(\psi)\left(y - y_r\right) \tag{5.6.b},$$

$$\psi_e = \psi - \psi_r \tag{5.6.c},$$

$$u_e = u - u_r \tag{5.6.d},$$

$$v_e = v - v_r \tag{5.6.e},$$

$$r_e = r - r_r \tag{5.6.f}.$$

Where u_r, v_r, r_r, x_r, y_r, ψ_r, $\tau_{u,r}$ and $\tau_{r,r}$ represent the reference coordinates which have to satisfy

$$\dot{x}_r = u_r C(\psi_r) - v_r S(\psi_r) \tag{5.7.a},$$

$$\dot{y}_r = u_r S(\psi_r) + v_r C(\psi_r) \tag{5.7.b},$$

$$\dot{\psi}_r = r_r \tag{5.7.c},$$

$$m_{11}\dot{u}_r = m_{22}v_r r_r - d_{11}u_r + \tau_{u,r} \tag{5.7.d},$$

$$m_{22}\dot{v}_r = -m_{11}u_r r_r - d_{22}v_r \tag{5.7.e},$$

$$m_{33}\dot{r}_r = (m_{11} - m_{22})u_r v_r - d_{33}r_r + \tau_{r,r} \tag{5.7.f}.$$

Differentiating the tracking errors will lead to the tracking error dynamics, which are given by

$$\dot{x}_e = u - u_r\cos(\psi_e) - v_r\sin(\psi_e) + r_e y_e + r_r(t)y_e \tag{5.8.a},$$

$$\dot{y}_e = v - v_r\cos(\psi_e) + u_r\sin(\psi_e) - r_e x_e - r_r(t)x_e \tag{5.8.b},$$

$$\dot{\psi}_e = r_e \tag{5.8.c},$$

$$\dot{u}_e = \frac{m_{22}}{m_{11}}(v_e r_e + v_e r_r(t) + v_r r_e) - \frac{d_{11}}{m_{11}}u_e + \frac{1}{m_{11}}(\tau_u - \tau_{u,r}) \tag{5.8.d},$$

$$\dot{v}_e = -\frac{m_{11}}{m_{22}}(u_e r_e + u_e r_r(t) + u_r r_e) - \frac{d_{22}}{m_{22}}v_e \tag{5.8.e},$$

$$\dot{r}_e = \frac{(m_{11} - m_{22})}{m_{33}}(u_e v_e + u_e v_r + u_r v_e) - \frac{d_{33}}{m_{33}}r_e + \frac{1}{m_{33}}\tau_r \tag{5.8.f}.$$

The goal now is to stabilize the tracking error dynamics with a suitable choice of control laws for τ_u in *surge* and τ_r in *yaw* in order to establish tracking control for the AUV. From now on a state feedback approach proposed by Lefeber in [83] and Lefeber, Pettersen and Nijmeijer in [88] is followed to asymptotically stabilize the tracking error dynamics. In these papers a state-tracking problem for an under-actuated ship (with only *surge* and *yaw* controlled) is solved by means of a global tracking controller. The author is of the opinion that a clear explanation of this approach will form a decent basis for the understanding of the underactuated control problem for the AUV, since the control law proposed has a simple structure and guarantees global exponential stability of the tracking error dynamics. From this basis further developments for the underactuated control of the AUV can more easily be made in further research.

In [88] it is experimentally proven that the control law has a certain robustness against modeling errors and disturbances due to currents and wave drift forces. The control law can easily be transformed to a control law suitable for the AUV, since the dynamical model of a ship and AUV are similar in the *x-y* plane.

A feedback control law for τ_r , given by

$$\tau_r = \tau_{r,r} - (m_{11} - m_{22})(uv - u_r v_r) + d_{33}r_e + m_{33}\upsilon \tag{5.9}$$

is proposed, which will change the tracking dynamics (5.8.c) and (5.8.f) into the linear system given by

$$\dot{\psi}_e = r_e \tag{5.10},$$

$$\dot{r}_e = \upsilon \tag{5.11},$$

respectively. The linear system can be stabilized by the linear control law given by

$$\upsilon = -k_1 r_e - k_2 \dot{\psi}_e, \qquad k_1 > 0,\ k_2 > 0 \tag{5.12},$$

which will change the control law for τ_r into

$$\tau_r = \tau_{r,r} - (m_{11} - m_{22})(uv - u_r v_r) - k_1 r_e - k_2 \dot{\psi}_e, \qquad k_1 > -d_{33},\ k_2 > 0 \tag{5.13}$$

and the tracking dynamics into

$$\begin{bmatrix} \dot{\psi}_e \\ \dot{r}_e \end{bmatrix} = \begin{bmatrix} 1 & 0 \\ -\dfrac{(d_{33} + k_1)}{m_{33}} & -\dfrac{k_2}{m_{33}} \end{bmatrix} \begin{bmatrix} \psi_e \\ r_e \end{bmatrix} \tag{5.14}$$

Under the assumption that (5.14) is stabilized and that r_e and ψ_e go to zero, one is able to rewrite the remaining error tracking dynamics, 5.8.a, 5.8.b, 5.8.d and 5.8.e, into

$$\dot{x}_e = u_e + r_r(t)\, y_e \tag{5.15}$$

$$\dot{y}_e = v_e - r_r(t)\, x_e \tag{5.16}$$

$$\dot{u}_e = \frac{m_{22}}{m_{11}} v_e r_r(t) - \frac{d_{11}}{m_{11}} u_e + \frac{1}{m_{11}} (\tau_u - \tau_{u,r}) \tag{5.17}$$

$$\dot{v}_e = -\frac{m_{11}}{m_{22}} u_e r_r(t) - \frac{d_{22}}{m_{22}} v_e \tag{5.18},$$

note that $r_e = 0$ and $\psi_e = 0$ are substituted and the error tracking dynamics denoted in matrix form is given by

$$\begin{bmatrix} \dot{x}_e \\ \dot{y}_e \\ \dot{u}_e \\ \dot{v}_e \end{bmatrix} = \begin{bmatrix} 0 & r_r(t) & 1 & 0 \\ -r_r(t) & 0 & 0 & 1 \\ 0 & 0 & -\dfrac{d_{11}}{m_{11}} & \dfrac{m_{22}}{m_{11}} r_r(t) \\ 0 & 0 & -\dfrac{m_{11}}{m_{22}} r_r(t) & -\dfrac{d_{22}}{m_{22}} \end{bmatrix} \begin{bmatrix} x_e \\ y_e \\ u_e \\ v_e \end{bmatrix} + \begin{bmatrix} 0 \\ 0 \\ \dfrac{1}{m_{11}} \\ 0 \end{bmatrix} \begin{bmatrix} \tau_u - \tau_{u,r} \end{bmatrix} \tag{5.19}$$

The controllability can now be checked with the lemma given in Appendix G.8 [83], which states that the tracking error dynamics (5.19) are uniformly completely controllable if the reference yaw velocity $r_r(t)$ is persistently exciting [83].

If the reference yaw velocity $r_r(t)$ is persistently exciting the system can be stabilized by the control law

$$\tau_u = \tau_{u,r} - k_3 u_e + k_4 r_r(t) v_e - k_5 x_e + k_6 r_r(t) y_e \tag{5.20}$$

where the parameters *k* have to following restrictions:

$k_3 > d_{22} - d_{11}$,

$$k_4 = \frac{k_6\left(k_6 + k_3 + d_{11} - d_{22}\right)}{\frac{m_{11}}{m_{22}}\left(d_{22}k_6 + m_{11}k_5\right)},$$

$$0 < k_5 < \left(k_3 + d_{11} - d_{22}\right)\frac{d_{22}}{m_{11}},$$

$k_6 > 0$.

Note that any other control law that is available in literature for stabilizing linear time-varying systems can be used. Since this control mechanism uses the *surge* velocity to correct an error in the *sway* degree of freedom, the controlled system explained above is only stable if $r_r(t)$ is persistently exciting, full stability proof can be found in [83].

A differential and integral gain are added to the *surge* control law (5.20) in order to improve the linear controller into a PID controller. The differential gain is denoted by

$$\dot{u}_e k_7, \quad k_7 > 0 \tag{5.21}$$

and the integral gain by

$$\int u_e k_8, \ k_8 > 0 \tag{5.22},$$

forming the *surge* control law

$$\tau_u = \tau_{u,r} - k_3 u_e - \int u_e k_8 - \dot{u}_e k_7 + k_4 r_r(t) v_e - k_5 x_e + k_6 r_r(t) y_e \tag{5.23}.$$

5.2 Simulation Results

For the simulation of the control laws the AUV will need to follow a circular trajectory where the *surge* and *yaw* velocity of the reference are set to 0.1 m/s and 0.05 rad/s, respectively. The AUV itself will start from a different initial position than the

reference trajectory, which means there is a starting error and the AUV will need to catch up with the reference trajectory. The control laws (5.13) and (5.20) derived in Section 5.1 are used to stabilize the system and keep the AUV on the reference trajectory.

The simulations are run in Matlab Simulink. The thrust rate is limited with a rate limiter at 200 *N*/s and saturated at -100 and 100 *N*. Noise is added to the position and velocity measurements of the AUV, 0.0197 [m]/[rad] for the position and 0.0197 [m/s]/ [rad/s] for the velocity.

The settings for the first simulation are described in Tables 5.1 to 5.3. Note that $m_{11} = m_{22} = m$, $m_{33} = I_{zz}$, $d_{11} = X_u$, $d_{22} = Y_v$ and $d_{33} = N_r$. The control gains given in Table 5.3 for control option 1 and 2 are found by trial and error. The resulting trajectory of the AUV in the x-y plane can be seen in Figure 5.1. Note that the reference trajectory starts at $[x, y, \psi] = [0, -1, 0]$ and the AUV starts at $[x, y, \psi] = [0, 0, 0]$.

Parameters	**Controller**	**Plant**
$m_{11} = m_{22}$ [kg]	160	160
m_{33} [kg]	15	15
d_{11} [Ns/m]	100	100
d_{22} [Ns/m]	100	100
d_{33} [Ns/m]	25	25

Table 5.1: Controller and plant parameters.

Parameters	**Reference**	**AUV**
x [m]	0	0
y [m]	-1	0
ψ [rad]	0	0
u [m/s]	0.1	0
v [m/s]	0	0
r [rad/s]	0.05	0

Table 5.2: Initial position reference and AUV.

	Option 1	**Option 2**
Parameters		
k_1	1	1
k_2	1	1
k_3	10	10
k_4	1	1
k_5	7	4
k_6	70	130
k_7	0	1
k_8	0	5
Noise	[m] [rad]	[m/s] [rad/s]
Position	0.0197	0.0197
Velocity	0.0197	0.0197

Table 5.3: Gains and Noise for options 1 and 2.

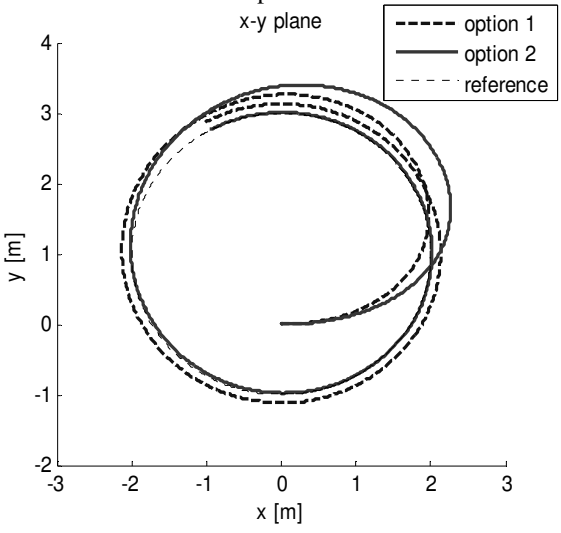

Figure 5.1: Trajectory of the reference and AUV in the *x*-*y* plane.

In case of the implementation of control option 1 the AUV tracks the reference trajectory with a steady state error in the *sway* degree of freedom of the AUV. To solve this problem, control option 2 is introduced which has an integral control term to correct the steady state error in *sway*, which can also be confirmed in Figure 7.1. Note that the introduction of the integral term also results in a larger overshoot, a consequence which is predicted in Appendix H.1. The *x* and *y* trajectory, *surge* and *yaw* thrust, velocity error and position error are all given in Appendix J.1.

Parameters	**Controller**	**Plant**
$m_{11} = m_{22}$ [kg]	160	160
m_{33} [kg]	15	15
d_{11} [Ns/m]	100	100
d_{22} [Ns/m]	100	100
d_{33} [Ns/m]	25	25

Table 5.4: Controller and plant parameters.

Parameters	**Reference**	**AUV**
x [m]	0	0
y [m]	-1	-2
ψ [rad]	0	0
u [m/s]	0.1	0
v [m/s]	0	0
r [rad/s]	0.05	0

Table 5.5: Initial position reference and AUV.

	Option 1	**Option 2**
Parameters		
k_1	1	1
k_2	1	1
k_3	10	10
k_4	1	1
k_5	7	4
k_6	70	130
k_7	0	1
k_8	0	5
Noise	[m] [rad] [m/s] [rad/s]	
Position	0.0197	0.0197
Velocity	0.0197	0.0197

Table 5.6: Gains and Noise for option 1 and 2.

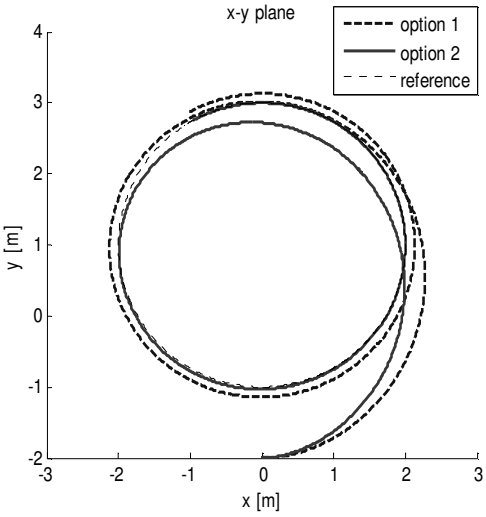

Figure 5.2: Trajectory of the reference and AUV in the *x*-*y* plane.

For the second simulation the initial position of the AUV is changed to $[x, y, \psi] = [0, -2, 0]$. The resulting trajectory can be seen in Figure 5.2 and all settings can be seen in Tables 5.4 to 5.6. The *x* and *y* trajectory, *surge* and *yaw* thrust, velocity error and position error are all given in Appendix J.2. Once again the control laws manage to bring the AUV back on track. Again an overshoot in the sway degree of freedom can be seen in combination with the PID controller, but the steady state error is solved.

For the third simulation, the mass/inertia parameters are perturbed, which can be seen in Table 5.7, the resulting *x-y* plane is given in Figure 5.3. Both control options still track the reference trajectory.

Parameters	Controller	Plant
$m_{11} = m_{22}$ [kg]	80	160
m_{33} [kg]	7	15
d_{11} [Ns/m]	100	100
d_{22} [Ns/m]	100	100
d_{33} [Ns/m]	25	25

Table 5.7: Gains and Noise for options 1 and 2.

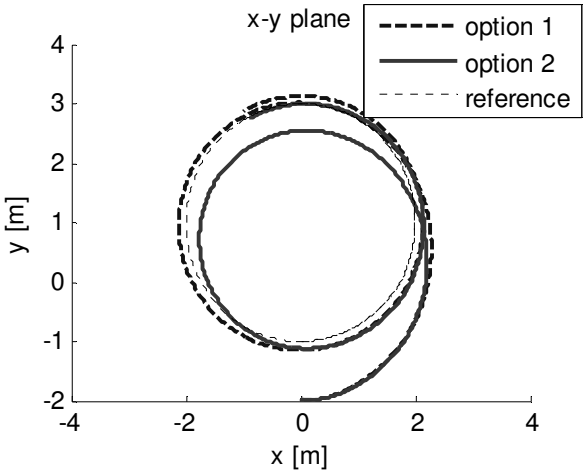

Figure 5.3: Trajectory of the reference and AUV in the *x-y* plane.

The simulations reveal that the state feedback control law is able to track a circular reference trajectory within a reasonable error and is not affected by measurement noise and perturbed mass and inertia parameters. However perturbed damping parameters seem to affect the control law, which means that damping parameters should be estimated close to the exact plant parameters or an adaption law should be used to tune the damping parameters online.

5.3 Summary

The under-actuated control problem is investigated assuming *sway* motion of the AUV is not negligible, so Coriolis and centripetal forces need to be considered. A state feedback control method is explained as a result of which the controlled system is able to follow a reference trajectory in the *x-y* plane. The only disadvantage is that the *yaw* degree of freedom of the reference trajectory needs to be persistently exciting, which makes following a straight line impossible. The control law uses the control in the *surge* degree of freedom to correct a position error in *sway*. The control law for the *yaw* degree of freedom is used to minimize the error in *yaw*. Simulations reveal that the state feedback control law is able to track a circular reference trajectory within a reasonable error and is not affected by measurement noise and perturbed mass and inertia parameters. However perturbed damping parameters seem to affect the control law,

which means that damping parameters should be estimated close to the exact plant parameters or an adaption law should be used to tune the damping parameters online.

Chapter 6

Conclusions and Recommendations

6.1 Conclusions

The kinematic and dynamic models of the AUV of the Department of Mechanical Engineering at the University of Canterbury are derived for its six degrees of freedom operating range. The following assumptions are made to the dynamic model: the AUV only moves with a relatively low speed, there is symmetry about the three planes, the aligning moment ensures horizontal stability, *roll*, *pitch* and *sway* motion can be neglected, and, the body-fixed frame of the AUV is positioned at the center of gravity. With these assumptions decoupling the degrees of freedom is possible, where only the *surge*, *heave* and *yaw* degrees of freedom will be controlled. Since one is dealing with a decoupled model only the mass/inertia and damping terms need to be estimated. A system identification approach is proposed which treats the *surge*, *heave* and *yaw* degree of freedom separately. The approach uses a static experiment to determine the damping terms, where the acceleration is zero, and, a dynamic experiment to determine the mass terms, with the use of constant acceleration. Unfortunately due to the failure of the IMU the acceleration could not be measured correctly. Therefore the unknown mass/inertia and damping terms could not be estimated and a parameter selection method is used instead. The parameter selection is based on parameter estimation results of software programs and a parameter comparison with other similarly shaped AUVs.

After comparing different control techniques a feedback linearizing control technique is chosen to design control laws for the *surge*, *heave* and *yaw* degrees of freedom. The feedback linearizing control technique changes the nonlinear dynamical

system into a linear system through a suitable chosen control input. The linear system is stabilized with the use of PID control. The feedback linearizing controller is extended to a tracking controller in order to track a trajectory in one degree of freedom. Simulations are performed to test the controller, which performed well under parameter perturbation and the implementation of noise on the feedback position and velocity signals of the plant. It should be noted that all states need to be available online to control the AUV. However during experiments full state measurement is not possible and the control law should be extended with an observer in order to estimate unmeasured states.

In the *x-y* plane the AUV is only able to move in the *surge* and *yaw* degrees of freedom caused by the trolling motor configuration. An under-actuated control problem arises, since one is only able to control two degrees of freedom while the AUV is able to move in three degrees of freedom. To steer the AUV with a smooth motion from an initial position *A* to a different position *B*, in the *x-y* plane, a path planning model is derived. The path planning model describes a path from *A* to *B* with the use of polar coordinates which the AUV is able to follow controlling only the *surge* and *yaw* degrees of freedom. The assumption is made that *sway*-motion of the AUV can be neglected. From simulations with the path planning model it could be concluded that the path planning model works correct, except for planning a straight line due to singularity reasons. This problem can be solved by introducing a switching controller which is able to switch between different path planning models.

The under-actuated control problem is again investigated, now assuming *sway* motion of the AUV is not negligible, so Coriolis and centripetal forces need to be considered. A state feedback control method is explained as a result of which the controlled system is able to follow a reference trajectory in the *x-y* plane. The only disadvantage is that the *yaw* degree of freedom of the reference trajectory needs to be persistently exciting, which makes following a straight line impossible. The control law uses the control in the *surge* degree of freedom to correct a position error in *sway*. The control law for the *yaw* degree of freedom is used to minimize the error in *yaw*. Simulations reveal that the state feedback control law is able to track a circular reference trajectory within a reasonable error and is not affected by measurement noise and perturbed mass and inertia parameters. However perturbed damping parameters seem to affect the control law, which means that damping parameters should be estimated close to the exact plant parameters or an adaption law should be used to tune the damping parameters online.

6.2 Recommendations

A few recommendations can be made about the AUV design, sensor equipment and future experiments. At first, the trolling motor configuration should be redesigned to improve the water flow, thrust power and weight of the vehicle. The frame which holds the trolling motors and battery compartments can be designed more compact, reducing the weight of the vehicle, and, the vertical trolling motors should be repositioned in order to improve the flow of the horizontal trolling motors.

New sensor equipment should be installed to determine the position and velocity of the AUV. Different sensors are available, but the best low-cost solution will be stereo vision. Two underwater cameras measure the displacement of the AUV with respect to objects placed on the bottom of a swimming pool determining the relative position and velocity of the AUV. If position and velocity measurements of the AUV are possible, the unknown parameters can be estimated with the use of the system identification approach explained in this report. The data acquisition is a very time consuming and challenging task and demands a proper setup and planning for correct measurements. Parameters should be estimated with the highest possible accuracy which finally will lead to better and more accurate control laws.

If the unknown parameters are estimated, control techniques explained in this report extended with state observers can be used for positioning the AUV. Although, for the under-actuated problem a global tracking controller still needs to be designed.

Bibliography

[1] D. Richard Blidberg. The Development of Autonomous Underwater Vehicles (AUV); A Brief Summary. Autonomous Undersea Systems Institute, 2000.

[2] P.J. Craven, R. Sutton and R.S. Burns. Control Strategies for Unmanned Underwater Vehicles. University of Plymouth, 1998; *Key Information: PID control, Gain-scheduling control, adaptive control, MRAC, indirect adaptive control, self-tuning control, sliding control, H-infinity robust control, fuzzy logic control*

[3] Ferial El-Hawary. The Ocean Engineering Handbook, The Electrical Engineering Handbook Series, 2001

[4] R. Cristi, F.A. Papoulias and A.J. Healey. Adaptive Sliding Mode Control of Autonomous Underwater Vehicles in the Dive Plane. IEEE journal of oceanic engineering, vol. 15, no. 3, pag. 152-160, july 1990

[5] R. Burgoyne, X. Huang, C. North, N. Schaal and K. Shaw. Final Year Project Report; Unmanned Underwater Vehicle. University of Canterbury; 2007; *Key Information: Design of the AUV of the University of Canterbury*

[6] G.N. Roberts and R. Sutton. Advances in unmanned marine vehicles. Book IEE control series 69, 2006

[7] K.P. Valanis, D. Gracanin, M. Matijasevic, R.Kolluru and A. Demetriou. Control architecture for autonomous underwater vehicles. IEEE Control Systems, issue no. *0272-1708l97l, pag. 48-60 Dec.*1997

[8] Thor I. Fossen. Underwater Vehicle Dynamics. Book TSI Press, Albuquerque, 1995.

[9] W. Wang and C. M. Clark. Modeling and Simulation of the VideoRay Pro III Underwater Vehicle. University of Waterloo, 2001; *Key Information: Kinematic Model, Dynamic model*

[10] B. Jalving. The NDRE-AUV flight control system. IEEE journal of Oceanic Engineering vol. 19, no. 4, pag. 497-501, oct.1994; *Key Information: PID control, autopilots, vehicle modeling*

[11] O. Fjellstad and T.I. Fossen. Position and attitude tracking of AUVs: a quaternion feedback approach. Department of Engineering Cybernetics, The Norwegian Institute of Technology, University of Trondheim, Nov 1994.

[12] G. Antonelli, S. Chiaverini, N. Sarkar, and M. West. Adaptive control of a autonomous underwater vehicle: experimental results on ODIN. IEEE Transactions on Control Systems Technology, vol. 9, no. 5, pag.756-765, sep. 2001; *Key Information: Adaptive Control, position control, AUV: ODIN*

[13] J. Healey and D. Lienard. Multivariable sliding model control for autonomous diving and steering of unmanned underwater vehicles. IEEE Journal of Oceanic Engineering, vol. 18, no. 3, pag. 327-339, 1993; *Key Information: Sliding Mode Control, Vehicle Modeling, Flight UUV*

[14] D.B. Marco, A.J. Healey. Command, control and navigation experimental results with the NPS ARIES AUV. IEEE Journal of Oceanic Engineering, vol. 26, no. 4, pag. 466-476, 2001; *Key Information: Kalman filter, Autopilot Control Laws, AUV: ARIES*

[15] J. Hu, C. Bohn, and H.R. Wu. Systematic H_∞ weighting function selection and its application to the real-time control of a vertical take-off aircraft. Control Engineering Practice 8, pag. 241-252 2000; *Key Information: H_∞ weighting function*

[16] C. Silpa-Anan. Autonomous underwater vehicle: Vision and control. Master's thesis, The Australian National University, 2001; *Key Information: AUV Thesis, AUV: Kambara*

[17] G. Indiveri. Modelling and Identification of Underwater Robotics Systems. PhD thesis, University of Genova, 1998; *Key Information: AUV Thesis, AUV: ROMEO*

[18] P. Brutzman. A Virtual World for an Autonomous Underwater Vehicle. PhD thesis, Naval Postgraduate School, 1994.

[19] D. Wettergreen et al. Development of autonomous underwater vehicle towards visual servo control. Proceedings of the Australian Conference on Robotics and Automation 2000, 2000.

[20] T. Fossen and I. Fjellstad. Robust adaptive control of underwater vehicles. 3rd

IFAC Workshop on Control Applications in Marine Systems (CAMS '95), pag. 1-9, 1995; *Key Information: Adaptive control*

[21] S. Sagatun and R. Johansson. Optimal and adaptive control of underwater vehicles. 4th Symposium on Robot Control, pag. 953-958, 1994; *Key Information: Adaptive control*

[22] J.Nie, T. Fossen et al. On-board sensor-based adaptive control of small uuvs in very shallow water. Proceedings of the IFAC Conference on Control Applications in Marine Systems (CAMS '98), pag. 441-452, 1998; *Key Information: Adaptive control*

[23] T. Fossen and S. Sagatun. Adaptive control of nonlinear underwater robotic systems. Journal of Robotic Systems, JRS-8(3): pag. 393-412, 1991; *Key Information: Adaptive control*

[24] Pascoal, Oliveira, Santos, and others. Robotic Ocean Vehicles for Marine Science Applications: the European ASIMOV Project; IEEE no. 0-7803-6551-8, 2000. *Key Information: Infante AUV, communication and sonar, sensors*

[25] T. Fossen and B. Foss. Sliding control of mimo nonlinear systems. Proceedings of the European Control Conference, pag. 1855-1860, 1991; *Key Information: Sliding mode control*

[26] J. Healey and D. Lienard. Adaptive sliding mode control of autonomous underwater vehicles in the dive plane. IEEE Journal of Oceanic Engineering, vol. 15, no. 3, pag. 152-161, july 1990; *Key Information: Sliding mode control*

[27] S. Feijun and S. Smith. Automatic design and optimization of fuzzy logic controllers for an autonomous underwater vehicle. OCEANS'2000 MTS/IEEE, no. 0-7803-6551-8, pag. 829-835, 2000;*Key Information: Fuzzy Logic Control*

[28] M. Kwiesielewicz et al. Predictive versus fuzzy control of autonomous underwater vehicle. IEEE International Conference on Methods and Models in Automation and Robotics, 2001.

[29] S. Feijun and S. Smith. Design of sliding mode fuzzy controllers for an autonomous underwater vehicle without system model. OCEANS'2000 MTS/IEEE, vol.2, pag 835-840, 2000.

[30] J.Jantzen. Design Of Fuzzy Controllers. Technical University of Denmark. 1998; *Key Information: Basic Explanation Fuzzy Control*

[31] B.Ashbaugh and J.Boitano. Advantages and Disadvantages of Controller Designs Using Fuzzy Logic. University of California, 1998. *Key Information: Fuzzy Logic Control*

[32] J. Ibaiiez-Guzmhl and R. Ketata. Fuzzy logic control experiments on a singlelink manipulator. PBle Atlantique de Genie Electrique; *Key Information: Fuzzy Logic Control*

[33] S.M. Smith, G.J.S. Rae, and D.T. Anderson. Applications of Fuzzy Logic to the Control of an Autonomous Underwater Vehicle. Advanced Marine Systems Group Department of Ocean Engineering, pag 1099-1106, 1992; *Key Information: Fuzzy Logic Control (heading, pitch and depth), AUV: Ocean Voyager*

[34] W. Naeem et al. Lqg/ltr control of an autonomous underwater vehicle using a hybrid guidance law. International Federation on Automatic Control Journal, 2003; *Key Information: Linear Quadratic Gaussian methods, Kalman Filter*

[35] D. Juul et al. Submersible control using the linear quadratic gaussian with loop transfer recovery method. Proceedings of the Symposium on Autonomous Underwater Technology, 1994.

[36] A. Santos, R.R. Bitmead. Nonlinear Control for an Autonomous Underwater Vehicle (AUV) Preserving Linear Design Capabilities. Conference on Decision & Control. 1995
Key Information: Linear Quadratic Gaussian methods, Extended Kalman Filter

[37] T.I. Fossen. Guidance and Control of Ocean Vehicles. Book: John Wiley and Sons Ltd. 1994

[38] T.I. Fossen. Marine Control Systems. Guidance, Navigation and Control of Ships, Rigs and Underwater Vehicles. Marine Cybernetics AS. 2002

[39] J.Lee, M.Roh, J.Lee and D.Lee. Clonal Selection Algorithms for 6-DOF PID Control of Autonoumous Underwater Vehicles. Department of Bio and Brian Engineering, KAIST; *Key Information: PID control*

[40] K.P. Valavanis, D. Gracanin, M. Matijasevic and others. Control Architectures for Autonomous Underwater Vehicles, IEEE Control Systems, no. 0272-1708, pag. 48-64, 1997; *Key Information: Comparison of different control techniques in different AUVs*

[41] R.Bachmayer, S.Humphris, D. Fornari, and others. Oceanographic Research Using Remotely Operated Underwater Robotic Vehicles: Exploration of Hydrothermal Vent Sites On The Mid-Atlantic Ridge At 37°North 32°West. 1996; *Key Information: Basic Information AUV, Navigation, Sonar, AUV: ARGO2*

[42] S.B. Williams, P.Newman, G.Dissanayake and others. A decoupled, distributed AUV control architecture. University of Sydney, 2006; *Key Information: Decoupled control, AUV: Oberon*

[43] P. Mhaskar, N.H. El-Farra and P.D.Christofides. A Method for PID Controller Tuning Using Nonlinear Control Techniques. University of California, 2004; *Key Information: PID control, tuning methods and nonlinear control*

[44] K.Hur. Brushless Motor Controller for an AUV. University of Texas, 2006; *Key Information: Basic AUV Information*

[45] L.A.Gonzales. Design, Modeling and Control of an Autonomous Underwater Vehicle. Mobile Robotics Laboratory, University of Western Australia, 2004; *Key Information: AUV Thesis, AUV: MAKO*

[46] M.H.Kim, Nonlinear Control and Robust Observer Design for Marine Vehicles. Virginia Polytechnic Institute and State University, 2000; *Key Information: Nonlinear control, Nonlinear observer, neural networks, sliding and adaptive*

[47] D.G.Biddle. Inertial Based Control on the Kambara. Australian National University, 2003; *Key Information: IMU control, AUV thesis, AUV: Kambara*

[48] O.E.Fjellstad. Control of Unmanned Underwater Vehicles in Six Degrees of Freedom, A Quaternion Feedback Approach. University of Trondheim. 1994; *Key Information: AUV Thesis, AUV: MOBATEL*

[49] I. Schjolber and T.I. Fossen. Modelling and Control of Underwater Vehicle Manipulator Systems. University of Trondheim; *Key Information: Dynamic model, feedback linearization*

[50] D.A. Jones, D.B. Clarke, I.B. Brayshaw and others. The Calculation of Hydrodynamic Coefficients for Underwater Vehicles. Australia; *Key Information: Dynamic model, Parameter Estimation, Identification*

[51] P.Ridao, J.Batlle and M.Carreras. Model Identification of a low-speed UUV. University of Girona, 2001; *Key Information: Parameter Estimation, Modeling, Identification*

[52] J. Wu, M.J. Zhang, Y.J. Wang. Research of system identification method for underwater vehicle based on neural network. Harbin Engineering University, 2007; *Key Information: Parameter estimation, system identification*

[53] P.Hsu, M. Bodson, S.Sastry and B.Paden. Adaptive Identification and Control for Manipulators without Using Joint Accelerations. University of California; *Key Information: Dynamic model, Parameter estimation, Adaptive Control, Identification*

[54] A. Tiano. Comparison of nonlinear identification methods for underwater vehicles. University of Pavia; *Key Information: Lyapunov Identification, Least Squares Identification, Parameter estimation, Modeling, Identification*

[55] D.A. Smallwoord. Adaptive Identification of Dynamically Positioned Underwater Robotic Vehicles; *Key Information: Adaptive Parameter Estimation, Dynamic model, Least Squares Method, Identification*

[56] P.Ridao, A.Tiano, A. El-Fakdi, M.Carreras, A.Zirilli. On the identification of nonlinear models of unmanned underwater vehicles. University of Girona, 2004; *Key Information: Dynamic model, Parameter Estimation, Identification*

[57] A.Alessandri, M.Caccia, G.Indiveri, F.Veruggio. Application of LS and EKF Techniques to the identification of underwater vehicles. University of Genoa, 1998; *Key Information: Dynamic model, Identification, Least Square, Extended Kalman Filter*

[58] A. Tiano, R.Sutton, A.Lozowicki, W.Naeem. Observer Kalman filter identification of an autonomous underwater vehicle, 2006; *Key Information: System identification, Parameter Estimation, Dynamic model*

[59] J.S. Geisbert. Hydrodynamic Modeling for Autonomous Underwater Vehicles Using Computional and Semi-Empirical Methods. Verginia Polytechnis Institute and State University, 2007; *Key Information: Kinematic model, Dynamic model*

[60] A.J. Healey, S.M. Rock and others. Toward an Improved Understanding of Thruster Dynamics for Underwater Vehicles. IEEE journal of oceanic engineering, vol 20, no. 4, pag. 354-361, okt. 1995; *Key Information: Thruster model*

[61] T.I.Fossen and O.E.Fjellstad. Robust Adaptive Control of Underwater Vehicles: A comparative study. University of Trondheim, IFAC workshop on Control Applications in Marine Systems (CAMS'95), 1995; *Key Information: Adaptive control, dynamic model, parameter estimation*

[62] D.B.Marco, A.Martins, A.J.Healey. Surge Motion Parameter Identification for the NPS Phoenix AUV, 1996; *Key Information: Parameter Estimation, Kalman filter*

[63] L.L. Whitcomb, D.R. Yoerger. Comparative Experiments in the Dynamic and Model-Based Control of Marine Thrusters, pag. 1018-1028, 1994; *Key Information: Thruster model*

[64] C.L. Tsukamoto, W.Lee, J.Yuh, S.K.Choi and J.Lorentz. Comparison study on advanced thruster control of underwater robots. University of Hawaii, 1997; *Key Information: Thruster model*

[65] J. Petrich, W.L.Neu and D.J.Stilwell. Identification of a simplied AUV pitch axis model for control design: Theory and experiments. Virginia Polytechnic Institute and State University, 2001; *Key Information: System Identification, modeling*

[66] M.Caccia, G.Indiveri and Gianmarco Veruggio. Modeling and Identification of Open-Frame Variable Configuration Unmanned Underwater Vehicles, IEEE journal of oceanis engineering, vol. 25, no. 2, pag. 227-241, apr. 2000; *Key Information: Parameter estimation, thruster model, decoupling*

[67] K.R.Goheen and E.R.Jefferys. Multivariable self-tuning autopilots for autonomous and remotely operated underwater vehicles. IEEE journal Oceanic Engineering, vol 15, no. 3, pag. 144-151, 1990; *Key Information: Thruster model, implementation of the thruster installation coefficient.*

[68] C.Moler. Numerical Computing with Matlab, Least Squares, Chpt 5. Mathworks, 2008; *Key Information: Least Squares Technique*

[69] D. Mills and C. Harris. Neurofuzzy modelling and control of a six degree of freedom auv. 1996.

[70] V. Filaretov et al. The sliding mode adaptive control system for autonomous underwater robot. *Proceedings of ICAR '95*, 1995.

[71] D. Sellers. An Overview of Proportional plus Integral plus Derivative Control and Suggestions for Its Successful Application and Implementation. Portland Energy Conservation Inc, 2003.

[72] P. Mhaskar, N. H. El-Farra and P. D. Christofides. A Method for PID Controller Tuning Using Nonlinear Control Techniques. Proceeding of the 2004 American Control Conference, no. 7803-8335-4, pag. 2925-3000, Jun 2004

[73] J.E.Slottine and W.Li. Applied nonlinear control. Book: Prentice-Hall, 1991; *Key Information: Nonlinear control techniques*

[74] H.K.Khalil. Nonlinear systems. Third edition. Book: Prentice-Hall, 2002; *Key Information: Nonlinear control techniques*

[75] G.F.Franklin, J.D.Powell and A.Emami-Naeini. Feedback control of dynamic systems. Fourth Edition. Book: Prentice-Hall, 2002; *Key Information: Feedback control*

[76] M.W.Spong, S.Hutchinson and M.Vidyasagar. Robot modeling and control. Book: Wiley, 2006; *Key Information: Path tracking*

[77] P.Egeskov, A.Bjerrum, et.al.. Design, construction and hydrodynamic testing of the AUV MARIUS. Proceedings of the AUV conference, 1994; *Key Information: Gain scheduling*

[78] M.Aicardi, G.Casalino, et.al. Closed loop steering of unicycle-like vehicles via Lyapunov Techniques. IEEE Robotics & Automation Magazine, pag. 27-35, mar.1995; *Key Information: Unicycle Path Planning*

[79] M.Aicardi, G.Casalino, et.al. Closed loop smooth steering of unicycle-like vehicles. IEEE proceedings of the 33rd Conference on Decision and Contol, no. 0-7803-1986-0, pag. 2455-2459, Dec 1994; *Key Information: Unicycle Path Planning*

[80] T.S.VanZwieten. Dynamic simulation and control of an autonomous surface vehicle. Florida Atlantic University, 2003; *Key Information: Unicycle Path Planning applied on a ASV*

[81] A.Micaelli and C.Samson. Trajectory tracking for unicycle-type and two-steering-wheels mobile robots. Unite´ de recherche INRIA Sophia-Antipolis, 1993; *Key Information: Unicycle Path Planning and tracking*

[82] A.P.Aguiar and J.P.Hespanha. Trajectory-Tracking and Path-Following of Underactuated Autonomous Vehicles With Parametric Modeling Uncertainty. IEEE Transactions on automatic control, vol 52, no. 8, pag. 1362-1379, aug 2007; *Key Information: Trajectory Tracking and Path Following of an AUV*

[83] A.A.J.Lefeber. Tracking control of nonlinear mechanical systems. Universiteit Twente, 2000; *Key Information: Tracking control of a ship and unicycle*

[84] K.D.Do and J.Pan. Robust and adaptive path following for underactuated autonomous underwater vehicles. The University of Western Australia, 2003; *Key Information: Path following of an AUV using backstepping*

[85] L.Lapierre and D.Soetanto. Nonlinear path-following control of an AUV. Ocean engineering, vol 34, pag. 1734-1744, 2007; *Key Information: Path following of an AUV using backstepping*

[86] L.Lapierre, D.Soetanto and A.Pascoal. Nonlinear Path Following with Applications to the Control of Autonomous Underwater Vehicles. Proceedings of the 42nd IEEE Conference on Decision and Control, no. 0-7803-7924-1, pag. 1256-1261, 2003; *Key Information: Path following of an AUV using backstepping and applications*

[87] P.Encarnasiio and A.Pascoal. 3D Path Following for Autonomous Underwater Vehicle. Proceedings of the 39th IEEE Conference on Decision and Control, no. 0-7803-6638-7, pag. 2977-2983, Dec 2000; *Key Information: 3D path following using backstepping*

[88] E.Lefeber, K.Y.Pettersen and H.Nijmeijer. Tracking Control of an Underactuated Ship. IEEE Transactions on control systems technology, vol 11, no. 1, pag. 52-61, jan 2003; *Key Information: Tracking control of a ship using cascaded controller design see also [83]*

[89] K.Y.Pettersen and H.Nijmeijer. Tracking control of an underactuated surface vessel. Norwegian University of Science and Technology, University of Twente, Technical Univeristy of Eindhoven, 1998; *Key Information: Tracking control of a ship*

[90] K.D.Do, Z.P.Jiang, J.Pan and H.Nijmeijer. Global output feedback universal controller for stabilization and tracking of underactuaded ODIN-an underwater vehicle. University of Western Australia, Polytechnic University NY USA, Eindhoven University of Technology. Proceedings of the 41st IEEE Conference on Decision and Control, no. 0-7803-7516-5, pag. 504-510, Dec 2002; *Key Information: Tracking control for the AUV named ODIN, see also [91]*

[91] K.D.Do, Z.P.Jiang, J.Pan and H.Nijmeijer. A global output-feedback controller for stabilization and tracking of underactuated ODIN: A spherical underwater vehicle. University of Western Australia, Polytechnic University NY USA, Eindhoven University of Technology. Automatica 40, 2004; *Key Information: Tracking control for the AUV named ODIN, see also [90]*

[92] K.Y.Pettersen and O.Egeland. Exponential stabilization of an underactuated surface vessel. Proceedings of the 35th IEEE Conference on Decision and Control, no. 0-7803-3590-2, pag. 967-973, Dec 1996; *Key Information: Underactuaded control*

[93] K.Y.Pettersen and O.Egeland. Time-varying Exponential Stabilization of the Position and Attitude of an Underactuated Autonomous Underwater Vehicle. Norwegian University of Science and Technology, 1997; *Key Information: Underactuaded control*

[94] T.Patterson, H.Rogers, D.Hewett, F.McKenzie and B.Burnell, Final Year Project Report; Unmanned Underwater Vehicle. University of Canterbury; 2008; *Key Information: Design of the AUV of the University of Canterbury*

Appendix A

A.1 Derivation of the rotation matrix

$$\underline{R}^{BW}(\varphi,\theta,\psi)=\underline{R}_z(\psi)\underline{R}_y(\theta)\underline{R}_x(\varphi) \quad \text{or} \quad \underline{R}^{30}(\varphi,\theta,\psi)=\underline{R}^{32}(\psi)\underline{R}^{21}(\theta)\underline{R}^{10}(\varphi) \tag{3.3}$$

$$\underline{R}^{BW}(\varphi,\theta,\psi)=\begin{bmatrix} C(\psi) & -S(\psi) & 0 \\ S(\psi) & C(\psi) & 0 \\ 0 & 0 & 1 \end{bmatrix}\begin{bmatrix} C(\theta) & 0 & S(\theta) \\ 0 & 1 & 0 \\ -S(\theta) & 0 & C(\theta) \end{bmatrix}\begin{bmatrix} 1 & 0 & 0 \\ 0 & C(\varphi) & -S(\varphi) \\ 0 & S(\varphi) & C(\varphi) \end{bmatrix}$$

$$\underline{R}^{BW}(\varphi,\theta,\psi)=\begin{bmatrix} C(\theta)C(\psi) & -S(\psi) & S(\theta)C(\psi) \\ C(\theta)S(\psi) & C(\psi) & S(\theta)S(\psi) \\ -S(\theta) & 0 & C(\theta) \end{bmatrix}\begin{bmatrix} 1 & 0 & 0 \\ 0 & C(\varphi) & -S(\varphi) \\ 0 & S(\varphi) & C(\varphi) \end{bmatrix}$$

$$\underline{R}^{BW}(\varphi,\theta,\psi)=\begin{bmatrix} C(\theta)C(\psi) & -C(\varphi)S(\psi)+S(\varphi)S(\theta)C(\psi) & S(\varphi)S(\psi)+C(\varphi)S(\theta)C(\psi) \\ C(\theta)S(\psi) & C(\varphi)C(\psi)+S(\varphi)S(\theta)S(\psi) & -S(\varphi)C(\psi)+C(\varphi)S(\theta)S(\psi) \\ -S(\theta) & S(\varphi)C(\theta) & C(\varphi)C(\theta) \end{bmatrix}$$

A.2 Derivation of the coordinate transform matrix

$\vec{\omega}_B = \underline{J}_2^{-1}\vec{\omega}_W$ which gives:

$$\vec{\omega}_B = \vec{e}^{\,B^T}\begin{bmatrix}\dot{\varphi}\\0\\0\end{bmatrix} + \vec{e}^{\,B^T}\underline{R}_x(\varphi)\begin{bmatrix}0\\\dot{\theta}\\0\end{bmatrix} + \vec{e}^{\,B^T}\underline{R}_x(\varphi)\underline{R}_y(\theta)\begin{bmatrix}0\\0\\\dot{\psi}\end{bmatrix}$$

Substitution of the rotation matrices:

$$\vec{\omega}_B = \vec{e}^{\,B^T}\begin{bmatrix}\dot{\varphi}\\0\\0\end{bmatrix} + \vec{e}^{\,B^T}\begin{bmatrix}1&0&0\\0&C(\varphi)&-S(\varphi)\\0&S(\varphi)&C(\varphi)\end{bmatrix}^T\begin{bmatrix}0\\\dot{\theta}\\0\end{bmatrix} + \vec{e}^{\,B^T}\begin{bmatrix}1&0&0\\0&C(\varphi)&-S(\varphi)\\0&S(\varphi)&C(\varphi)\end{bmatrix}^T\begin{bmatrix}C(\theta)&0&S(\theta)\\0&1&0\\-S(\theta)&0&C(\theta)\end{bmatrix}^T\begin{bmatrix}0\\0\\\dot{\psi}\end{bmatrix}$$

$$\vec{\omega}_B = \vec{e}^{\,B^T}\begin{bmatrix}\dot{\varphi}\\0\\0\end{bmatrix} + \vec{e}^{\,B^T}\begin{bmatrix}1&0&0\\0&C(\varphi)&S(\varphi)\\0&-S(\varphi)&C(\varphi)\end{bmatrix}\begin{bmatrix}0\\\dot{\theta}\\0\end{bmatrix} + \vec{e}^{\,B^T}\begin{bmatrix}1&0&0\\0&C(\varphi)&S(\varphi)\\0&-S(\varphi)&C(\varphi)\end{bmatrix}\begin{bmatrix}C(\theta)&0&-S(\theta)\\0&1&0\\S(\theta)&0&C(\theta)\end{bmatrix}\begin{bmatrix}0\\0\\\dot{\psi}\end{bmatrix}$$

$$\vec{\omega}_B = \vec{e}^{\,B^T}\begin{bmatrix}\dot{\varphi}\\0\\0\end{bmatrix} + \vec{e}^{\,B^T}\begin{bmatrix}0\\\dot{\theta}C(\varphi)\\-\dot{\theta}S(\varphi)\end{bmatrix} + \vec{e}^{\,B^T}\begin{bmatrix}C(\theta)&0&-S(\theta)\\S(\varphi)S(\theta)&C(\varphi)&S(\varphi)C(\theta)\\C(\varphi)S(\theta)&-S(\varphi)&C(\varphi)C(\theta)\end{bmatrix}\begin{bmatrix}0\\0\\\dot{\psi}\end{bmatrix}$$

$$\vec{\omega}_B = \vec{e}^{\,B^T}\begin{bmatrix}\dot{\varphi}\\0\\0\end{bmatrix} + \vec{e}^{\,B^T}\begin{bmatrix}0\\\dot{\theta}C(\varphi)\\-\dot{\theta}S(\varphi)\end{bmatrix} + \vec{e}^{\,B^T}\begin{bmatrix}-\dot{\psi}S(\theta)\\\dot{\psi}S(\varphi)C(\theta)\\\dot{\psi}C(\varphi)C(\theta)\end{bmatrix}$$

$$\vec{\omega}_B = \vec{e}^{\,B^T}\begin{bmatrix}1&0&-S(\theta)\\0&C(\varphi)&S(\varphi)C(\theta)\\0&-S(\varphi)&C(\varphi)C(\theta)\end{bmatrix}\begin{bmatrix}\dot{\varphi}\\\dot{\theta}\\\dot{\psi}\end{bmatrix}$$

$$\vec{\omega}_B = \underline{J}_2^{-1}\vec{\omega}_W \qquad \text{with} \qquad \underline{J}_2^{-1} = \begin{bmatrix}1&0&-S(\theta)\\0&C(\varphi)&S(\varphi)C(\theta)\\0&-S(\varphi)&C(\varphi)C(\theta)\end{bmatrix}$$

$$\underline{J}_2 = \begin{bmatrix}1&S(\varphi)T(\theta)&C(\varphi)T(\theta)\\0&C(\varphi)&-S(\varphi)\\0&S(\varphi)/C(\theta)&C(\varphi)/C(\theta)\end{bmatrix}$$

Appendix B

B Design of the AUV

The design of the AUV is separated into a mechanical and an electrical part. The mechanical part of the AUV consists of: the design of the hull, the materials that are selected, the waterproof sealing, the inner sliding mechanism, the buoyancy system and depth control, and, the propulsion and steering mechanism. The electrical part consists of: the power supply, the central processing unit, sensors and motor controllers. More information about the design of the AUV and comparison of different design aspects can be found in [5].

B.1 Hull Design

The hull of an AUV houses the electrical systems of the AUV waterproof. The hull, needs to have enough room for the electrical systems (and future expansion), has to have a good accessibility, needs to be corrosion resistant, has to be able to withstand an impact and at the same time needs to be capable of withstanding the water pressure.

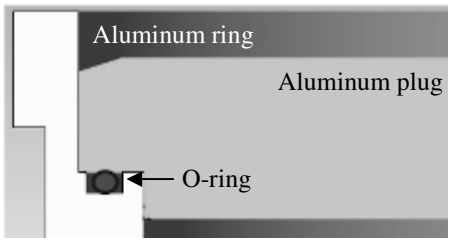

Figure B.1: Cross-section of the end cap, note the o-ring sealing of the AUV hull

A cylindrical shape is chosen for the hull because it has a favorable geometry for both pressure and dynamic reasons, at the same time it offers also enough room for the electrical systems. The hull is made out of a thick PVC pipe which keeps the hull relatively cheap, corrosion free and able to withstand an impact. The PVC pipe is closed with two aluminum end caps. The cap consists of an aluminum ring which is permanently fixed to the hull and a removable aluminum plug. Sealing between the ring and the plug is ensured by an o-ring, see Figure B.1. Sealing is provided in the axial direction of the PVC pipe which means that water pressure will ensure more tension on the sealing area when the vehicle is submerged, since the water pressure will press the end caps against the PVC pipe. A transparent sphere of synthetic material is implemented in one end cap. In this way a webcam, which is mounted inside the hull, can deliver an underwater view. The transparent sphere is also useful to see warning lights of the central processing unit from outside the hull. The complete assembly of the hull can be seen in Figure B.2.

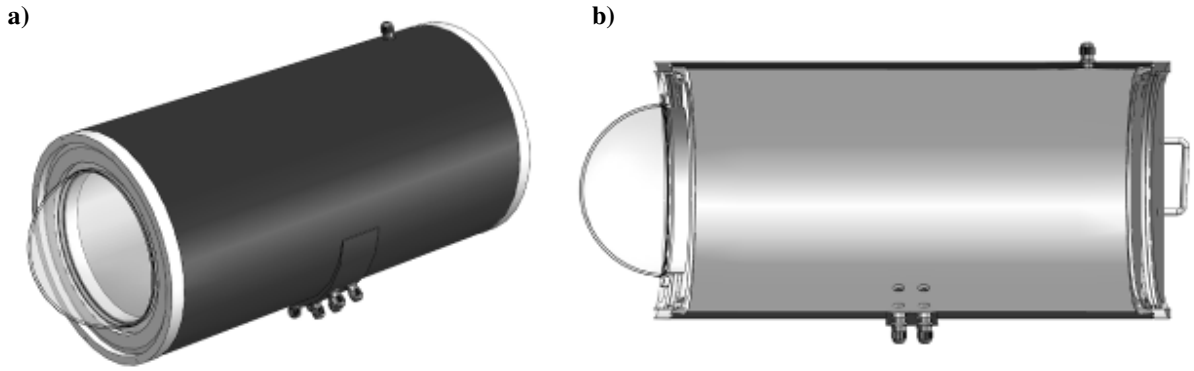

Figure B.2: Final assembly of the AUV hull. a) 3D view. b) Cross-section.

B.2 Buoyancy System

The AUV buoyancy system is based on a dynamic diving method. This method requires the AUV to be slightly positively buoyant, vertically mounted thrusters will then control the depth of the AUV. A drawback of this method is the large energy consumption the system will need to control depth, since thrusters must remain powered to keep the AUV submerged. An advantage of this system is that when the thrusters are switched off buoyancy will ascend the vehicle, which means that the vehicle will surface itself when there are electrical problems. Other advantages of this method lay in the economic reasoning, for example, there are no complex sealing methods needed for depth control. A further explanation about different buoyancy systems and depth control methods can be found in [5].

B.3 Propulsion and Steering

The propulsion or thrust of the AUV is delivered by six trolling motors, two horizontally mounted and four vertically mounted. The horizontal motors ensure motion in the *surge* and *yaw* directions[*]. The vertical motors ensure stability (in the *roll* and *pitch* directions) and motion (in the *heave* direction). The position of the motors on the AUV can be seen in Figure B.3.

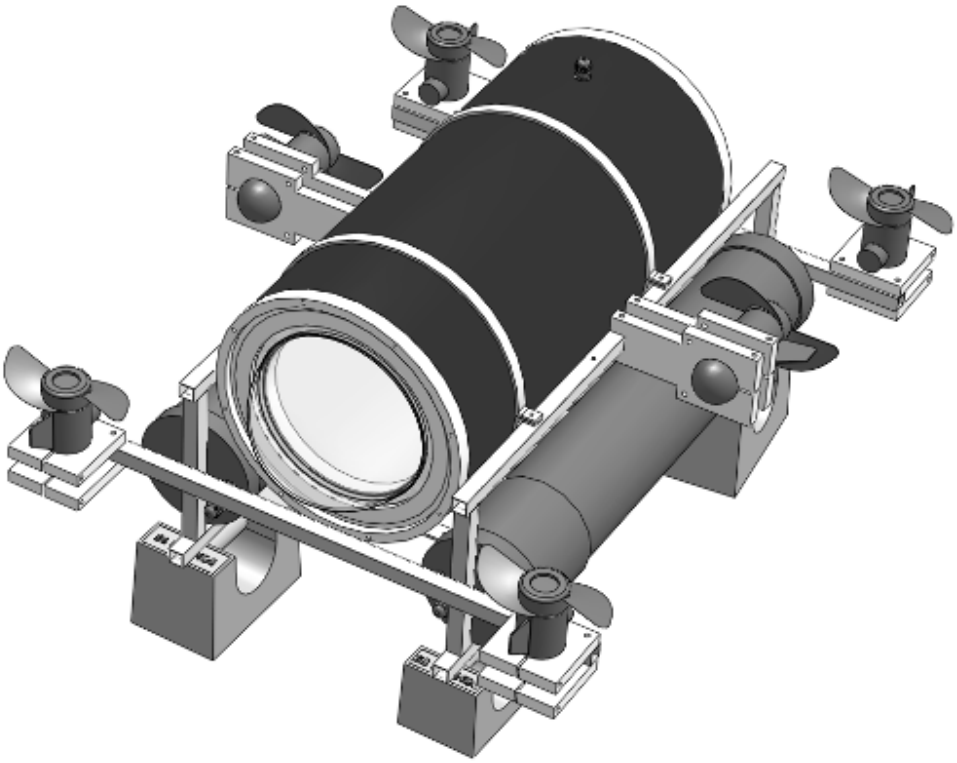

Figure B.3: The 3D image made in Solid Works showing the final assembly of the AUV

The trolling motors used are 12 V DC motors. The force output of the trolling motor with respect to the duty cycle of the Roboteq controller is measured to determine the thruster characteristics. Therefore the trolling motor is mounted in a test rig with a load cell and strain gauge amplifier. Every trolling motor used is tested to account for minor abnormalities between different motors. The test results of the trolling motors are given in Figure B.4. In the voltage to duty cycle diagram can be seen that there is small abnormality between the trolling motors. Although this small abnormality exists the team

[*] If the reader is not familiar with the *surge*, *sway*, *heave*, *roll*, *pitch* and *yaw* notation, which are the six degrees of freedom of the AUV, a further explanation of these terms can be found in Chapter 2.

decided to use the same force to duty-cycle curve for every trolling motor. The force to duty-cycle curve can be seen in Figure B.4 is calculated with the calibration of the load cell and strain gauge amplifier. Note that the force to duty-cycle diagram is linear with a duty-cycle offset of ±10%. The offset is caused by the static friction of the propeller. More information is given in Appendix D.1.

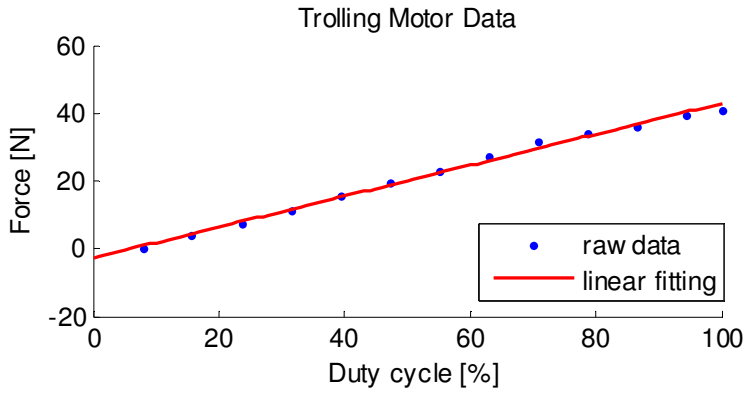

Figure B.4.a: The force to duty cycle used for all trolling motors is given. b) The voltage to duty cycle data is displayed for all trolling motors.

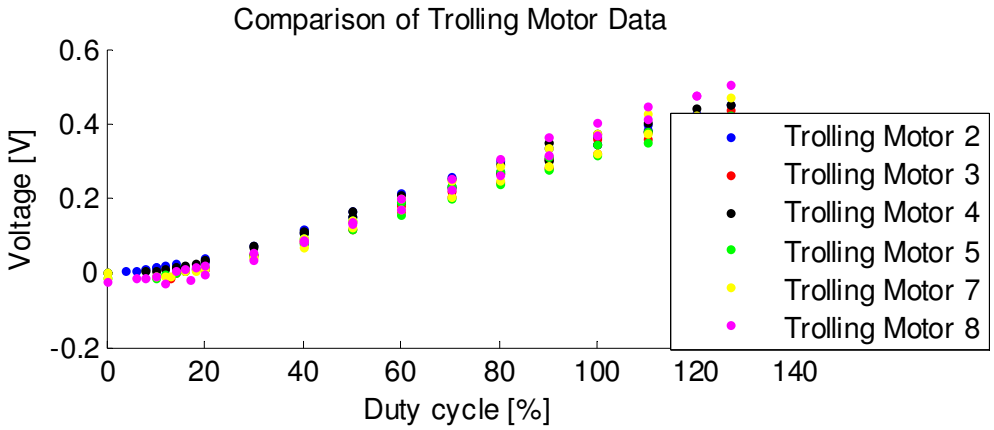

Figure B.4.b: The voltage to duty cycle data is displayed for all trolling motors.

B.4 Power System

Sealed lead acid (SLA) batteries are chosen for the onboard power supply of the AUV. The advantage of these batteries is that they have a high capacity, deliver a high current, are mechanical robust and work in every orientation. A drawback is that they have a high weight to capacity ratio compared to other types of batteries. In order to

supply enough current five batteries are parallel connected on an aluminum bus, see Figure B.5. The AUV has three different battery compartments, one in the main hull and two external tube battery compartments. Every compartment has 5 parallel connected batteries. The benefit of using two tube battery compartments is that, when operating in field, it is easier to interchange the batteries. The two tube battery compartments are used to power the trolling motors and the main hull battery is used to power the onboard electrical equipment. The SLA battery from Exide Powergard delivers 12 V and has a 12 AH@10 hrs current.

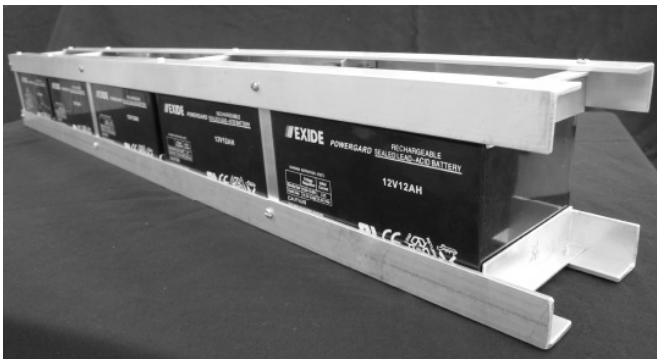

Figure B.5: Five parallel connected batteries which together form one battery compartment housed in an aluminum bus.

B.5 Central Processing Unit

The central processing unit in the AUV is responsible for accessing sensors, processing data and setting control outputs. An ADM Sempron 3000+ processor and Asus M2N-PV motherboard are used to form this central processing unit, see Figure B.6. This processing unit delivers adequate processing power, has enough connection ports for the diverse range of peripherals and has an ethernet module for a remote control connection.

Figure B.6: ADM sempron 3000+ processor and Asus M2N-PV motherboard, forming the central processing unit of the AUV.

B.6 Motor Controllers

Three Roboteq AX2500 motor controllers, see Figure B.7, are used to control the trolling motors. The controller is able to control motors up to 120 amps. This is more than enough to control the trolling motors used on the AUV, which only need 25 amps. For future expansion an over specified controller is chosen. The controller uses a 7 bit interface, is connected via a RS232 serial port and a C++ library is written to change the motor controller to either manual or automated control programs. Detailed specifications of the Roboteq controller can be found on the website of the manufacturer.

Figure B.7:.Roboteq controller used to control the trolling motors of the AUV.

B.7 Sensors

B.7.1 Depth Sensor

The depth sensor, see Figure B.8, is used to determine the vertical position or depth of the AUV. The depth sensor chosen is a Bürkert pressure transmitter with a range from 0 to 1 bar (where the pressure reference is relative pressure [atmospheric]). This means that the pressure sensor is able to measure the depth of the AUV up to 10 meters underwater, which is enough for pool experiments but it will need to be replaced if deep water experiments are performed. The specifications of the depth sensor are given in Table B.1, further specifications can be found on the website of the manufacturer.

Figure B.8:.The pressure sensor of the AUV.

Pressure range	Accuracy	Pressure max.	Bursting pressure	Power supply	Output signal
0-1[bar]	≤ 0.005 [bar]	5[bar]	5 [bar]	10-30V DC	4…20mA

Table B.1: Specifications of the Bürkert pressure transmitter

B.7.2 IMU, Inertial Measurement Unit

The Mircostrain 3DM-GX1 IMU combines three angular rate gyros with three orthogonal DC accelerometers, three orthogonal magnetometers, multiplexer, 16 bit A/D converter, and embedded microcontroller, to output its orientation in dynamic and static environments. The IMU can operate over the full 360 degrees of angular motion on all three axes. The IMU provides orientation in matrix, quaternion and Euler formats. The digital serial output can also provide temperature compensated calibrated data from all nine orthogonal sensors at update rates of 350 Hz. The IMU can be seen in Figure B.9.

Figure B.9:.The IMU of the AUV.

By measuring the current angular and linear acceleration of the vehicle, it is possible to determine the linear acceleration of the vehicle in the inertial reference frame. Performing integration on the inertial accelerations using the correct kinematic equations yields the inertial velocities of the system, and integration again yields the inertial position.

All inertial navigation systems suffer from integration drift. Small errors in the acceleration measurement are integrated into progressively larger errors in velocity,

which is compounded into still greater errors in position. This is a inherent problem in every open loop control system.

The specifications of the IMU are given in Table B.1, detailed specifications can be found on the website of the manufacturer.

Orientation range (Pitch, Roll, Yaw)	360° all axes (orientation matrix, quarternion) ± 90°, ± 180°, ± 180° (Euler angles)
Sensor range	Gyros: ± 300°/sec FS Accelerometers: ± 5 g Magnetometers: ± 1.2 Gauss FS
A/D resolution	16 bits
Accelerometer nonlinearity Accelerometer bias stability	0.2% 0.010 g
Gyro nonlinearity Gyro bias stability	0.2% 0.7°/sec
Magnetometer nonlinearity Magnetometer bias stability	0.4% 0.010 Gauss
Orientation resolution	<0.1° minimum
Repeatability	0.20°
Accuracy	0.5° typical for static test conditions 2.0° typical for dynamic (cyclic) test conditions & for arbitrary orientation angles
Digital output rates	100Hz for Euler, Matrix, Quaternion 350Hz for none orthogonal sensors only

Table B.2: Specifications for the Mircostrain IMU

B.8 Inner-Sliding-Mechanism

The inner-sliding-mechanism for the autonomous underwater vehicle designed by J.H.A.M. Vervoort (author) and made by J.H.A.M. Vervoort and R.C. Engelaar is used for an easy mounting/dismounting of the electronic-systems in the AUV. The mechanism will save installing time and will protect the electronic systems from damage. The electronic systems on the tray can be connected to the thrusters and batteries on the AUV with a simple plug and socket connector.

The inner-sliding-mechanism consists of two metal strips mounted along the length of the AUV, on both sides of the hull, and, a tray where all the electronics systems are mounted on. The tray will slide in the hull over the two strips, see Figure B.10.

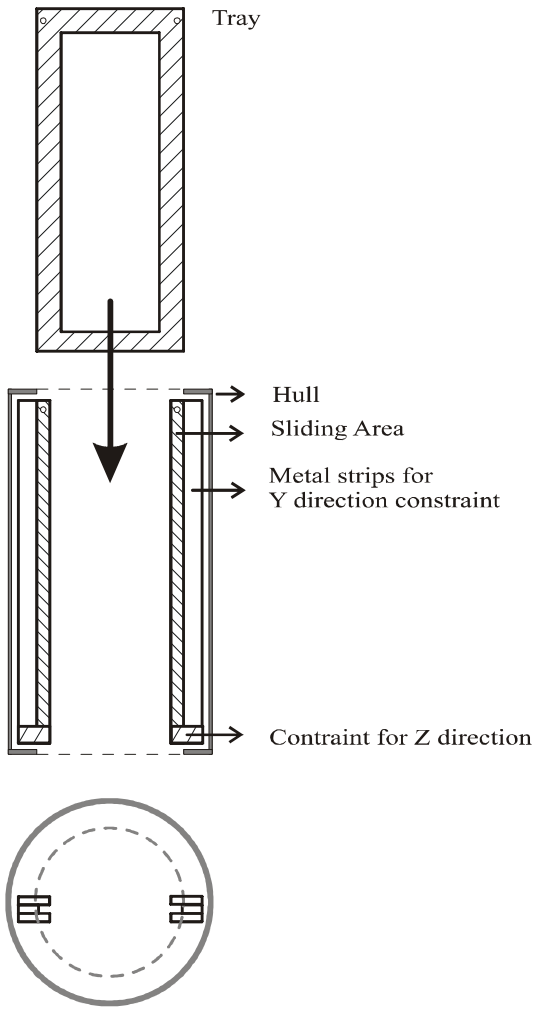

Figure B.10: Drawing of the inner-sliding-mechanism.

It is important that the tray of the sliding mechanism, when installed in the AUV, is constrained in all directions to prevent damage to the electronic systems and to prevent accelerometer measurement errors when the vehicle is moving. Along the length of the AUV a small metal strip is mounted on both sliding strips, to constrain motions in the Y direction. This constraint will also give support when sliding the tray in the vehicle to prevent collision of the electronic systems with the hull. The tray is constrained in the X and Z directions at the front end of the AUV with two metal strips and at the back end with two bolts. Bolts are only used on one side of the AUV, since it is desired to remove only one end cap of the AUV to install the tray.

The tray holds all electronics systems inside the hull of the AUV except for the inside batteries. It is possible to mount the inner batteries to the tray but this will make the tray unnecessarily heavy. The added weight could cause back injury to anyone

working with the tray, therefore the batteries are separately mounted to the hull of the AUV and can not be slided out of the vehicle. All other electronic systems are mounted on the tray. The tray has limited available space and all electronic systems have requirements. The processors on the motherboard need ventilation space for cooling, which means that nothing can be stored above the motherboard. The IMU measures the magnetic field of the earth which can be disrupted by the hard disk drive so these two can not be placed next to each other. The Roboteq controllers need cooling space and can therefore only be stacked with an inner space. The final implementation of all electronic systems on the tray can be seen in Figure B.11.

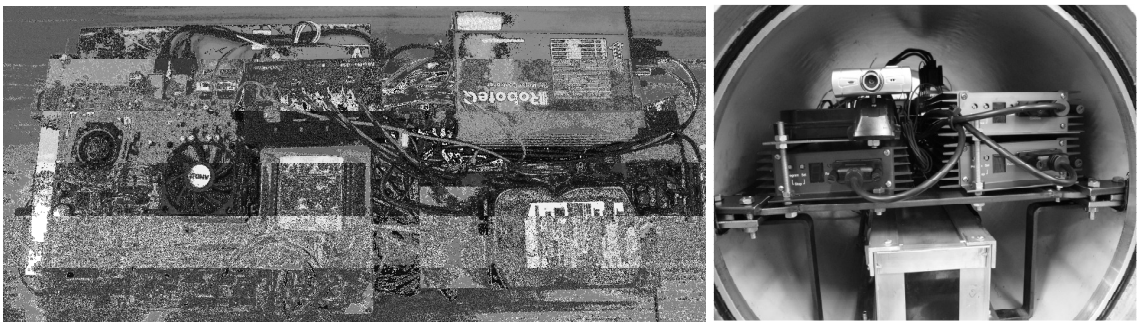

Figure B.11: Picture of the tray of the inner sliding mechanism.

Appendix C

C Dynamic Model Including Ocean Currents

The dynamic model (2.8) of the AUV did not include ocean currents. This dynamic model is sufficient to model the AUV for swimming pool experiments. But the final goal is to use the AUV in harbors and for this purpose it is interesting to see how the AUV will respond to environmental disturbances. The environmental disturbances of an AUV are ocean currents. Here wave induced currents are neglected because an AUV is deeply submerged. Ocean currents are horizontal and vertical circulating systems of ocean water, produced by gravity, wind friction and water density variation in different parts of the ocean [6]. Note that if the AUV is used in a sea harbor also tides can form a current.

The effect of ocean currents in six DOFs can be expressed with the use of relative motion in

$$\nu_r = \begin{bmatrix} u - u_c^b & v - v_c^b & w - w_c^b & p & q & r \end{bmatrix}^T \tag{C.1},$$

where u_c^b, v_c^b and w_c^b are body-fixed current velocities. The dynamic model including the ocean currents is given in

$$\underbrace{\underline{M}_{RB}\dot{\nu} + \underline{C}_{RB}(\nu)\nu}_{\text{rigid-body terms}} + \underbrace{\underline{M}_A\dot{\nu}_r + \underline{C}_A(\nu_r)\nu_r + \underline{D}(\nu_r)\nu_r}_{\text{hydrodynamic terms}} + \underbrace{\underline{g}(\eta)}_{\text{hydrostatic terms}} = \tau \tag{C.2}.$$

It is common to assume that the current velocity vector is slowly varying, which means that $\dot{\nu}_r \approx 0$. This simplifies the dynamic model (C.2) into

$$\underline{M}\dot{\nu} + \underline{C}_{RB}(\nu)\nu + \underline{C}_A(\nu_r)\nu_r + \underline{D}(\nu_r)\nu_r + \underline{g}(\eta) = \tau \tag{C.3}.$$

The ocean current speed is normally defined in the W-frame but can be transformed into the B-frame with the use of the transposed Euler angle rotation matrix given in equation (2.3).

Appendix D

D.1 Trolling Motor Model

The parameters of the one degree of freedom dynamical model (3.2) are estimated assuming that the input force/torque $\tau_{\dot{x}}$ is known. The voltage and duty cycle send to the trolling motors are measured during the experiment and the force provided by the trolling motors can be calculated with the use of

$$\tau_{\dot{x}} = 0.46 D_{cycle} - 2.76 \quad \text{(D.1)},$$

where D_{cycle} is the duty cycle percentage and $\tau_{\dot{x}}$ the force/torque term. The force to duty cycle properties of the trolling motors are determined in a separate experiment. The data retained from this experiment is given in Figure D.1. Note that the linear fitting equation (D.1) of the trolling motor data displayed is in Figure D.1. Note also that the force provided by the trolling motor is zero from 0 to 8% duty cycle, which means that (D.1) is only valid from 8 to 100% duty cycle.

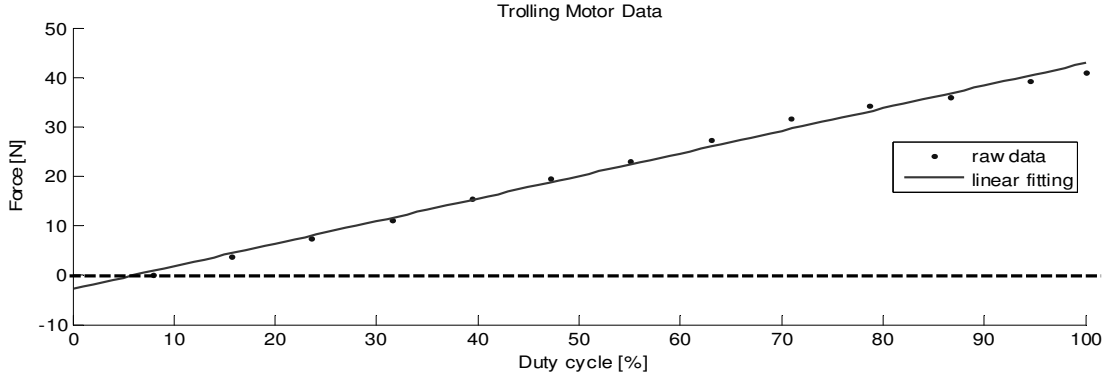

Figure D.1: The force to duty cycle properties of the trolling motors

A drawback of this method is that the thruster to thruster and the thruster to hull interaction that occurs while the vehicle is operating is not taken into account, since the force to duty cycle properties of the trolling motor are measured for each single trolling motor separately. This problem is solved by Goheen and Jefferys [67] by adding a trolling motor installation coefficient, $\eta_{\dot{x}}$, to the one degree of freedom dynamical model,

$$m_{\dot{x}}\ddot{x} = \eta_{\dot{x}}\tau_{\dot{x}} - d_{\dot{x}}\dot{x} - d_{\dot{x}|\dot{x}|}\dot{x}|\dot{x}| - g_{\dot{x}} \quad \text{(D.2)}.$$

In this way the reduction in the trolling motor force can be taken into account to have an even more accurate model. The installation coefficient can be tuned during the underwater experiments, but for now the assumption is made that $\eta_{\dot{x}}$ is equal to one.

Another assumption made in the trolling motor model is that the trolling motor is able to provide the same power running forwards and backwards. The difference in forward and backward power can be implemented into the model by choosing a different trolling motor efficiency coefficient for the forward and backward direction, but for now it is assumed that the forward and backward power is the same.

D.2 Static Experiment, Identification of the Damping Terms

In the static experiment a constant force/torque is provided by the trolling motors in the right mapping for the specific degree of freedom. The experiment starts when the steady state condition is reached, where velocity is constant and the acceleration zero. Under steady state conditions the dynamic model (3.2) changes into

$$0 = \tau_{\dot{x}} - d_{\dot{x}}\dot{x} - d_{\dot{x}|\dot{x}|}\dot{x}|\dot{x}| - g_{\dot{x}}, \qquad Where\ \ddot{x} = 0 \tag{D.3}$$

Note that $\ddot{x} = 0$, which means that the $m_{\dot{x}}$ term is canceled out off the dynamic model. The force/torque term $\tau_{\dot{x}}$ and the gravitational and buoyancy term $g_{\dot{x}}$ are fully known parts of (D.3), for a proper least square estimation (D.3) is rewritten into

$$\underbrace{\tau_{\dot{x}} - g_{\dot{x}}}_{y} = \underbrace{\begin{bmatrix} \dot{x} & \dot{x}|\dot{x}| \end{bmatrix}}_{X} \underbrace{\begin{bmatrix} \alpha & \beta \end{bmatrix}^T}_{\theta} + \underbrace{\varepsilon}_{\varepsilon} \tag{D.4}$$

The unknown parameters of D.4 are the linear and quadratic drag coefficients, which can be estimated with use of the least square technique. For an explanation of the least square technique and the application of the least square technique on the dynamical model (D.4) one is referred to Appendix E.

D.3 Dynamic Experiment, Identification of the Mass and Inertia Term

In the dynamic experiment a sinusoidal force/torque in one specific degree of freedom is applied to the AUV. The only unknown parameter left is the inertia and mass term, $m_{\dot{x}}$, since the drag parameters are already identified in the static experiment. The one degree of freedom dynamic model (4.2) changes into

$$\underbrace{\tau_{\dot{x}} - d_{\dot{x}}\dot{x} - d_{\dot{x}|\dot{x}|}\dot{x}\left|\dot{x}\right| - g_{\dot{x}}}_{y} = \underbrace{\ddot{x}}_{X}\underbrace{m_{\dot{x}}}_{\theta} + \varepsilon \qquad \text{(D.5)},$$

where the known terms, *y,* are formed by $\tau_{\dot{x}}$, $g_{\dot{x}}$, $d_{\dot{x}}$ and $d_{\dot{x}|\dot{x}|}$, and the unknown term, θ, is $m_{\dot{x}}$. The unknown term can be estimated with the use of the least square technique which is explained in Appendix E.

Appendix E

E.1 Least Squares Technique

The least squares (LS) technique is a frequently used approach to solve (approximate) over-determined or inexactly specified systems of equations [68]. Instead of solving the equations exactly the LS technique minimizes the sum of residuals. This subsection explains the LS technique, gives the normal equations in matrix form (which are needed to estimate the unknown parameter) and provides the standard deviation of the estimated parameters and parameter error equations. More information about the LS technique can be found in [17, 45, 51, 56, 66, 68].

Let *t* be the independent variable and let *y(t)* denote an unknown function of *t* that needs to be approximated. Assume that there are *m* observations, i.e. values of *y* measured at specified values of *t*,

$$y_i = y(t_i), \qquad i = 1,...,m \tag{E.1}$$

The idea is to model *y(t)* by a linear combination of *n* basis functions,

$$y(t) \approx \theta_1 \phi_1(t) + ... + \theta_n \phi_n(t) \tag{E.2}$$

The design matrix, $x_{i,j} = \phi_j(t_i)$, is a rectangular matrix of order *m* by *n*, which normally has more rows than columns. The matrix-notation of E.2 is given by

$$y \approx X\theta \tag{E.3}$$

After an experiment there are more equations than unknowns, so the system is over-determined, which means that the system can not be solved exactly. The goal of the least square estimation is now to find the values $\hat{\theta}_j$, which fit the equations best. In other words, it has to find the minimum possible value of the sum of squares of the residuals. The residuals are the differences between the observations and the model, given by

$$r_i = y_i - \sum_{1}^{n} \hat{\theta}_j x_{i,j}, \qquad i = 1,...,m \tag{E.4}$$

or in matrix notation given by

$$r = y - X\hat{\theta} \tag{E.5}$$

The least square method minimizes the sum of squares of the residuals, which is given by

$$\|r\|^2 = \sum_{1}^{m} r_i^2 \tag{E.6}$$

$\|r\|^2$ is minimized when its gradient with respect to each parameter is equal to zero, this is defined by

$$\frac{\partial \|r\|^2}{\partial \hat{\theta}_j} = 2\sum_{i}^{m} r_i \frac{\partial r_i}{\partial \hat{\theta}_j} = 0, \qquad \text{i} = 1,...,m, \qquad j = 1,...,n$$

Where: $\dfrac{\partial r_i}{\partial \hat{\theta}_j} = -x_{i,j}$ (E.7).

Substitution of (E.4) in (E.7) gives

$$\frac{\partial \|r\|^2}{\partial \hat{\theta}_j} = -2\sum_{i=1}^{m} x_{i,j}\left(y_i - \sum_{j=1}^{n} \hat{\theta}_j x_{i,j} \right) = 0 \tag{E.8}$$

and rearrangement gives

$$\sum_{i=1}^{m}\sum_{j=1}^{n} x_{i,j} x_{i,j} \hat{\theta}_j = \sum_{i=1}^{m} x_{i,j} y_i \tag{E.9},$$

which form the normal equations of the least square estimation. The normal equations written in matrix notation are given by

$$\left(X^T X\right)\hat{\theta} = X^T y \tag{E.10}.$$

So the estimate of the parameters can be found from

$$\hat{\theta} = \left(X^T X\right)^{-1} X^T y \tag{E.11}.$$

Note that to invert the normal equations matrix, the $X^T X$ matrix needs to be well-conditioned and positive definite, the $X^T X$ matrix has to have full rank. The standard deviation of this estimated parameter is computed [17] with

$$\hat{\sigma}_\theta = \sqrt{\text{diag}\left(\left(X^t X\right)^{-1} \sigma_\varepsilon^2\right)} \tag{E.12},$$

where $\hat{\sigma}^2$ is the estimated Gaussian zero mean measurement noise variance, which is defined by

$$\hat{\sigma}_{\varepsilon}^{2} = \frac{\left(Y - X\hat{\theta}\right)^{T}\left(Y - X\hat{\theta}\right)}{\dim(Y) - \dim(\theta)} \qquad \text{(E.13).}$$

The standard deviation and estimate of the parameters can be used to determine the parameter relative percentile error, which is defined by

$$\varsigma = 100\frac{\hat{\sigma}_{\theta}}{\left|\hat{\theta}\right|} \qquad \text{(E.14),}$$

where Indiveri [17] gives the following explanation for *statistically insignificancy*:

"*If the parameter variance is too large the parameter itself is said to be statistically insignificant and it might just as well be put to zero. More precisely given the two hypothesis* h_0 *and* h_1 *:*

$$\left.\begin{array}{l} h_0 : \theta_i = 0 \\ h_1 : \theta_i \neq 0 \end{array}\right\} \text{such that } p(\textit{accept } h_1 \mid h_0 \textit{ true}) \;=\; \alpha$$

Being θ_i *normaly distributed with the standard deviation* σ_{θ_i} *and* α *some arbitrary constant (usually 5%), the hypothesis is accepted if* $\frac{\left|\hat{\theta}_i\right|}{\hat{\sigma}_{\theta_i}} > c(\alpha)$ *being* $c = 1.96$ *if* $\alpha = 5\%$ *.*

In percentile notation it can be said that if the parameter relative percentile error ς *is larger than 51.02%, see 4.19, there is a 95% confidence limit that the parameter itself is statistically insignificant and the hypothesis* $h_0 : \theta_i = 0$ *is better to be accepted.*

$$100\frac{\hat{\sigma}_{\theta}}{\left|\hat{\theta}\right|} > \frac{100}{1.96}\% \rightarrow \varsigma > 51.02\% \qquad \textit{(E.15)"}$$

E.2 Least Square Applied

The LS technique explained above can be applied on the one degree of freedom dynamical model (4.2), to estimate the inertia and drag parameters, $m_{\dot{x}}, d_{\dot{x}}$ and $d_{\dot{x}|\dot{x}|}$ for each degree of freedom. The one degree of freedom dynamical model can be rewritten into

$$\ddot{x} = \gamma\left(\tau_{\dot{x}} - g_{\dot{x}}\right) + \alpha\dot{x} + \beta\dot{x}\left|\dot{x}\right| + \varepsilon \qquad \text{(E.16),}$$

where α, β and γ are defined by

$$\alpha = -\frac{d_{\dot{x}}}{m_{\dot{x}}} \tag{E.17},$$

$$\beta = -\frac{d_{\dot{x}|\dot{x}|}}{m_{\dot{x}}} \tag{E.18}$$

and

$$\gamma = \frac{1}{m_{\dot{x}}} \tag{E.19},$$

Respectively, and ε is a measurement noise term. Note that $m_{\dot{x}}$ defines the rigid body and added mass, for $surge: m_{\dot{x}} = m - X_{\dot{u}}$, for $heave: m_{\dot{x}} = m - Z_{\dot{w}}$ and for $yaw: m_{\dot{x}} = m - N_{\dot{r}}$. Note also that $g_{\dot{x}}$ is zero for the *surge* and *yaw* degrees of freedom.

The dynamic model (E.16) rewritten into a matrix form gives

$$\ddot{x} = \begin{bmatrix} \dot{x} & \dot{x}|\dot{x}| & \tau_{\dot{x}} - g_{\dot{x}} \end{bmatrix} \begin{bmatrix} \alpha & \beta & \gamma \end{bmatrix}^T + \varepsilon \tag{E.20}.$$

If a decoupled experiment is run with N samples, (E.20) expands to N rows as can be seen in

$$\underbrace{\begin{bmatrix} \ddot{x}_1 \\ \ddot{x}_2 \\ \vdots \\ \ddot{x}_N \end{bmatrix}}_{y} = \underbrace{\begin{bmatrix} \dot{x}_1 & \dot{x}|\dot{x}|_1 & \tau_{\dot{x},1} - g_{\dot{x},1} \\ \dot{x}_2 & \dot{x}|\dot{x}|_2 & \tau_{\dot{x},2} - g_{\dot{x},2} \\ \vdots & \vdots & \vdots \\ \dot{x}_N & \dot{x}|\dot{x}|_N & \tau_{\dot{x},N} - g_{\dot{x},N} \end{bmatrix}}_{X} \cdot \underbrace{\begin{bmatrix} \alpha_1 & \beta_1 & \gamma_1 \\ \alpha_2 & \beta_2 & \gamma_2 \\ \vdots & \vdots & \vdots \\ \alpha_N & \beta_N & \gamma_N \end{bmatrix}}_{\theta} + \underbrace{\begin{bmatrix} \varepsilon_1 \\ \varepsilon_2 \\ \vdots \\ \varepsilon_N \end{bmatrix}}_{\varepsilon} \tag{E.21},$$

which now has the same form as E.3. Now the LS estimation can be applied on E.21 to estimate the vector of unknowns θ.

Appendix F

F Remote Control

The AUV needs to be remotely controlled in order to execute the static and dynamic experiments. The remote control has to enable the correct thrusters and set up predefined thrust levels to move the AUV in one specific degree of freedom, so one is able to estimate the parameters of this degree of freedom.

The program “LabVIEW” is used to write the software to remotely control the AUV. The software developed communicates with the RoboteQ motor controllers, and is able to specify the direction and power of thrust of all six trolling motors. Next to this the software performs voltage and current output readings and keeps track of the temperature of both RoboteQ motor controllers. The software for the Roboteq controllers is written by T.Patterson, H.Rogers, D.Hewett, F.McKenzie and B.Burnell, final year bachelors students of the University of Canterbury [94]. A visual programming technique is used in LabVIEW by creating Virtual Instruments (VIs) which can either stand alone or depend on other VIs. An example of visual programming can be seen in Figure F.1.

Next to the RoboteQ motor controller software, software is written to setup the sensors and store sensor data in an array form. Software to read the pressure from the depth sensor is written by the bachelor students named above and the LabVIEW code is calibrated according to the manual. The IMU is a digital sensor and has its own software to read the analog signals from the different sensors within the IMU. LabVIEW software needs to send a data request signal (in 7 bit format) which is followed by a reply of the sensor containing the demand data. The LabVIEW software to configure and read the data from the IMU is made by the author of this paper, J.H.A.M.Vervoort, with the use of existing LabVIEW software provided by the manufacturer of the IMU “Microstrain” and can be seen in Figure F.1.

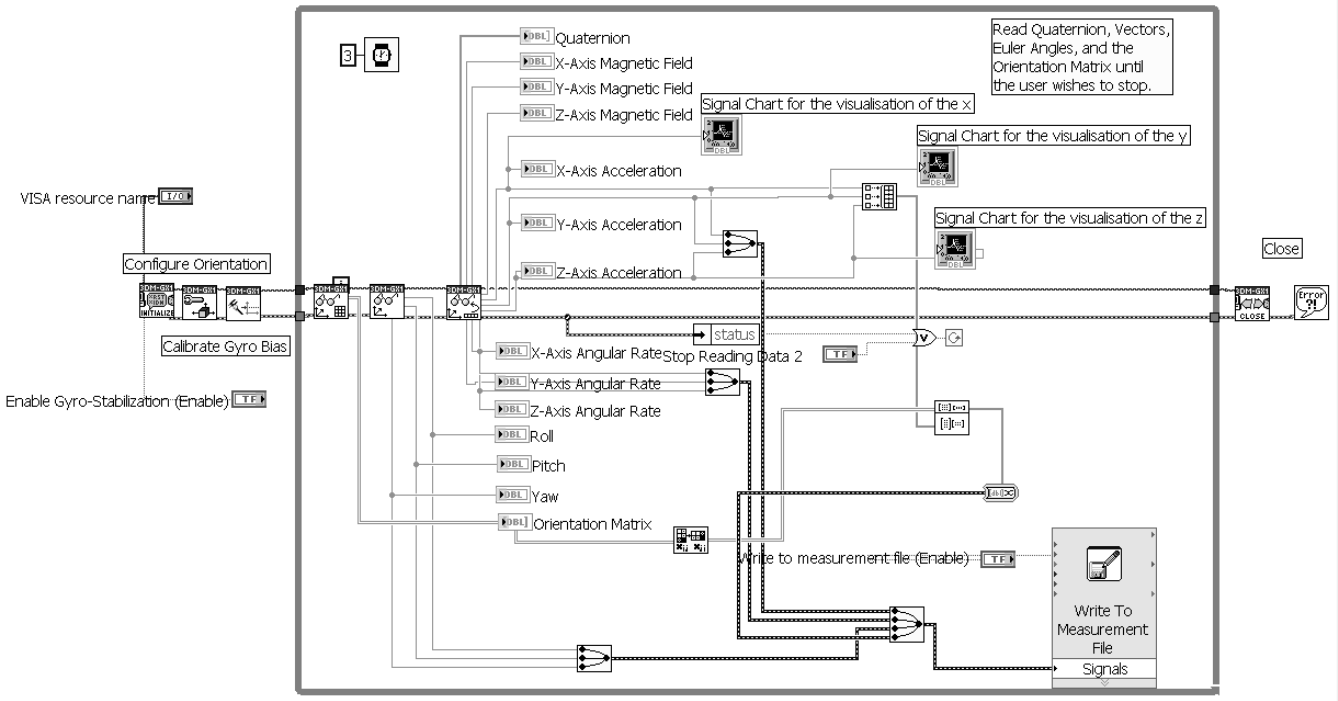

Figure F.1: VI for configuring and reading data from the IMU.

The LabVIEW software is able to read the data from the IMU with a maximum sampling rate of 12 Hz which is significantly lower than the sampling rate reached by the standalone software from Microstrain which reaches a sampling rate of 100 Hz. The rather complicated but necessary LabVIEW code which is used for interaction between the IMU and the program causes the drop in maximum sampling rate. The data obtained by LabVIEW consists of the acceleration in the *u*, *v* and *w* directions, the angular rates of *roll*, *pitch* and *yaw*, and, the angle in *roll*, *pitch* and *yaw* between the earth fixed frame and the body fixed frame. All this data is stored in a ".lvm" file which can be read by a Matlab m-file written by J.H.A.M.Vervoort and R.C.Engelaar. The m-file reads the data from the .lvm file, transforms the data to the earth fixed frame and filters the data with a low pass hamming filter and afterwards plots the obtained data. The m-file is given in Appendix D.

A general user interface (GUI) is made in combination with the LabVIEW software, so the operator of the AUV is able to easily define the thrust power and set-points for all degrees of freedom, read all the RoboteQ controller outputs and can keep track of all sensor information, see Figure F.2 for a visual impression of this interface.

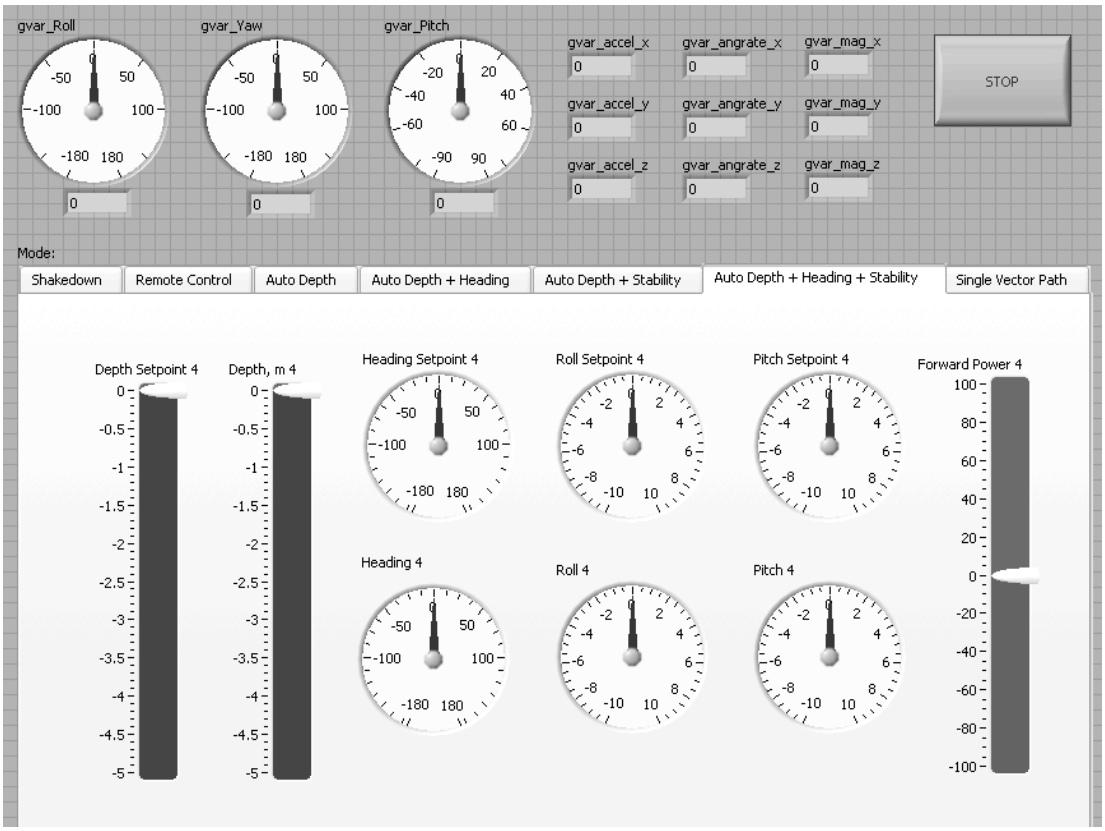

Figure F.2: The GUI developed to remotely control the AUV.

Appendix G

G.1 Input-output linearization

The choice for the state feedback control law *u* given in (4.7) can be confirmed by the input-output linearization of the state equation (4.6), which is already in normal form. For the input-output linearization it is important to know the relative degree of the nonlinear system. The relative degree ρ is the number of times the output *y* has to be differentiated before the input *u* appears. The relative degree can be determined with the use of a definition defined by H.K.Khalil [74], see Appendix G.2, note that this definition makes use of *Lie Derivatives*. If the relative degree of the nonlinear system is known then the state feedback control *u* can be determined with

$$u = \frac{1}{L_g L_f^{\rho-1} h(x)} \left[-L_f^{\rho} h(x) + v \right] \qquad \text{(G.1)},$$

where $L_g L_f h(x) = \frac{\partial \left(L_f h \right)}{\partial x} g(x)$ with $L_f h = \frac{\partial h}{\partial x} f(x)$ and $L_f^2 h(x) = \frac{\partial \left(L_f h \right)}{\partial x} f(x)$. Here the notation of H.K.Khalil is used in combination with the *Lie Derivatives*.

The relative degree of the state equation is determined by the differentiation of the output, which results in

$$y = x_1 \qquad \text{(G.2.a)},$$

$$\dot{y} = \dot{x}_1 = x_2 \qquad \text{(G.2.b)},$$

$$\ddot{y} = \dot{x}_2 = -a x_2 - b x_2 \left| x_2 \right| + du \qquad \text{(G.2.c)},$$

where the input *u* appears in $\ddot{y}$, $\rho = 2$, which also verified by the definition of H.K.Khalil in Appendix G.3.

With the relative degree known the state feedback control law *u* can be determined with the use of (G.1), which gives

$$u = \frac{1}{L_g L_f h(x)} \left(-L_f^2 h(x) + v \right) = \frac{1}{d} \left(a x_2 + b x_2 \left| x_2 \right| + v \right) \qquad \text{(G.3)},$$

where $L_g L_f h(x) = d$, $L_f h = x_2$ and $L_f^2 h(x) = -a x_2 - b x_2 \left| x_2 \right|$. The state feedback control law (G.3) is similar to (4.7) and reduces the input-output map to $\ddot{y} = v$. This means that the state equation (4.6) is indeed input-output linearizable. Note that the relative degree is

similar to the number of states, $\rho = n$, which means that there are no internal dynamics. The system has no zero dynamics and by default is said to be minimum phase [73 74].

G.2 The definition of Khalil

[Khalil [74], "Nonlinear Systems", Third edition, Definition 13.2]

The nonlinear system is said to have a relative degree ρ, $1 \le \rho \le n$, in a region $D_0 \subset D$ if

$$L_g L_f^{i-1} h(x) = 0, \quad i = 1, 2, \ldots, \rho - 1; \quad L_g L_f^{\rho-1} h(x) \neq 0 \tag{G.4}$$

for all $x \in D_0$ □

G.3 The definition of Khalil applied

[Khalil [74], "Nonlinear Systems", Third edition, Definition 13.2]

The definition of Khalil applied to calculate the relative degree of the state equation (4.6):

$$L_g L_f^{i-1} h(x) = L_g h(x) = \frac{\partial h}{\partial x} g(x) = \frac{\partial h}{\partial x_2} d = 0, \qquad i = \rho - 1 = 1 \tag{G.5}$$

$$L_g L_f^{\rho-1} h(x) = L_g L_f h(x) = \frac{\partial \left(L_f h \right)}{\partial x} g(x) = d \neq 0, \quad \rho = 2 \tag{G.6}$$

G.4 Eigenvalue determination

Calculations to prove that (4.13) is only Hurwits for $k_1 > 0$ and $k_2 > 0$:

$$\det(A - KB - \lambda I) = 0 \tag{G.7}$$

Where $A - BK = \begin{bmatrix} 0 & 1 \\ 0 & 0 \end{bmatrix} - \begin{bmatrix} 0 & 0 \\ k_1 & k_2 \end{bmatrix} = \begin{bmatrix} 0 & 1 \\ -k_1 & -k_2 \end{bmatrix}$

$$\det\left(\begin{bmatrix} -\lambda & 1 \\ -k_1 & -k_2-\lambda \end{bmatrix}\right)=0 \tag{G.8}$$

$$\lambda\left(k_2+\lambda\right)+k_1=0 \tag{G.9}$$

$$\lambda^2+k_2\lambda+k_1=0 \tag{G.10}$$

$$\lambda_{1,2}=-\frac{1}{2}k_2\pm\frac{1}{2}\sqrt{\left(k_2\right)^2-4k_1} \tag{G.11}$$

G.5 Lyapunov's stability theorem

[Khalil [74], "Nonlinear Systems", Third edition, Theorem 4.1]

Let $x=0$ be an equilibrium point for $\dot{x}=f(x)$ and $D\subset R^n$ be a domain containing $x=0$. Let $V:D\to R$ be a continuously differentiable function such that

$$V(0)=0 \text{ and } V(x)>0 \text{ in } D-\{0\} \tag{G.12}$$

$$\dot{V}(x)\le 0 \text{ in } D \tag{G.13}$$

Then, $x=0$ is stable. Moreover, if

$$\dot{V}(x)<0 \text{ in } D-\{0\} \tag{G.14}$$

Then, $x=0$ is asymptotically stable. □

G.6 Barbalat's Lemma

[Slotine and Li [73], Applied nonlinear control, Barbalat's lemma]

If the differentiable function $f(t)$ has a finite limit as $t\to\infty$, and if $\dot{f}$ is uniformly continuous, then $\dot{f}(t)\to 0$ as $t\to\infty$. □

G.7 Lyapunov-Like Lemma

[Slotine and Li [73], Applied nonlinear control, lemma 4.3]

If a scalar function $V(x,t)$ satisfies the following conditions:

1. $V(x,t)$ is lower bounded
2. $\dot{V}(x,t)$ is negative semi-definite
3. $\dot{V}(x,t)$ is uniformly continuous in time

then $\dot{V}(x,t) \to 0$ as $t \to \infty$. □

G.8 [A.A.J.Lefeber [83], Corollary 2.3.4]

Consider the system

$$\dot{x} = A(r_r(t))x + Bu \tag{G.15}$$

$$y = Cx \tag{G.16}$$

Where $A(r_r)$ is continuous, $A(0) = 0$, $r_r : \square \to \square$ continuous. Assume that for all $s \neq 0$ the pair $(A(s), B)$ is controllable (respectively the pair $(A(s), C)$ is observable). If $r_r(t)$ is bounded, Lipschitz and constants $\delta_c > 0$ and $\varepsilon > 0$ exist such that $\forall t \geq 0$, $\exists s : t - \delta_c \leq s \leq t$ such that $|r_r| \geq \varepsilon$ then the system in 7.41 and 7.42 is uniformly completely controllable (respectively observable). □

Appendix H

H Control Techniques

H.1 PID Control

PID control or Proportional-Integral-Derivative control is a control loop feedback mechanism, which is used to correct the error between a measured variable and a desired reference variable (or set-point) with a corrective action. To correct, for example, the error between the current and desired depth of the AUV by enabling the vertical thrusters. The PID controller consists of three different parameters or gains, namely the proportional, integral and derivative gain. The proportional gain determines the reaction to the current error. The integral gain determines the reaction based on the sum of recent errors. The derivative gain determines the reaction to the rate at which the error has been changing. The weighted sum of these three actions is used to adjust the output, for instance the power of the thrusters of the AUV [6 10 19]. The PID algorithm is given by

$$u = k_p e + k_i \int e + k_p \dot{e} \tag{H.1}$$

Where, u is the output of the PID controller, k_p is the proportional gain, k_i is the integral gain, k_d is the derivative gain and e is the error signal.

The three different gains within the PID controller all have there own influence. Enlarging the k_p gain will result in a faster response of the controller, although an excessively larger chosen proportional term will lead to instability and oscillation. Enlarging the k_i gain will imply a quicker elimination of steady state errors but the drawback is a larger overshoot. A larger k_d gain will decrease the overshoot but slows down the response of the system and causes signal noise amplification in the differentiation of the error which may lead to instability. The effect of increasing gains is given in Table H.1 and can also be found in [39].

Gains	Rise Time	Overshoot	Settling Time	Steady state error
Increase k_p	Decrease	Increase	Small Change	Decrease
Increase k_i	Decrease	Increase	Increase	Eliminate
Increase k_d	Small Decrease	Decrease	Decrease	None

Table H.1: Effect of increasing PID control gains [39].

In Table H.1, the rise time is the time required for the system response to rise from 10% to 90% of the final steady state value of the desired response. The overshoot is the maximum peak value of the response curve measured from the desired response of the system. The settling time is the time that is required for the response of the system to reach and stay within a specified error band which is usually chosen symmetrical about the final value. The steady state error is the error that exists as time goes to infinity, when the response reaches a steady state [71].

P.J. Craven, et al. [2] recommend to have high proportional gain and high derivative gain for the control of underwater vehicles. The high proportional gain ensures a rapid response to error and decreases steady state errors. The stability of the system will be reduced by this high proportional gain and therefore a high derivative gain is needed to ensure stability.

A problem with a PID controller is the fact that it is linear. So if it is used for an AUV, which is a high nonlinear system, the performance of the PID controller is variable. Therefore a linear representation of the nonlinear dynamics of the AUV can be made. At specific points the nonlinear dynamics can be linearised as a series of linear functions across the operating range [72]. For every linear function a PID controller can be designed, an interpolating function is often used to aid transition between operating points, this method is also known as gain scheduling [73]. However the further the system diverges from the point of linearization the more ineffective the control will be. Gain scheduling is successfully applied on the AUV named “Marius” by P.Egeskov, A.Bjerrum, et al. [77]. PID control is also used in combination with feedback linearization. Feedback linearization changes the nonlinear system into a linear system through a change of variables and a suitable control input, PID control is then often used to stabilize the resulting linear equation [73].

A disadvantage of the derivative term of the PID controller, as also noted above, is that small amounts of measurement noise can cause large changes in the output.

Measurements are therefore filtered with a low pass filter to remove high frequency noise. However reducing noise of the sensors (in a instrumental way) is preferred, since low pass filtering and derivative control can cancel each other out [2].

H.2 Linear Quadratic Gaussian Controllers

The Linear Quadratic Gaussian or LQG controller assumes a linear system, quadratic cost function and Gaussian noise. The LQG control is an optimal control problem and tries to achieve a certain optimality criterion with a combination of a Kalman filter, i.e. a Linear-Quadratic Estimator (LQE) and a Linear-Quadratic Regulator (LQR) to optimize the controller [6, 34, 35].

A.Santos and R.R.Bitmead have tested a flying AUV with a LQG controller [36]. They implemented the LQG controller in a linear and nonlinear controller for the AUV. Linear altitude control of the AUV resulted in a chattered control signal of the AUV, which caused skidding of the vehicle. The altitude deviations are mostly caused by the poor estimator. Nonlinear control reduced the chattering in the control, the altitude deviations are reduced and the response is faster. An extended kalman filter (EKF) was introduced, which was also primarily responsible for the improvements.

H.3 Fuzzy Logic Control

Fuzzy control is control with logics (sentences) rather than equations [30]. An example of the program rules of a fuzzy logic controller:

1. If *error* < *0* and *change in error* < *0* then *output* = *NB*

2. If *error* < *0* and *change in error* = *0* then *output* = *NM*

The rules (given above) are in the if-then format and are applied in a rule based controller. The computer is able to execute the rules and compute a control signal depending on the measured inputs. An advantage of a fuzzy controller is that the control strategy is stored in a natural language, which is easier to understand for a non-specialist end-user. A disadvantage is that a non-fuzzy logic controller can be designed much more quickly [31 32 33]. The fuzzy controller is useful when a mathematical model is not known well or not known at all. Implementing fuzzy control on an AUV can avoid the complex hydrodynamic modeling of the vehicle. Fuzzy logic controllers are implemented with success on AUVs in several cases [20, 21, 22]. Note that when a mathematical model is available the use of classical control theory is more appropriate.

H.4 Adaptive Control

Adaptive control is a form of non-linear control used for uncertain or time-varying systems and it is mainly applied on systems with a known dynamic structure with unknown constant or slowly-varying parameters [73, 74]. Adaptive control is useful for AUV's due to the changing dynamics in the ocean. The controller can adapt itself to varying ocean currents or to a different vehicle mass when new equipment is installed. According to P.J. Craven, R. Sutton, et al. [2], the most successful AUV control studies include some form of adaptive control strategy.

J.Nie, T. Fossen et al.[22] presented a sensor-based navigation system and an adaptive control system for shallow water UUVs. All control gains were initially set to zero and adjusted by the adaptive control law, which resulted in accurate control of the UUV in six degrees of freedom using the estimated position and velocity from the on-board sensor-based navigation system. G. Antonelli, S. Chiaverini, et. al. [12] presented experimental results of adaptive control using the AUV named "ODIN". Other interesting research on adaptive control is done by T. Fossen and I. Fjellstad [20], S. Sagatun and R. Johansson [21], and, T. Fossen and S. Sagatun [23].

H.5 Sliding Mode Control

Another nonlinear control technique is Sliding Mode Control or SMC, which leads to robust control under parameter uncertainties [73 74]. SMC is frequently used to control AUVs and consists of a switching control law that transforms the state trajectory of the plant onto a sliding surface. The control law is designed in such a way that the system will diverge to the sliding surface. Afterwards the control law constrains the system so it stays on the sliding surface where it has desired dynamics [2, 46, 70]. Interesting research on sliding mode control is performed by J. Healey and D. Lienard [13, 26], D.B. Marco, A.J. Healey [14] and in T. Fossen and B. Foss [25].

Appendix I

I Simulation Results

The following simulations are run:

- In Appendix I.1: Mass/Inertia and damping parameters of the controller and plant are exactly the same. High proportional and derivative gains are chosen
- In Appendix I.2: The mass of the controller is half the mass of the plant, so a perturbed parameter situation is created; the results of a PD controller with high proportional and derivative gains are compared with a P controller with a low proportional gain.
- In Appendix I.3: The controllers from Appendix I.2 stay the same, but now noise is added to the measured position and velocity of the plant.
- In Appendix I.4: The PD controller, with high proportional and derivative gains, is tested under the same conditions as in Appendix I.3, except for the fact that the rate limiter is now left out.
- In Appendix I.5: The PID controller is tested under extreme parameter perturbation, where the mass and linear damping of the controller is three times higher and the quadratic damping is four times higher than the parameters of the plant.

I.1 High Gain PD control, No Noise, No Perturbation

Parameters	Controller	Plant
$m_{\dot{x}}$	160	160
$d_{\dot{x}}$	60	60
$d_{\dot{x}\|\dot{x}\|}$	90	90
$g_{\dot{x}}$	0	0

Table I.2: Controller and plant parameters.

	Option 1	Option 2
Parameters		
k_p	100	-
k_i	0	-
k_d	20	-
Noise		
Position	0	-
Velocity	0	-

Table I.3: PID gain terms for options 1 and 2.

Maximum tracking error	Option 1	Option 2
Position	e_{mach}	-
Velocity	e_{mach}	-

Table I.4: Maximum tracking error for options 1 and 2.

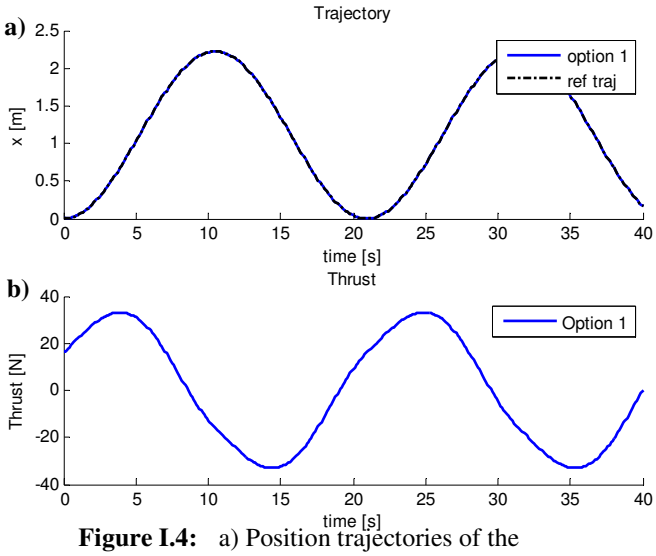

Figure I.4: a) Position trajectories of the reference, options 1 and option 2. b) Thrust input of options 1 and 2.

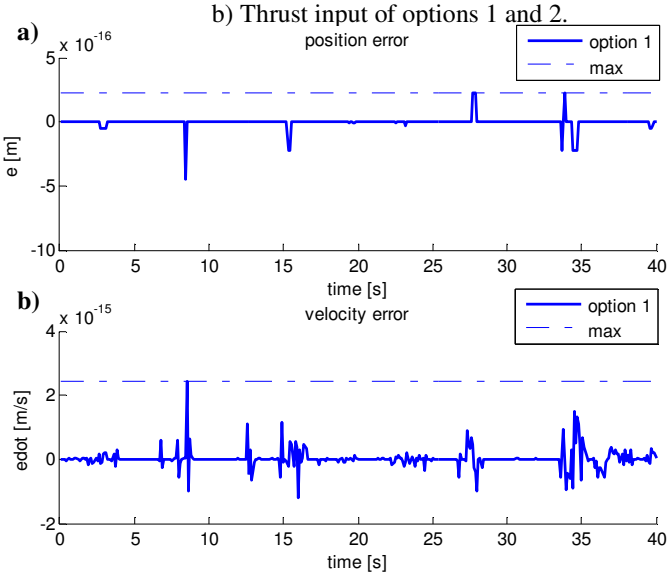

Figure I.5: a) Position error. b) Velocity error.

In this simulation there is no parameter perturbation, the controller and plant parameters can be seen in Table I.2. There is no noise added to the measured signals and the linear controller within the tracking controller is a PD controller with high proportional and derivative gains, see Table I.3. In Figure I.4 it can be seen that the AUV exactly tracks the reference trajectory, which can also be seen in Figure I.5 where the position and velocity error are e_{mach}, see Table I.4. This is an obvious result since the parameters plant were exactly known and there are no disturbances.

I.2 Low Gain P control and High Gain PD control, No Noise, With Perturbation

Parameters	Controller	Plant
$m_{\dot{x}}$	80	160
$d_{\dot{x}}$	60	60
$d_{\dot{x}\|\dot{x}\|}$	90	90
$g_{\dot{x}}$	0	0

Table I.5: Controller and plant parameters.

	Option 1	Option 2
Parameters		
k_p	1	100
k_i	0	0
k_d	0	20
Noise		
Position	0	0
Velocity	0	0

Table I.6: PID gain terms for options 1 and 2.

Maximum tracking error	Option 1	Option 2
Position	0.2323	9.999e-4
Velocity	0.1197	2.999e-4

Table I.7: Maximum tracking error for options 1 and 2.

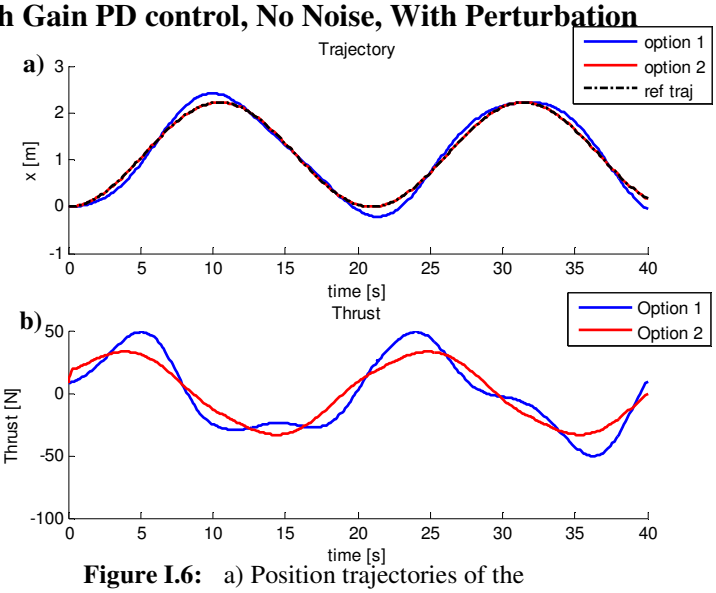

Figure I.6: a) Position trajectories of the reference, options 1 and option 2. b) Thrust input of options 1 and 2.

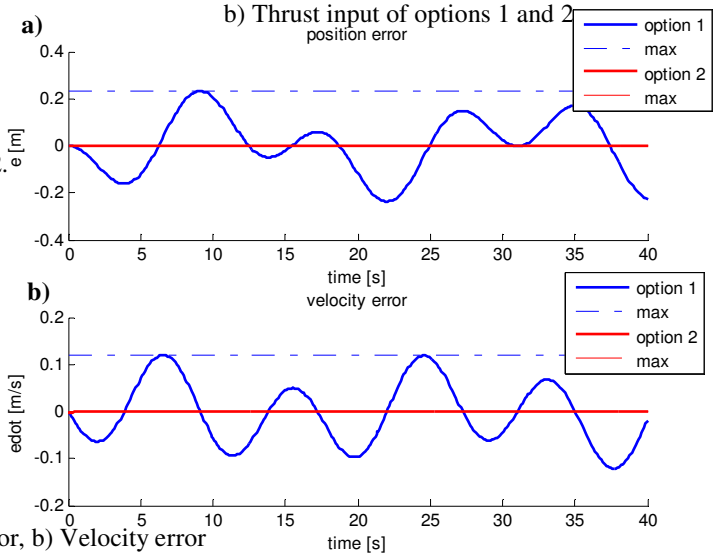

Figure I.7: a) Position error, b) Velocity error

In this simulation there is parameter perturbation, the controller and plant parameters can be seen in Table I.5. There is no noise added to the measured signals, see Table I.6. The linear controller within the tracking controller for option one is a P controller with a low proportional gain and for option 2 is a PD controller with high proportional and derivative gains, the P and PD gains are shown in Table I.5. In Figure I.6 it can be seen that control option 1 tracks the reference trajectory, with a reasonable error of 0.23 *m*. However control option 2 manages to follow the trajectory with only a position error of 1 mm, which is also an obvious result since the high proportional and derivative gains will immediately response to an error.

I.3 Low Gain P control and High Gain PD control, With Noise and Perturbation

Parameters	Controller	Plant
$m_{\dot{x}}$	80	160
$d_{\dot{x}}$	60	60
$d_{\dot{x}\lvert\dot{x}\rvert}$	90	90
$g_{\dot{x}}$	0	0

Table I.8: Controller and plant parameters.

	Option 1	Option 2
Parameters		
k_p	1	100
k_i	0	0
k_d	0	20
Noise		
Position [m]	0.0093	0.0093
Velocity [m/s]	0.0186	0.0186

Table I.9: PID gain terms for options 1 and 2.

Maximum tracking error	Option 1	Option 2
Position	0.2352	5.5224
Velocity	0.1292	1.1176

Table I.10: Maximum tracking error for options 1 and 2.

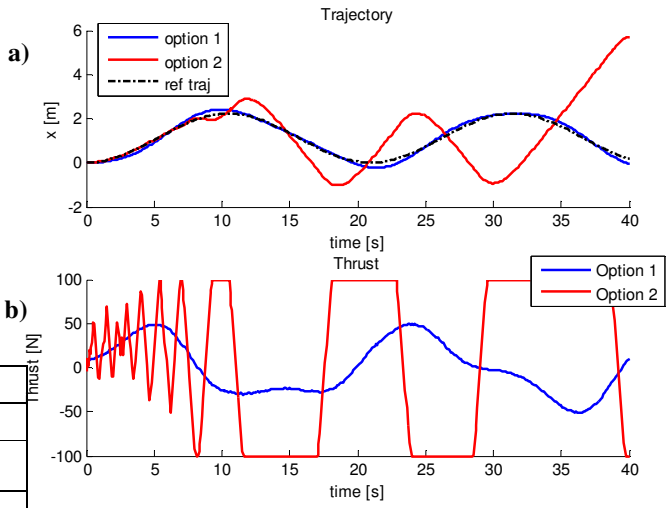

Figure I.8: a) Position trajectories of the reference, options 1 and option 2.
b) Thrust input of options 1 and 2.

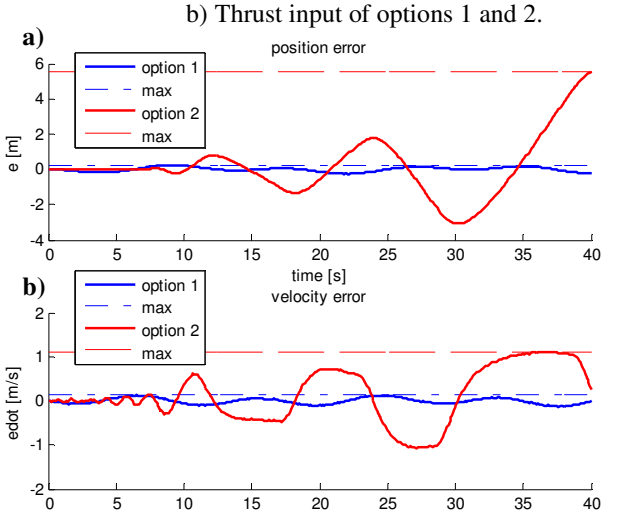

Figure I.9: a) Position error.
b) Velocity error.

In this simulation the same conditions and controllers apply as in subsection I.2, except for the fact there is noise added to the measured signals, see Table I.9. In Figure I.8 it can be seen that control option 1 still tracks the reference trajectory, with a similar reasonable error of 0.23 *m*. Only control option 2 has now become unstable and the error keeps increasing over time, see Figure I.9. This is obviously caused by the too high chosen gains of the PD controller. In theory the k_p and k_d gains can be chosen arbitrarily above zero and larger k_p and k_d will give a more robust system, which could be seen in subsection I.2. However the k_p and k_d are also bounded from above, caused by the higher bandwidth and triggering of higher order dynamics. Note in Figure I.8 that the thrust saturation works at 100 and -100 *N* and that the thrust rate limiter limits the change of thrust to 200 *N* in one sec.

I.4 High Gain PD control, With Noise and Perturbation, No Thrust Rate Limiter

Parameters	Controller	Plant
$m_{\dot{x}}$	80	160
$d_{\dot{x}}$	60	60
$d_{\dot{x}\|\dot{x}\|}$	90	90
$g_{\dot{x}}$	0	0

Table I.11: Controller and plant parameters.

	Option 1	Option 2
Parameters		
k_p	100	-
k_i	0	-
k_d	20	-
Noise		
Position [m]	0.0093	-
Velocity [m/s]	0.0186	-

Table I.12: PID gain terms for options 1 and 2.

Maximum tracking error	Option 1	Option 2
Position	0.0104	-
Velocity	0.0473	-

Table I.13: Maximum tracking error for options 1 and 2.

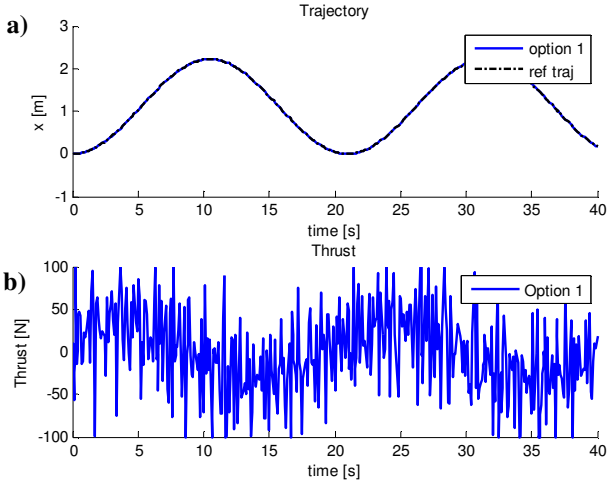

Figure I.10: a) Position trajectories of the reference, options 1 and option 2.
b) Thrust input of options 1 and 2.

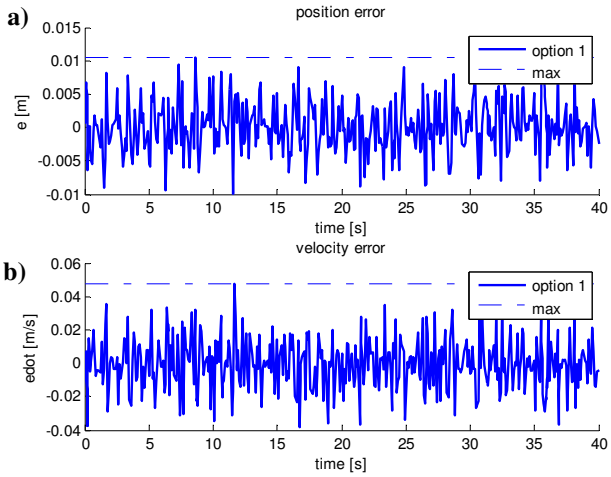

Figure I.11: a) Position error.
b) Velocity error.

This subsection is added as an intermezzo to show what would happen to the system, which has the same conditions and PD controller defined in subsection I.3, if there is no rate limiter applied to the thrust input. The system is no longer unstable as can be seen in Figure I.10, the controller manages to stabilize the system by continuously changing the sign of the thrust input. It can be seen that it is important to implement a rate limiter to the thrust input; otherwise this PD controller would in theory be better, which it obviously is not, since the thrust sign can not be changed immediately caused by the propeller inertia.

I.5 PID control, With Noise and Extreme Perturbation

Parameters	Controller	Plant
$m_{\dot{x}}$	500	160
$d_{\dot{x}}$	200	60
$d_{\dot{x}\|\dot{x}\|}$	400	90
$g_{\dot{x}}$	0	0

Table I.17: Controller and plant parameters.

	Option 1	Option 2
Parameters		
k_p	9	-
k_i	10	-
k_d	6	-
Noise		
Position [m]	0.0093	-
Velocity [m/s]	0.0186	-

Table I.18: PID gain terms for options 1 and 2.

Maximum tracking error	Option 1	Option 2
Position	0.0141	-
Velocity	0.0477	-

Table I.19: Maximum tracking error for options 1 and 2.

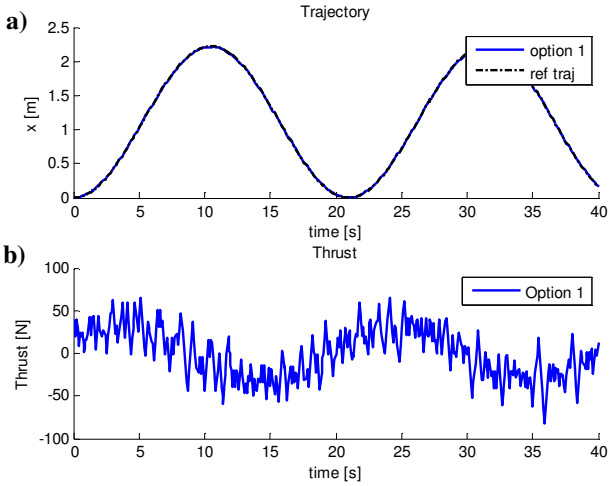

Figure I.14: a) Position trajectories of the reference, options 1 and option 2.
b) Thrust input of options 1 and 2.

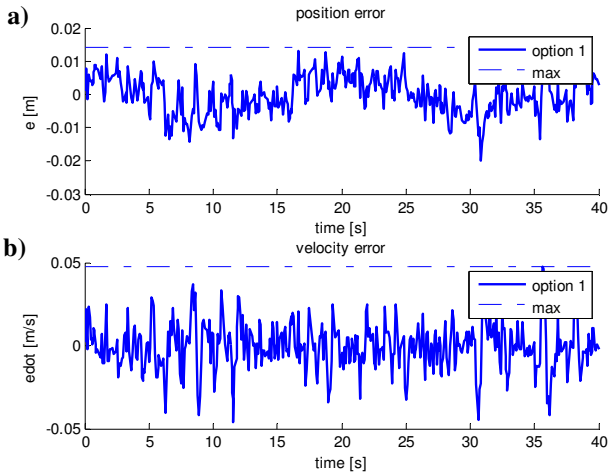

Figure I.15: a) Position error.
b) Velocity error.

The last simulation is to see how the derived PID controller from Section 4.2, will behave under extreme parameter perturbation, added noise and no change of the control gains. The extreme parameter perturbation consists of giving the controller model a three times higher mass and linear damping and a four times higher quadratic damping, this can be seen in Table I.17. The PID controller keeps the system stable and the position error increases from 0.011 *m* to 0.014 *m*, which is a slight increase but still a reasonable and acceptable error.

Appendix J

J.1 Simulation Results

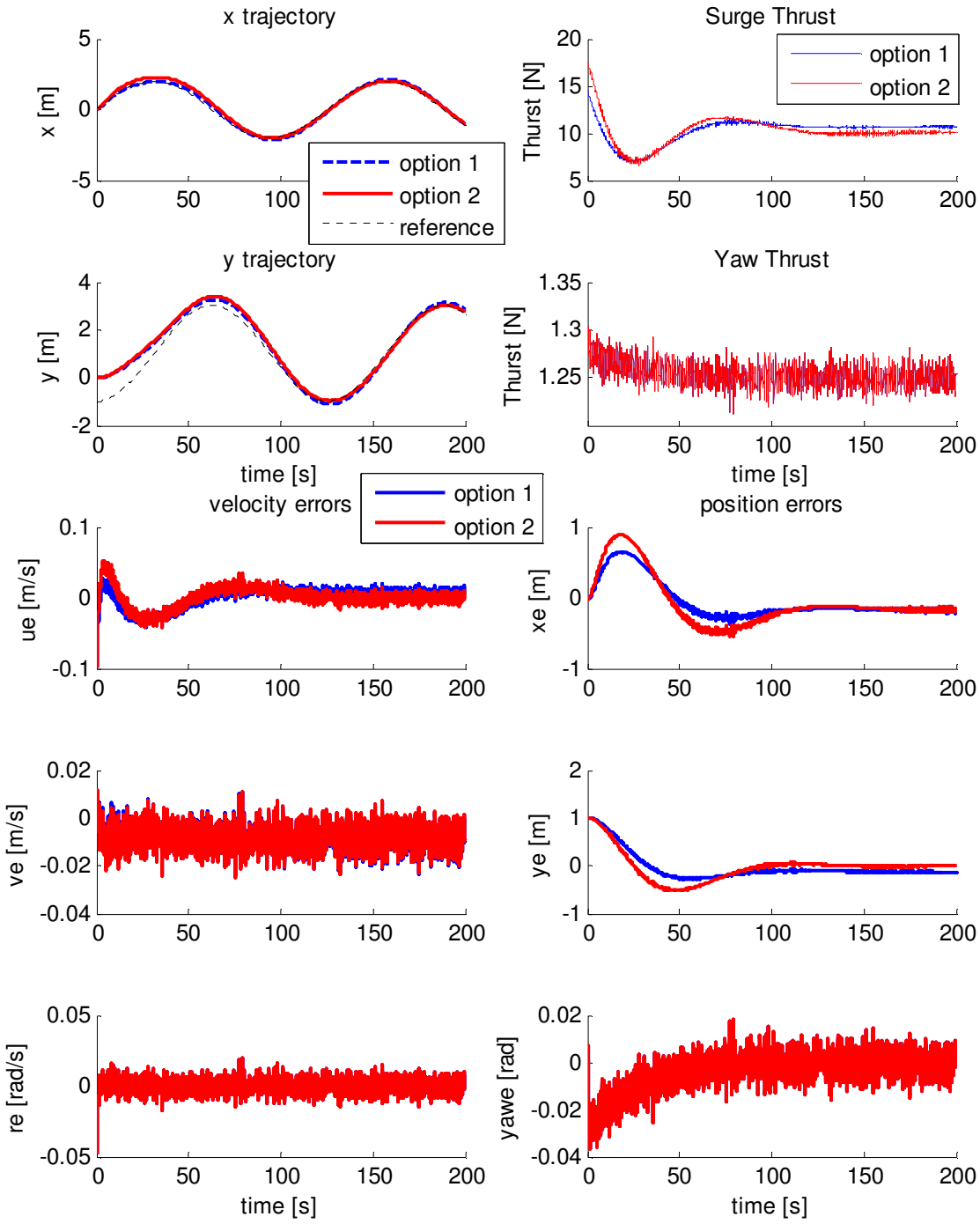

Figure J.1: Initial position of the AUV is (x,y)=(0,0).

J.2 Simulation Results

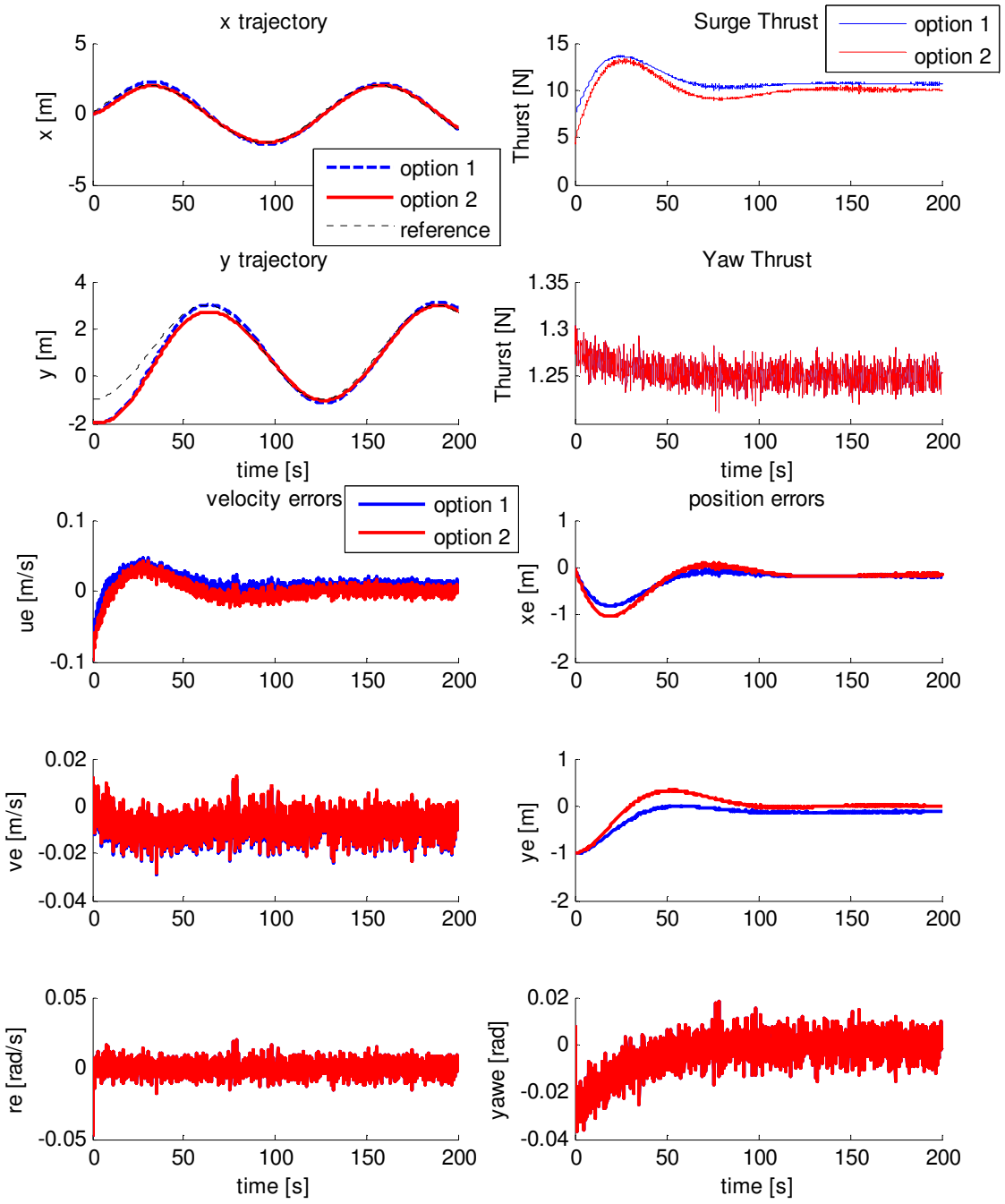

Figure J.2: Initial position of the AUV is (x,y)=(0,-2).

Appendix K

K Matlab Simulink Implementation

Simulations will be run in Matlab Simulink to test the control law defined in (4.22). To be able to run a simulation a reference and plant model are made. The reference model defines a reference trajectory for the AUV to follow. Note that the reference signals r, $\dot{r}$ and $\ddot{r}$ need to be available online. The plant model will replace the real AUV and represent the AUV dynamics.

A cosine function will define the reference signal for acceleration, with a frequency of 0.3 Hz and an maximum amplitude of 0.1 m/s^2. The cosine function will be integrated twice to obtain the reference signals for velocity and position. Table K.1 shows the maximum r, $\dot{r}$ and $\ddot{r}$ values reached; the AUV was able to reach these values during wet tests.

Max($\ddot{r}$)	0.10 m/s^2
Max($\dot{r}$)	0.33 m/s
Max(r)	2.22 m
Function	$\ddot{r} = 0.1\cos(0.6\pi t)$

Table K.1: Reference model information.

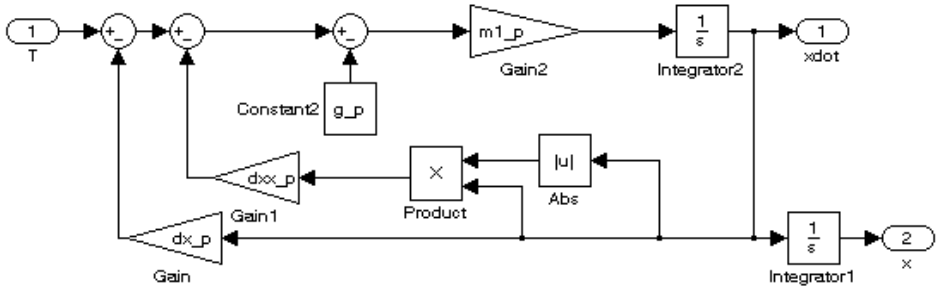

Figure K.1: Plant model built in Simulink Matlab, to represent the AUV dynamics.

The plant model is defined by

$$\ddot{x} = \frac{\tau_{\dot{x}} - d_{\dot{x}}\dot{x} - d_{\dot{x}|\dot{x}|}\dot{x}|\dot{x}| - g_{\dot{x}}}{m_{\dot{x}}} \qquad \text{(K.1)},$$

which is the one degree of freedom dynamical model of the AUV, also defined in (4.1). The input signals of the plant model are the thrust and plant velocity and the output signal

is the current acceleration which is integrated to obtain the current velocity and integrated twice to obtain the current position of the AUV. The plant model, which can be seen in (K.1), is built within Simulink, as shown in Figure K.1

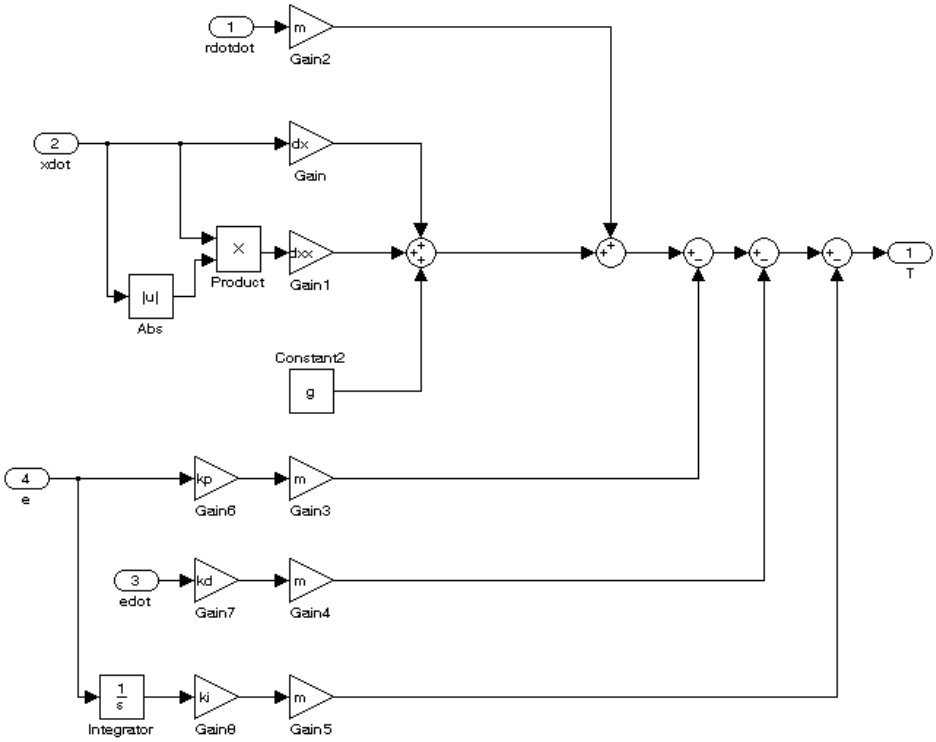

Figure K.2: Control model built in Simulink Matlab.

The control law defined in (4.22), for ease shown again in (K.2), is implemented within Simulink and shown in Figure K.2. The input signals are the reference acceleration $\ddot{r}$, the velocity of the plant $\dot{x}$, the velocity error $\dot{e}$ and the position error e and the output is the thrust $\tau_{\dot{x}}$.

$$\tau_{\dot{x}} = d_{\dot{x}}\dot{x} + d_{\dot{x}|\dot{x}|}\dot{x}|\dot{x}| + g_{\dot{x}} + m_{\dot{x}}\ddot{r} - m_{\dot{x}}k_1 e - m_{\dot{x}}k_2\dot{e} - m_{\dot{x}}k_i\int e \qquad \text{(K.2)}$$

The reference model, control model and plant model are now connected with each other within Simulink. In reality the current position and velocity of the AUV (or plant) will be measured with a certain level of noise, therefore white noise is added to the determined position and velocity of the plant. The noise amplitude of the position will be 0.01 m or 10 cm and 0.02 m/s for the velocity.

A rate limiter is added to the thrust output, since in reality the trolling motors are not able to immediately switch thrust, from for instance -50 N to +50 N, since the propeller has an inertia. The rate limiter will limit the rate of change of thrust to

maximum 100 *N* in one second per trolling motor, for the *surge* degree of freedom this will mean a maximum change of 200N since the AUV has two trolling motors operating in this degree of freedom.

Saturation is also added to the thrust output, since in reality the trolling motors can only get a certain amount of power (i.e. thrust). One trolling motor is able to deliver a maximum thrust of 50 N, and the assumption is made that it will be able to do this in both directions. For the *surge* degree of freedom this means that the saturation is set to 100 N, since two trolling motors are operating in this degree of freedom.

The complete system built within Simulink is shown in Figure K.3.

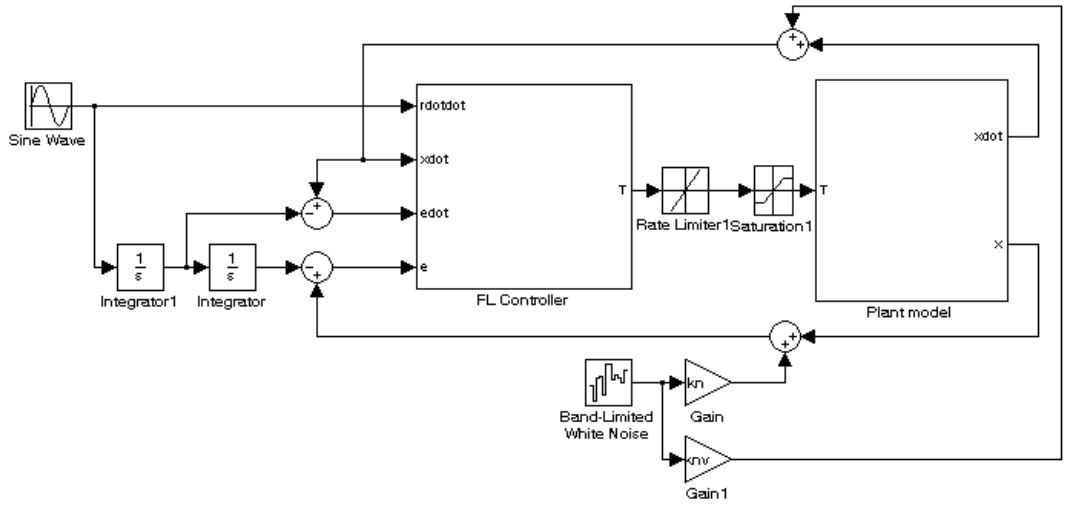

Figure K.3: Control model built in Simulink Matlab.